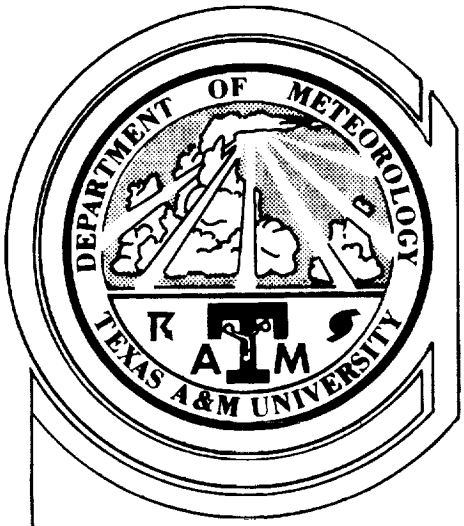

TEXAS A&M UNIVERSITY

DEPARTMENT OF METEOROLOGY

TROPICAL PACIFIC MOISTURE VARIABILITY: ITS DETECTION, SYNOPTIC STRUCTURE AND CONSEQUENCES IN THE GENERAL CIRCULATION

December 6, 1986 - August 31, 1990

Submitted September 1990

FINAL REPORT, Contract No. NAS8-37284

James P. McGuirk

Department of Meteorology

Texas A&M University

College Station TX 77843-3146

Prepared for

George C. Marshall Space Flight Center

Marshall Space Flight Center, Alabama 35812

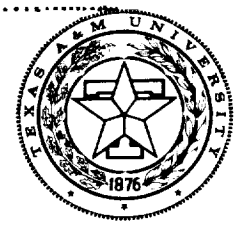

TROPICAL PACIFIC MOISTURE VARIABILITY: ITS DETECTION, SYNOPTIC STRUCTURE AND CONSEQUENCES IN THE GENERAL CIRCULATION

December 6, 1986 - August 31, 1990

Submitted September 1990

FINAL REPORT, Contract No. NAS8-37284

James P. McGuirk

Department of Meteorology

Texas A&M University

College Station TX 77843-3146

Prepared for

George C. Marshall Space Flight Center

Marshall Space Flight Center, Alabama 35812

ACKNOWLEDGEMENT

The principal investigator acknowledges the contributions of the following people in the completion of this research:

Aylmer H. Thompson, who collaborated during the first part of the research period as a Co-Principal Investigator, before his retirement; and,

The following graduate students:

Drs. G.A. White, J.R. Schaefer, C.A. Askue, and K.G. Blackwell; and D.J. Ulsh, P.M. Hayes, D.C. Sautter, R.E. Havholm, J.D. Fink, D.E.W. Smith, R.J. Liles, and K.B. Batson.

Finally, the contribution of **Joseph Gerrity** and **Eugenia Kalnay** of the National Meterological Center's Development Division, who made the collaborative work at NMC possible, is acknowledged.

1. INTRODUCTION AND SUMMARY

The body of this final report summarizes the accomplishments and findings of the research effort carried out under NAS-37284. This NASA grant is about two scientific issues:

i. Synoptic scale circulation systems over the tropical Pacific Ocean and their interaction with the larger scale circulation; and,

ii. Development of the satellite analysis tools to accomplish (i).

The most intensely studied event is referred to as a tropical plume. (Old terminology refers to it as a moisture burst.) Tropical plumes are defined as extensive bands of clouds extending out of the ITCZ and across 15°N to link tropics and middle latitudes. This study has been expanded to examine all convective features along the ITCZ, middle latitude troughs which extend into the tropics and subtropics, and East Asian cold surges (cold air masses which cross China and the South China Sea and trigger systems which can cross the Pacific completely). The most successful view of these synoptic features over the data sparse Pacific is through satellites, and in particular, through the observation of moisture and cloud fields.

The structure of synoptic systems and the interaction of synoptic and larger scale systems is a convenient scientific framework for the development of satellite analysis tools. The two techniques most used in this research are:

i. Statistical multi-variate analysis (empirical orthogonal function analysis, canonical discriminant analysis, clustering, compositing, and non-linear regression and linear filtering); and,

ii.A radiative transfer model for the TOVS instruments (estimating TOVS brightness temperatures from operational analysis and from radiosondes).

The technical details resulting from this research are embodied in the five refereed publications, seventeen conference presentations and proceedings, three doctoral dissertations and six master's theses listed in Section 3. In the list of findings in Section 2, the reference citations refer to the publications and documents listed in Section 3. Appendix A consists of the abstracts of the publications, the dissertations and the theses; complete texts of these documents are available in the journals themselves or through Texas A&M University. Appendix B consists of reproductions of available conference proceedings papers The only papers that are currently unavailable are two presentations made to the IUGG in 1987 (McGuirk and Thompson [1987] and Thompson et al. [1987]).

The remainder of this document extracts, synthesizes and summarizes relevant information from the sources listed in Section 3. Although this project was scheduled to be completed in December 1989, the P.I. (JPM) spent 8.5 months with the National Meterological Center's (NMC) Development Division under joint sponsorship of the University Corporation

for Atmospheric Research, NMC, and NASA under this grant. For this reason, the contract period was extended through August 1990, at no additional cost to NASA. Secondly, after the contract was initiated, the budget was reduced by NASA Headquarters from $462,075 to $309,000. This "descoping" occurred in early 1988, approximately at the 40% completion point of the contract. Because of this adjustment and added funding for the NMC effort, it was not possible to follow precisely the original work statement.

The fulfillment of the objectives and work statement for this contract is summarized in Section 1. Section 2 specifies, in detail, many of the important conclusions of this study. Section 3 lists publications generated through this contract. Finally, the appendices contain abstracts of theses, dissertations and publications, and reprints of the proceedings papers.

The initial contract work statement (before the contract was descoped) states as the overall objective:

> **To develop techniques to resolve and describe atmospheric moisture variability over the data-sparse tropical Pacific.**

Individual tasks were enumerated:

i. Utilize channel radiance data to describe synoptic scale systems;

ii. Apply multi-channel techniques to correct data uncertainties and synthesize three dimensional results;

iii.Describe weather system moisture budgets, utilizing

satellite observations;

iv. Describe the interaction of the synoptic scale and the general circulation over the Pacific;

v. Expand the understanding of moisture bursts (hereafter denoted tropical plumes), including dynamical and moisture budget mechanisms and enhanced temporal resolution;

vi. Utilize radiative transfer models to identify and interpret synoptic signals in satellite observations and operational analyses.

[The following general objective is added to account for the shared funding with NMC and UCAR.]

vii.Assess the use of additional satellite information in the operational NMC analysis/forecast model.

a. Fulfillment of the Objective

The overall objective was met well. Several new data sets were implemented in this study: VAS water vapor imagery, outgoing long wave radiation fields, and SMMR microwave observations (at 19 and 22 gigahertz). In addition, infrared imagery and full channel TOVS sounding radiances continued to play a large part in research analysis. VAS water vapor imagery, SMMR precipitable water estimates and TOVS moisture channels were used to describe synoptic scale water vapor distributions. A radiative transfer model (developed by Susskind et al. [1983] at NASA Goddard) was used both to

extract additional information from satellite sounding data and to verify operational analyses and observations in data sparse regions; both of these procedures emphasized horizontal and vertical water vapor distributions. Tropical plumes, East Asian cold-surge-spawned system, a variety of tropical thermal waves, and active ITCZ systems and their interactions with larger scale circulation features were documented. Again, the role of moisture within these systems was examined; in fact, most of these systems were identified, quantified and tracked by their specific moisture distributions. Finally satellite, synoptic and dynamic-modelling analyses were applied to expand our understanding of the processes involved in tropical plume formation and evolution.

b. Fulfillment of the Work Statement

Because of the descoping of the research effort, item (iii) and the dynamical aspects of item (v) were not attempted. The remainder of the itemized tasks were completed, as well as a number of associated tasks which suggested themselves as profitable endeavors during the course of fulfilling the listed tasks.

i. Nearly all of the papers listed in Section 3 pertain to the utilization of channel radiance data. The weather systems studied have been listed above as have been the satellite data sets. The crucial result is that vapor imagery has been so successful in depicting the temporal

evolution of tropical plumes, that skillful forecast of plume development can be made solely on VAS water vapor imagery.

ii. Schaefer's (1988) dissertation and the survey by McGuirk(1988) are the most direct fulfillments of the removal of contamination from satellite data and application of decomposition of satellite individual channel radiance data. Three component waves associated with tropical plume development were isolated and quantified.

iii.This task was descoped, although Blackwell's (1987) thesis dealt with estimating vertical motion from satellite observed moisture fields. Reliable estimates of strong subsidence within the subtropical high can be made from TOVS water vapor channels.

iv. McGuirk and Ulsh (1990) and the theses of Hayes (1988) and Sautter (1988) and the dissertation of Askue (1989) examined and quantified interaction between the synoptic scale and the tropical general circulation. Features examined included interactions between middle latitude synoptic scale systems, tropical plume, the ITCZ, monsoonal systems and tropical normal modes.

v. The same studies listed in item (iv) examined causative mechanisms of tropical plumes, as well as the studies by McGuirk and Ulsh (1990), McGuirk et al. (1988) and the syntheses presented by McGuirk (1987,1989). Tropical plumes are barotropic in nature, although the triggering mechanisms appear to be convective and baro-

clinic.

vi. White's (1988) dissertation and Smith's (1989) thesis dealt extensively with the GLA radiative transfer model to identify and interpret synoptic signals in radiance data. The former quantified vertical synoptic structure; the latter used radiation model output and TOVS observations to evaluate operational analysis.

vii.In the added task (reflecting the increased funding from NMC and UCAR), experiments were run on the NMC global spectral model which incorporated additional operation satellite information. Improvements were observed in the 48 h tropical forecasts.

2. Major conclusions

Progress has been accomplished in five general areas. The nature of the work in these areas is summarized, followed by a listing of the major significant findings.

a. Satellite tools

One major goal of this research is to develop analysis tools to use satellite data more effectively. Most of these tools are statistical in nature--empirical orthogonal function analysis, compositing, classification, and other multi-variate techniques. Others are physical or operational--radiative transfer models, operational forecast models. The first set of findings refers to the tools themselves. Physical meteorological results follow later.

EOF Techniques. Empirical orthogonal function analysis continues to be a fruitful data summary procedure useful for reducing the massive quantity of satellite data into a much smaller body of information. EOF analysis works well because of the high correlation among individual radiance channels. Four months of daily full channel brightness temperature soundings in early 1984 were analyzed extensively over the eastern tropical Pacific. The analysis extracted synoptic scale, planetary scale and moisture patterns from the syn-

thesized data set. This work is described in Schaefer's (1988) dissertation, and by McGuirk (1990, 1989) and McGuirk et al. (1989b). A second application of EOF analysis involved observed channel radiances and radiances computed with a radiative transfer model from ECMWF analyses and reanalyses during the FGGE Special Observing Periods in 1979. The EOF patterns and amplitudes were used as the basis of comparison between observed and calculated radiances. In this manner the satellite observations could be used directly as a ground truth comparison of operational analysis. Smith's (1989) thesis describes the calculations with some results presented by McGuirk and Smith (1990) and McGuirk et al. (1989b). Finally, White's (1988) dissertation describes the use of EOF analysis, canonical discriminant analysis and classification procedures to extract additional signal for satellite sounding retrievals. Statistically generated data were analyzed to separate soundings into different synoptic classes, and to subject each class to additional analysis to estimate quantitative structural details, such as inversion strengths or moisture content. Results are presented by White and McGuirk (1989, 1987), White et al. (1988) and McGuirk et al. (1989b).

Findings:

* EOF analysis is a technique that can summarize planetary scale features in only a few (about 3) EOF patterns of horizontal and vertical structure.
* Results depend on preprocessing (such as smoothing, compo-

siting or enhancing the "moisture variance" to bring out moisture features).

* Patterns are insensitive to moderate changes of domain size and to time interval.
* EOF analysis is an excellent filtering tool for extracting errors or extraneous signal (such as "scan angle", or limb-darkening, affects or surface emissivity variations.
* EOF analysis can, under controlled circumstances, extract accurate synoptic patterns on a number of different spatial scales.
* EOF decomposition of output (soundings or three-dimensional analysis) from a radiative transfer model provides a near ideal framework for the use of satellite observations as "ground truth" for analyses.
* Operational analyses can be evaluated in terms of descriptive statistics, time series behavior and EOF parameters.
* Synoptic scale variability revealed by EOF decomposition is sensitive to both geographical location and type of synoptic system.
* The general quality of a sounding (inversion? moist tropical? frontal?) can be distinguished easily through canonical discriminant analysis (a variation of EOF analysis).
* Structural estimates within sounding classes (how strong an inversion) show positive skill but are not highly reliable.
* Sounding retrieval will be more accurate if radiance soundings are first sorted into synoptic sub-classes. This procedure essentially improves the first guess.

* Chernov patterns can be used to obtain a quick qualitative assessment of the detailed structure of a sounding.

Compositing. Compositing is one of the most powerful techniques we have employed in the analysis of satellite data, particularly in the attempt to identify synoptic patterns. We have composited outgoing longwave radiation (OLR) gridded data, Tiros operational vertical sounder (TOVS) point data analyzed to a grid, and VISSR atmospheric sounder (VAS) water vapor imagery, all successfully. All of these satellite sets have been composited for tropical plumes; in Schaefer's (1988) dissertation for TOVS, in Ulsh's (1988) thesis for VAS imagery, and by McGuirk (1989) for OLR observations. All of these data sets reveal the same essential structure, but show important physical and observational differences as well. The intercomparison of composites from different satellite sensors yields additional information. These issues are discussed by McGuirk (1989, 1990) and McGuirk et al. (1989b).

In addition to the compositing of tropical plumes, Hayes's (1988) thesis describes the compositing of convective episodes along the Pacific ITCZ; and, Sautter's (1988) thesis composites synoptic disturbances triggered by East Asian cold surges. Both analyses used OLR data. These composite studies have synthesized convectively quiescent periods, as well as plumes. Compositing essentially applies a smoothing filter by averaging across a number of similar systems, each of which varies somewhat in strength and structural detail. The

composited mappings reproduce only those features that are robust across the data sample of composited events.

Findings (synoptic and other meteorological detail are presented later):

* Compositing of weather systems observed by TOVS allows signals from regions that are normally, but not always, cloud covered to be estimated. The danger, however, is that the uncloudy estimates may be unrepresentative.
* Composites from 6.7 and 7.3 μm channels on VAS (images from a geostationary satellite) and on TOVS (cloud-cleared point estimates from a polar orbiter) exhibit significant differences in regions of deep or high extensive clouds. TOVS generally underestimates the moistness of such regions.
* Compositing reveals unambiguous signatures of tropical plumes in moisture, cloud and temperature fields.
* Compositing on synoptic systems removes possible uncorrected signal bias due to limb darkening.
* The behavior of migratory synoptic systems is sufficiently consistent across the Pacific that compositing yields well-behaved meaningful propagating patterns.
* Resultant patterns are sensitive to the choice of compositing parameter (for example, convectively active ITCZ patterns depend strongly on whether events are selected based on zonal mean convection, point convection, or both; tropical plumes vary somewhat depending on whether they are registered to the tropical convective center or to the

middle latitude triggering trough).

Vapor signal interpretation. It is exceedingly difficult to interpret infrared radiances in the water vapor absorption bands quantitatively. Strictly speaking, the channels in the 6.7 μm band "see" only the top 0.5 cm of precipitable water, or less. The degree to which small amounts of upper tropospheric moisture "contaminates" moisture estimation is described in Blackwell's (1987) thesis. Applications are described by Blackwell et al. (1988), Thompson et al. (1987), McGuirk et al. (1989a) and McGuirk and Blackwell (1990).

Fink's (1989) thesis intercompares precipitable water estimates from TOVS 6.7 and 7.3 μm channels, from OLR radiances, from SMMR microwave algorithms, and from ECMWF analysis. Besides comparisons, he also developed statistical predictive models of SMMR-estimated column precipitable water from the other moisture estimators. These results are reported by Fink and McGuirk (1989) and McGuirk and Fink (1990).

In addition to these direct studies of satellite technology, applications related to vapor imagery interpretation are described by McGuirk and Hayes (1989), Thompson et al. (1988) and by McGuirk and Ulsh (1990).

Findings:

* Upper tropospheric streaks of moisture (amounting to less than 1.0 mm of precipitable water) can "contaminate" the

moisture channels by up to 20 °C in brightness temperature (about 50% of the observed brightness temperature range).

* Under some conditions upper tropospheric moisture sensing can be used to estimate vertical motion, particularly in regions of strong subsidence; a technique for this calculation is verified.
* Synoptic scale regions of exceptionally dry and intense subsidence appear in the north Pacific subtropical high, but not in the east Pacific equatorial dry zone.
* The warmest vapor brightness temperatures always occur in conjunction with tropical plumes.
* Radiosondes are normally not sufficiently accurate (in dry layers) to compute accurate brightness temperatures.
* Correlation between SMMR estimated precipitable water and other estimators is only moderate over the tropical Pacific:

SMMR and TOVS 6.7 μm:	-0.61
SMMR and TOVS 7.3 μm:	-0.48
SMMR and OLR:	-0.56
SMMR and ECMWF analysis (1979):	0.70

* These correlations become much smaller (and may not be statistically reliable) when restricted to specific synoptic features.
* Satellite observations improve operational analysis estimates by about 10% of the total moisture variance.
* The FGGE reanalysis improved variance explained by about 10% over the original analysis; the 10% improvement by

satellite estimates remained unchanged.

* Infrared estimators have the greatest difficulty in dry atmospheres; however, when TOVS indicates dryness, the atmosphere is unambiguously dry.
* Operational analyses are not sufficiently accurate to yield moisture budgets that are correct even in sign over synoptic time and space scales.
* Satellite moisture sensing normally gives accurate horizontal moisture patterns.
* Vapor channels can define developing synoptic patterns, even in the absence of significant cloud.
* In the presence of cloud, cloud cleared radiances can often extract synoptic patterns, but these patterns are normally weaker than those detected in OLR or vapor imagery.
* OLR can detect the evolution and temporal/spatial continuity of synoptic systems in both the tropics and middle latitudes and over long synoptic scales.

b. Radiative Transfer Modelling

A radiative transfer model developed by Susskind at NASA Goddard Laboratory for Atmospheres, appropriate for TOVS radiance bands, has been used successfully in a number of studies. Its primary application has been to convert vertical soundings, either analyzed temperature and moisture profiles or those measured by radiosondes, into equivalent channel brightness temperatures of the TOVS instrument.

Satellite interpretation. The sensitivity of observed brightness temperatures to changes in the vertical structure of atmospheric composition or temperature cannot be determined directly from the satellite observations. Thus, the meaning of varying observed brightness temperature in a single TOVS channel is not always related to the assumed primary relationship; for example, variations in the moisture channels do not relate simply to varying moisture amount. Comparison of satellite observations with calculated estimates based on collocated radiosondes affords a means of interpreting the original satellite observations. Blackwell's (1988) thesis used this technique to estimate moisture channel brightness temperatures from radiosonde profiles for comparison with collocated satellite observations. Results are described by McGuirk and Blackwell (1990) and McGuirk et al. (1989a).

Findings:

* Radiative transfer model computations and subsequent comparison with satellite radiance observations is a powerful technique for evaluation of observations.
* Operational radiosonde procedures which set the default dew point depression to 30°C in dry atmospheres and delete humidity data above 300 mb can each lead to brightness temperature errors of 10°C in estimated moisture channel radiances.
* If radiosonde moisture profiles are accurate, radiative

transfer estimates in the moisture channels are accurate.

* Water vapor radiances can accurately locate the pressure level of the "top of the moisture layer."
* Under certain conditions, radiosondes can measure moisture above 300 mb and dew point depressions greater than 30°C, or even up to 50°C, accurately.

Ground truth for operational analyses. One of the more powerful applications of the radiative transfer model is its use in the evaluation of operational analysis over data sparse regions. In these situations, the tropical Pacific being a good example, the verifying state of the atmosphere simply is not known. Satellite observations provide the best coverage, but they are not directly comparable with the analyses. A radiative transfer model can convert the analyses into equivalent brightness temperatures, so that the analysis can then be compared directly with observations. This approach of "flying a satellite through the analysis" allows the satellite observations to be used as a ground truth for the analysis. Smith's (1989) thesis performed such computations to compare TOVS radiance observations directly with ECMWF operational analyses. Results are presented by McGuirk and Smith (1990) and McGuirk et al. (1989b).

Findings:

* 1979 ECMWF analysis is biased towards "over stability" with upper tropospheric channels too warm and boundary layer and

window channels too cold.

* Estimated analysis brightness temperatures are more variable spatially than are observations over the same space.
* Analysis brightness temperatures in the vapor channels are too warm (dry) and too variable.
* The FGGE reanalysis (based on a 1986 analysis model) reduced, but did not eliminate the over stability bias, barely improved the over sensitivity, and dramatically improved moisture estimation.
* General circulation features are accurately represented in ECMWF analyses.
* The ECMWF analysis is generally unsuccessful in reproducing observed detail within synoptic systems in both the thermal and moisture fields.
* ECMWF analysis does not reproduce accurately temporal changes in strongly and rapidly evolving synoptic systems.
* Patterns of temporal variance are not reproduced accurately by ECMWF analysis.
* Except for moisture patterns, the ECMWF accurately simulates observed atmospheric persistence, in spite of the weak synoptic scale performance.
* The ECMWF analysis does not reproduce observed diurnal variations.

Sounding retrieval. White's (1988) dissertation used the radiative transfer model to generate a large collection of

fictitious tropical soundings with known statistical properties. This data base was used to develop multi-variate statistical procedures to improve the fine structure of sounding retrievals. The procedure involved canonical discriminant analysis to sort the soundings into groups of similar soundings and to invoke various classification procedures to interpret the soundings and assign new soundings to groups. Further multivariate statistical techniques were applied to each group to quantify individual sounding characteristics. Results are described by McGuirk et al. (1989), White and McGuirk (1989, 1987) and by White et al. (1988).

Findings:

* Radiative transfer models can be used to generate large data sets of vertical soundings with known statistical properties: Synoptic scale features (inversions, etc.), vertical correlation, mean temperature, fixed moisture amount, fixed lapse rate, specific feature amplitudes (inversion strengths, etc.), and many more.
* Statistical procedures can sort soundings of satellite brightness temperatures into groups based on their radiation structure; these groups are identical to those obtained by sorting the actual temperature and moisture soundings.
* Further sorting of individual groups can often, but not always, resolve additional vertical fine structure.

c. Synoptic/Planetary Scale Systems

The second major objective, in fact the reason for developing satellite and statistical techniques, is the understanding of atmospheric circulation systems on the synoptic and general circulation scale. Although most of the work at Texas A&M is centered on a synoptic scale phenomenon called a tropical plume, results and conclusions are not focused exclusively on plumes.

Plumes. The structure and behavior of tropical plumes are described in detail by McGuirk et al. (1988) and McGuirk et al. (1989a). Recent studies of tropical plumes include: Ulsh's (1988) thesis which composited 35 tropical plumes viewed in VAS water vapor imagery; Hayes's (1988) thesis which examined plume/ITCZ interactions through OLR; Sautter's (1988) thesis which examined plume/east Asian cold surge interactions, also using OLR; Blackwell's (1987) thesis, which examined moisture distributions in tropical plumes; Schaefer's (1989) dissertation which examined composites of 17 plumes in TOVS multi-channel radiances; and, Askue's (1989) dissertation which included a case study analysis of wind and vorticity fields. Some of these results have been presented in the literature and at conferences described in the final report prior to this research (NAS8-35182, submitted June 1987). In addition, McGuirk and Hayes (1989), Askue and McGuirk (1989b), Thompson et al. (1988), McGuirk (1987),

McGuirk and Thompson (1987) and Thompson et al. (1987) describe various aspects of tropical plumes.

Findings (limited to recent contract period):

* Plumes evolve in a consistent, repeatable pattern in water vapor imagery. This evolution is marked by:
  i. a precursor composed of a moist/dry wave along the ITCZ, a moist middle latitude trough to the northwest, separated by a very dry subtropical high;
  ii. an evolving moist/dry dipole separated by a sharp SW/NE-oriented moisture gradient
  iii. a pattern spanning at least 72 h and drifting slowly ENE.
* The precursor signal normally is not evident in OLR patterns; therefore, it is a vapor signal, not a cloud signal.
* The evolutionary pattern is contrasted with a synoptically quiescent pattern which is nearly zonally symmetric and, on average, more moist.
* As plumes commence evolution, a zonally symmetric moist tropical Pacific must <u>dry out</u> as meridional and zonal eddy patterns evolve.
* Plumes evolve from a middle latitude disturbance and a tropical disturbance; both seem to be required.
* Plumes weaken and dissipate normally when the tropical and middle latitude portions separate.
* The dry subtropical high to the northwest of the plume contains the driest observations (by TOVS) of anywhere in

the Pacific. These observations suggest that less than 1 mm of precipitable water resides above 700 mb.

* Plumes are linked only weakly to general ITCZ convection.
* When a tropical plume develops, other tropical convective systems in the region seem to be suppressed.
* The origin of about half of all plumes can be traced back to East Asian cold surges; this link is through the middle latitudes, not the tropics.
* Upper tropospheric vorticity fields provide evidence that the zonal winds are barotropically unstable, or nearly so, when some tropical plumes develop.
* In at least strong plumes, a low level synoptic wave is generally present with the upper level disturbance.
* Plumes are associated with three wavy features in TOVS observations: A planetary scale, tropospheric deep thermal wave; a 3000 km thermal wave similar to the first baroclinic mode; and a 6000 km wave in the moisture field, which is the plume.

Planetary thermal waves. Schaefer (1988) and McGuirk (1990) examine aspects the interaction of a tropical planetary scale wave in the tropospheric averaged temperature and tropical plumes. In the former, EOF decompositions were used to isolate the wave and to link its position and strength to tropical plumes. In the latter, the wave was identified in operational satellite observations, and in operational NMC analysis and forecasts for a single January 1989 case study.

Findings:

* A 17 event composite and case studies indicate that tropical plumes develop along the temperature gradient of a large scale (at least planetary wave number four) thermal wave; the warm air lies to the west, and the cold air to the east, of the plume.
* This feature propagates slowly eastward and is well resolved by the NMC operational analysis.
* Although this wave resembles a Kelvin wave, it extends well into middle latitudes to link with the trough associated with plume formation.

Synoptic thermal waves. Schaefer (1988) also described significant synoptic scale thermal waves associated with tropical plumes. These waves were also detected by Sautter (1988). A quantitative description of this wave was obtained using a non-linear regression procedure of both individual events and of a seventeen event composite. The composites also linked this wave to tropical plumes and Asian cold surge phenomenon. A number of tests were devised to demonstrate that the wave was not a product of observational practices.

Findings:

* Tropical plumes also evolve in a preferred location with respect to a 3000 km wave.
* This wave, commonly occurring in tropical data sets, is

approximately 3000 km in zonal length, moves eastward at a speed between 4 and 8 ms^{-1}, and is similar to the first tropical baroclinic mode (warm over cold, or cold over warm).

* Tropical plumes develop when the less statically stable portion of this wave crosses the temperature gradient of the planetary scale wave.
* The wave is most detectable at times near 00 GMT and in channels with weighting function peaks at, or above, the tropopause (such as MSU 3 or HIRS 3). It is only weakly resolved in channels at, or lower than, 700 mb.
* The wave amplitude is steady until plume evolution; then it increases slightly before weakening as the plume dissipates.
* Since the wave length is approximately equal to the swath width of individual TOVS passages, care must be taken to remove observational aliasing.
* The origin and type of wave is still unresolved.

East Asian cold surges. Sautter's (1988) thesis used OLR to examine synoptic scale disturbances that are triggered by East Asian cold surges. These surges are massive infusions of cold air which move out over the East China Sea sporadically during winter. Although they themselves are normal synoptic frontal passages, the resulting monsoonal convection interacts with much of the general circulation. McGuirk (1987) also presented some of these results. The approach involved selecting

a large number of cold surges based on published objective definition, and then examining composited behavior and individual cases studies.

Findings:

* One or two significant events exist each cool season month.
* Cold surges trigger middle latitude cyclones (many of them "bombs") which propagate into the central Pacific, lasting an average of 5 d, before dissipating in the mid Pacific ridge.
* OLR composites centered on the cyclones delineate a strong tropical plume signal, about 2000 km to their southeast and along the ITCZ. A 3000 km wave is observed weakly as well.
* No significant propagation of tropical convection is detected, contrary to theories presented by Webster (Penn. St.).

ITCZ disturbances. Hayes's (1988) thesis and McGuirk and Hayes (1989) describe fluctuations in Pacific ITCZ convection, as observed in temporally and spatially filtered OLR. The data base spanned 8 six-month cool seasons. Periods of anomalous convection in small regions of the Pacific and for periods averaged across the Pacific were both examined and intercompared. Statistical properties of these convective episodes were calculated.

Findings:

* Three common types of convective activity were identified:
  i. Small spatial and temporal scales (less than 3000 km and 10-20 d) and restricted to the eastern Pacific.
  ii. Larger spatial scales (5000-10000 km) but short time scales and no regional restriction.
  iii. Medium spatial scales (2000-6000), long time scales, and quasi-stationary.
* Episodes of zonal average convective activity, lasting 3-4 weeks, occurred a few times each season, with the ITCZ moving southward as it intensified.
* The location of active convection is bimodal, with frequency peaks just north of the equator and at about 13°N.
* Convection is not bimodally distributed during El Nino.
* Active convection at points along the ITCZ was only weakly related to zonally averaged active convection.
* Point convection is meridionally oriented.
* Episodes of both active convection at a point and zonal averaged active convection are marked with a distinctive zonal wave pattern and symmetric orientation about the equator. These episodes resemble tropical plumes in the Northern Hemisphere.

Intense localized subsidence. Blackwell's (1987) thesis documented intense localized subsidence occurring on synoptic temporal and spatial scales in association with tropical plume development. The phenomenon was described by Thompson et al.

(1987) and Blackwell et al. (1988), as well. This feature, observed in TOVS moisture channels, is considered as evidence of a crucial forcing mechanism of tropical plumes and forms the basis for a body of new work to be performed under new NASA contract.

Findings:

* Extremely warm pockets of TOVS moisture channel brightness temperatures develop before and during tropical plume formation.
* These warm brightness temperatures are not observed anywhere else over the Pacific (not even in the east Pacific equatorial dry zone) and must owe their existence to anomalous intense subsidence.
* The frequency distribution of TOVS 6.7 μm brightness temperatures is bimodal, with a broad peak of "normal observations" comprising about 90% of the observations and a second, warm peak, well separated from "normal observations.

d. Dynamical Mechanisms

Although most of the dynamical research was "descoped" and removed from the research tasks of this contract due to budget reduction, some work was initiated. A highly idealized shallow water model, constructed by Askue (1989), was developed to examine tropical wave-wave interaction. The jointly

funded effort (NASA, NMC and UCAR) by McGuirk (no publications to date) examined the evolution of tropical plumes in the NMC operational medium range forecast model (MRF). These results are an extension of results from satellite analysis which identified waves relevant to tropical plume evolution. The most important satellite studies are those of Schaefer (1988) and McGuirk and Ulsh (1990).

Observational evidence. The three waves described by Schaefer (1988) and the evolution of plumes in water vapor imagery described by McGuirk and Ulsh (1990) above suggest that plumes develop from a common dynamical mechanism. Additional work by Blackwell (1987) suggest the importance of localized subsidence, perhaps triggered from surges in the Walker circulation. These observations imply that the triggering mechanism for plumes must be one occurring commonly over the tropical Pacific. On the other hand, Sautter (1988) showed that many middle latitude troughs cross the Pacific without ever becoming involved with tropical plumes. The observations thus suggest a simple common mechanism but one which may not be operative during all conditions of the tropical general circulation.

Findings:

* The structure of the atmosphere in the vicinity of plumes suggests that baroclinic instability is not a relevant mechanism, at least when plumes first evolve. This conclu-

sion seems to be the case in spite of the small scale wave of the first baroclinic mode and the apparent strong surge of the Walker circulation.

* The interaction of waves of three different scales suggests a barotropic interaction of waves, either two waves against a complicated basic state, or a triad interaction.
* These waves are almost certainly equatorial normal modes because of the frequency of tropical plume formation.
* Because plumes are not common occurrences during summer or during strong El Nino, plume formation must be sensitive to the form of the basic state circulation.

Normal mode behavior. Askue's (1989) dissertation describes a first attempt to simulate tropical normal mode interaction in an effort to simulate tropical plume circulation features. Results are described by Askue and McGuirk (1989 a,b). All three papers describe integrations of an equatorial, beta plane, shallow water model under constant zonal flow basic state. Experiments were run with two interacting waves, with triads, and small scale perturbations on one or two wave flows. Gravity modes, Kelvin modes, Yanai waves and equatorial Rossby waves were examined.

Findings:

* In most cases, Kelvin wave self interaction eventually leads to wave breaking. As the Kelvin waves initially become unstable, flow around the convergence axis resembles

that of tropical plumes.

* As smaller scale waves propagate toward and through the Kelvin wave convergence axis, non-linear processes distort the waves into configurations that often resemble plume circulations. These experiments support P. Webster's energy accumulation hypothesis; that is, transient energy accumulates regions of specific zonal gradients of the zonal wind and that these regions also exchange wave energy between tropics and middle latitudes.
* Perturbations moving downstream of the divergence axis of Kelvin waves surprisingly resemble tropical plume circulations.
* The most successful triad interaction involves three planetary equatorial Rossby waves. These waves probably would not interact commonly over the tropical Pacific.

e. Prediction Implications

Vapor imagery. Ulsh's (1988) thesis developed a qualitative forecast scheme for tropical plumes based on water vapor imagery. Readily identifiable features appear on images 36 to 48 h before a tropical plume develops. A forecast experiment was run over a period of four months of water vapor imagery, in which these "precursor" features were used to predict plume evolution. Twenty nine plumes developed over the experimental period. Experimental results are described by McGuirk and Ulsh (1990), McGuirk (1989a) and Thompson et al. (1988).

Findings:

* The appearance of an exceedingly dry subtropical high, two moist maxima along the ITCZ, and a cold and moist middle latitude trough to the north are sufficient to anticipate plume development.
* 61% of tropical plumes were forecast correctly, by time and location of evolution, during the four month forecast experiment.
* Forecast errors were systematic, with overforecasts made in regions where tropical plumes normally do not develop, and errors made in complex forecasting situations.
* Most tropical plumes can be anticipated in water vapor imagery well before any detectable signature appears in cloud imagery.

Initial condition improvement. McGuirk, in yet to be published work, designed forecast experiments which attempted to insert more satellite information into initializations of NMC's global MRF model. The experiments were based on a pair of tropical plumes which developed in January 1989. Signals, based on the three wave patterns described by Schaefer (1988), were extracted from the TOVS satellite radiances routinely archived on NMC's operational history tapes. These signals were converted into model compatible perturbations to the model initialization, and a series of 48 h forecasts were made. Preliminary results were prepared by McGuirk (1990).

Findings:

* Signals of the 3000 km and planetary scale thermal waves, and the 5000 km wave in the moisture field could be extracted from operational satellite observations.
* Patterns of forecast perturbations resulting from the perturbed initialization matched closely the patterns of the 48 h operational forecast error, although the magnitudes were too weak.
* A weak tropical disturbance, to the west of the modelled tropical plume, was forecast to develop into a tropical plume correctly, an event not forecast operationally.
* Intense convection was forecast to develop within the "source" regions of both tropical plumes.
* Forecast improvements were obtained for both initialized and uninitialized perturbations.
* Forecast improvements required adjustments of the moisture fields.

3. PUBLICATIONS

a. Refereed Publications

McGuirk, J. P., and K. G. Blackwell, 1990: Contamination and interpretation of quantitative satellite water vapor observations. Being edited for *J. Appl. Met.*

_____, and J. D. Fink, 1990: Tropical moisture estimation from satellite and model analysis. Being edited for *J. Appl. Met.*

_____, and D. J. Ulsh, 1990: Evolution of tropical plumes in VAS water vapor imagery. *Mon. Wea. Rev.,118* (September).

_____, A. H. Thompson and L. L. Anderson, 1989: Synoptic scale moisture variation over the tropical Pacific Ocean. *Mon. Wea. Rev., 117*, 1076-1091.

_____, _____ and J. R. Schaefer, 1988: An eastern Pacific tropical plume. *Mon. Wea. Rev., 116*, 2505-2521.

b. Conference Proceedings

McGuirk, J. P., and D. E. W. Smith, 1990: TOVS channel radiances as a "ground truth" for ECMWF analysis, AMS 5th Conf. on Satellite Meteorology and Oceanography, London, September 1990.

_____, 1990: Use of satellite-derived spatial patterns in synoptic-scale numerical forecasts, *op. cit.*

_____, J. R. Schaefer, D. E. W. Smith and G. A. White, 1989: Effects of satellite observational characteristics on EOF structure, AMS 11th Conf. on Probability and Statistics in the Atmospheric Sciences, Monterrey, CA, October 1989.

_____, and P. M. Hayes, 1989: Active modes of the Pacific ITCZ, AMS 18th Conf. on Hurricanes and Tropical Meteorology, San Diego, May 1989.

Askue, C. A., and J. P. McGuirk, 1989: Dynamical characteristics of tropical plumes, *op. cit.*

McGuirk, J. P., 1989: Tropical synoptic composites in VAS, OLR and TOVS radiance data, AMS 4th Conf. on Satellite Meteorology and Oceanography, San Diego, May 1989.

Fink, J. D., and J. P. McGuirk, 1989: Tropical synoptic scale moisture fields observed form the Nimbus-7 SMMR, *op. cit.*

White III, G. A., and J. P. McGuirk, 1989: Unique signatures of synoptic features in TIROS N radiance data, *op. cit.*

Askue, C. A., and J. P. McGuirk, 1989: Barotropic mechanisms associated with tropical plume formation, AMS 7th Conf. on Atmospheric Waves and Stability, San Francisco, March 1989.

McGuirk, J.P., 1988: Horizontal and vertical pattern recognition in satellite radiance data, Cooperative Institute for Research of the Atmosphere, Colorado State University, Ft. Collins CO, September 1988.

Thompson, A. H., J. P. McGuirk and D. J. Ulsh, 1988: Tropical synoptic signatures in composited 6.7 micrometer water vapor imagery, AMS 3rd Conf. on Satellite Meteorology and oceanography, Anaheim, CA, February 1988.

Blackwell, K. G., J. P. McGuirk and A. H. Thompson, 1988: Temporal and spatial variability and contamination in 6.7 and 7.3 micrometer water vapor radiance data, *op. cit.*

White III, G. A., J. P. McGuirk and A. H. Thompson, 1988: Identification and recovery of discontinuous synoptic features in satellite-retrieved soundings using a radiative transfer model, *op. cit.*

_____, and _____, 1987: Canonical discriminant analysis of synoptic signatures in satellite channel brightness temperature data, AMS 10th Conf. on Probability and Statistics in Atmospheric Science, Edmonton, Canada, October 1987.

McGuirk, J. P., 1987: Climatology of various synoptic systems over the tropical North Pacific, NOAA 12th Climate Diagnostics Workshop, Salt Lake City, October 1987.

_____, and A. H. Thompson, 1987: Tropical synoptic scale momentum budgets during FGGE SOP 1, 19th IUGG General Assembly, Vancouver, Canada, August 1987.

Thompson, A. H., J. P. McGuirk and K. G. Blackwell, 1987: Synoptic scale moisture transports using ECMWF analysis and satellite data, *op. cit.*

c. Doctoral Dissertations

Askue, C. A., 1989: Barotropic mechanisms associated with tropical plume formation, 188pp.

Schaefer, J. R., 1988: Synoptic scale tropical waves in multi-channel satellite radiance data, 117pp.

White, G.A., 1988: Identification and quantification of synoptic structure in simulated TIROS N radiance soundings, 149pp.

d. Master's Theses

Smith, D. E. W., 1989: A comparison of model-generated and satellite-observed radiances, 150 pp.

Fink, J. D., 1989: Tropical synoptic scale moisture fields observed from the Nimbus-7 SMMR, 74pp.

Sautter, D. C., 1988: Synoptic-scale East Asian cold surge-induced phenomena, 115pp.

Hayes, P. M., 1988: Active modes of the Pacific ITCZ, 102pp.

Ulsh, J. D., 1988: Moisture burst structure in satellite water vapor imagery, 112pp.

Blackwell, K. G., 1987: Synoptic scale sensitivity of TIROS-N moisture channels in the tropics, 137pp.

Appendix A

Abstracts of refereed publications, theses and dissertations.

Synoptic Scale Sensitivity of TIROS-N Moisture Channels in the Tropics

James P. McGuirk and Keith G. Blackwell

Texas A&M University

College Station, Texas

Submitted to J. Appl. Met.

ABSTRACT

Water vapor radiance data obtained from a satellite-borne radiometer were evaluated for synoptic information content and accuracy over the tropical eastern Pacific Ocean.

An upper moist layer was defined in terms of precipitable water by integrating the sounding data downward from 300 mb. The varying pressure of this upper moist layer was correlated with collocated 6.7 and 7.3 mm water vapor (WV) brightness temperatures (BT)s.

Although high correlations were obtained between satellite BTs and upper moist layer pressures, minute quantities of upper tropospheric moisture above 300 mb produced large changes in BTs. The inability of conventional rawinsondes to measure moisture in the cold, tropical upper troposphere often leads to discrepancies between rawinsonde-derived and satellite-inferred moisture profiles. Using a radiative transfer model, these discrepancies were quantified and shown to result in an unsatisfactory compatibility between the two methods.

A persistent cluster of warm (dry) BTs was observed over the subtropical Pacific adjacent to the western flank of a series of tropical plumes. Collocated rawinsonde soundings and satellite BTs consistently showed excellent agreement within this region, indicating extreme dryness in the middle and upper troposphere. The anomalous lack of upper tropospheric moisture, the tight clustering of abnormally large BTs, and the close proximity to a large area of active convection suggests these elevated BTs occur only as an occasional synoptically induced feature.

Synoptic Scale Estimators of Precipitable Water in the Tropics

James P. McGuirk and Jeffrey D. Fink

Texas A&M University

College Station, Texas

Submitted to J. Appl. Met.

ABSTRACT

Nimbus-7 SMMR brightness temperatures from 7 d in January 1979 and 3 d in May 1979 are used to estimate precipitable water and precipitation over the tropical eastern Pacific Ocean. These estimates are made from algorithms are developed by Wilheit and Chang (1980) for precipitable water and given by Lipes (1981) for precipitation. The SMMR estimates are compared with moisture estimates from TIROS-N infrared moisture channels, TIROS-N outgoing longwave radiation, 1979 ECMWF model analysis and an ECMWF reanalysis using a 1986 analysis model. Comparisons are made within the context of 5 typical tropical synoptic scale features: Tropical plumes, the subtropical high; the convectively active ITCZ; the convectively inactive ITCZ; and the equatorial dry zone.

SMMR precipitable water estimates provide detailed information on the horizontal moisture structure in all areas of the tropics except in areas of heavy precipitation. Most of the information present in the TIROS-N and ECMWF data identify synoptic features, but not variations within the features. The 1986 reanalysis has a more accurate moisture distribution, at least compared with SMMR observations; the reanalysis, however, is biased such that wet areas are analyzed as too dry, and dry areas are too wet. SMMR observations identified plume precipitable water content as statistically identical to a quiescent ITCZ, and plume precipitation as statistically identical to an active ITCZ.

Prediction of SMMR precipitable water using TIROS-N and the ECMWF reanalysis explained 72% of the variance in SMMR observations, while the ECMWF reanalysis alone explained 65% of the variance. Contribution by satellite signals was not affected by the reanalysis.

Reprinted from Monthly Weather Review, Vol. 119, No. 9, September 1990

Evolution of Tropical Plumes in VAS Water Vapor Imagery

JAMES P. MCGUIRK AND DAVID J. ULSH

Texas A&M University, College Station, Texas

(Manuscript received 13 April 1989, in final form 21 February 1990)

ABSTRACT

Tropical plumes are common tropical synoptic disturbances marked by continuous upper tropospheric cloud bands extending out of the ITCZ into midlatitudes. Thirty-five tropical plumes over the northeast Pacific are composited in GOES VAS water vapor imagery at four time periods throughout their evolution, from a precursor stage 48 h before they fulfill an objective plume definition until they mature 24 h after this definition stage. A "quiescent" composite is constructed for 35 days in which no synoptic activity is occurring. Composites of outgoing longware radiation data are constructed using the same days, for comparison.

Precursor signals are identified in the vapor imagery before clouds develop: a moist midlatitude trough, a synoptic scale wave in the moisture/cloud field along the ITCZ, and an anomalously dry intervening subtropical high, all appearing in an anomalously dry tropical environment. This pattern is contrasted with the synoptically quiescent composite, a nearly zonally symmetric pattern in vapor imagery, with a convectively active ITCZ, flanked by a linearly shaped subtropical high; the quiescent tropics are generally moist. The plume evolves as a stationary, tropical, dry/moist dipole, separated by an exceptionally strong cloud/moisture gradient. All features within individual composites and most variations from stage to stage are statistically robust. Tropical plume evolution is accompanied by a systematic drying of the tropical eastern Pacific atmosphere before development, and moistening and increased cloudiness with development. The precursor pattern is used as a forecasting tool applied to an independent set of vapor imagery; 65% of 29 plumes were forecast correctly by position and time of evolution. Forecasting errors were systematic.

Reprinted from MONTHLY WEATHER REVIEW, Vol. 117, No. 5, May 1989
American Meteorological Society

Synoptic Scale Moisture Variation over the Tropical Pacific Ocean

JAMES P. MCGUIRK, AYLMER H. THOMPSON AND LLOYD L. ANDERSON, JR.

Texas A & M University, College Station, Texas

(Manuscript received 20 August 1987, in final form 21 October 1988)

ABSTRACT

Moisture observing capability is surveyed over the tropical northeast Pacific Ocean. Data are taken from late January 1979 during FGGE. Emphasis is on diagnosis of synoptic scale systems in data sparse areas. The capabilities and limitations of five observing systems are examined: surface observations, satellite cloud imagery, radio- and dropsondes, satellite individual channel brightness temperatures, and model analysis from the European Center for Medium Range Weather Forecasts. Both qualitative and quantitative intercomparisons are made.

Surface observations carry almost insignificant moisture information over the tropical oceans. The capability of GOES imagery is well known; however, clouds mask important moisture structure and do not always define moisture patterns well, even at cloud level. Soundings were adequate for synoptic diagnosis, *if* there were enough of them; however, FGGE dropsondes were limited in detail. Satellite channel data provide thorough coverage and show some detail even in nearly overcast regions; ambiguity of interpretation remains a problem. Given the lack of moisture observations for initialization, the ECMWF analysis provides surprisingly realistic moisture patterns.

Quantitative intercomparison of data is generally discouraging. Field comparisons of model analysis and satellite observations are poor, with only marginal statistical significance. Both systems, however, clearly define the synoptically active regions in their variability statistics; they both perform better in moist regions, where quantitative estimates of moisture are most important. Comparisons with radiosondes are poor as well. Correspondence of analysis, satellite and radiosondes is good in moist regions, but all three have serious observational problems when radiosonde-observed relative humidity falls below 50%.

Each of the five systems describes detail not contained in the other systems. Most importantly, quantitative satellite moisture channel data can be used synoptically, and model analysis provides useful synoptic moisture information, even without initial moisture observations.

Reprinted from MONTHLY WEATHER REVIEW, Vol. 116, No. 12, December 1988
American Meteorological Society

An Eastern Pacific Tropical Plume

JAMES P. MCGUIRK, AYLMER H. THOMPSON AND JAMES R. SCHAEFER

Texas A&M University, College Station, Texas

(Manuscript received 26 June 1987, in final form 9 June 1988)

ABSTRACT

Synoptic-scale cloud systems, called tropical plumes, develop from disturbances in the eastern Pacific ITCZ and in conjunction with amplifying troughs to the north; a common spatial pattern and temporal evolution accompany most events. A blend of disparate data and analyses yields a three-dimensional description of a case study during the FGGE January 1979 special observing period. That this tropical plume is typical is corroborated with a climatology of 41 systems and a less detailed climatology encompassing over 200 plumes.

Tropical plumes are accompanied by intense drying and subsidence within the trough to the northwest and a strong subtropical jet within the plume. Wind observations for the case study show that the jet originates near the equator. A disturbance in the low-level easterly trades exists independently from the upper trough when the plume initiates; such anticyclonic curving wind patterns are common at initiation. The plume developed simultaneously out of several disturbances along its axis. A frontal pattern of intensifying moisture gradient, developing thermal gradient and inversion, strengthening jet level winds, solenoidal overturning, and deepening of the tradewind inversion appears along the northwest flank and downstream of the plume. Plumes cease normally when their tropical and nontropical aspects become separated.

ABSTRACT

Barotropic Mechanisms Associated with

Tropical Plume Formation. (December 1989)

Cecilia Ann Askue, B.S., Mississippi State University;

M.S., University of Southern California; M.S. Colorado State University

Chair of Advisory Committee: Dr. James P. McGuirk

The tropical plume is an upper level phenomenon with greatest frequency of occurrence over the northeast Pacific. Primarily wintertime events, plumes transport energy poleward and may be transient systems comprising a Hadley circulation. Previous studies of tropical plumes have focused on plume development and on describing plume structure and statistical properties. This study investigates possible mechanisms involved in plume initiation.

From a case study, barotropic mechanisms are hypothesized to be important in initiating tropical plumes. These mechanisms are investigated by means of a one-layer, barotropic, gridpoint model using the shallow water equations on an equatorial β-plane. Particular attention is given to wave-wave interaction occurring between equatorially trapped normal modes and between these modes and perturbations from higher latitudes. The numerical results indicate that interaction among equatorially trapped Rossby modes shows promise as being a key element in plume initiation. The effects are particularly apparent when the Rossby wave state is perturbed by a disturbance resembling an upper level cyclonic circulation, such as frequently occurs when a midlatitude trough intrudes into the tropics. The effects of a Kelvin-wave-like

basic state are limited: active responses to the disturbance are observed only in the westerly regime of the Kelvin wave, but the disturbance does not interact strongly with the Kelvin wave itself.

ABSTRACT

Synoptic Scale Tropical Waves in Multichannel Satellite Radiance Data.

(December 1988)

James Royal Schaefer, B.S., University of Wisconsin at Eau Claire;

B.S., University of Utah;

M.S., Texas A&M University

Chair of Advisory Committee: Dr. James P. McGuirk

Diagnosis of tropical weather systems on the synoptic scale is limited severely by a near total absence of conventional *in situ* observations, particularly over the North Pacific. Analysis procedures are developed to minimize the limitations of satellite sounding data: compositing of numerous events to increase the data coverage and thereby fill in gaps due to cloud contamination and smooth the contamination associated with individual satellite passes; Empirical Orthogonal Function (EOF) decomposition to account for the high vertical correlation within observations; averaging and filtering to isolate and identify weak and poorly observed signals; and, non-linear regression to quantify previously detected synoptic signals.

Three months (January-March 1984) of multichannel radiance data from sounders on NOAA-7 and 8 are analyzed to extract the synoptic scale information content. Two synoptic systems are isolated and investigated: tropical plumes; and, a 2800 km tropospheric thermal wave believed to be a newly observed feature of the tropical atmosphere.

Seventeen tropical plumes are composited at 12 h time increments from 48 h before until 96 h after plume initiation. The composite model shows that previous plume case studies are typical of the composite model. Deleting the climatological mean from the composite proved that the pre-initiation signal is primarily a result of climatology and large scale semi-stationary waves. The EOF decompositions demonstrated that the synoptic signals found in individual case studies are consistent with the composite. These decompositions also display the existence of a tropospheric thermal wave aligned closely with the tropical plume.

The tropospheric thermal wave is a vertical mode three zonal wave; its extrema are located approximately at 300, 700 and 900 mb and it moves eastward at about 4.5 to 6.5 m s^{-1}. It possesses no detectable moisture structure. Its detection was facilitated by removal of the dominant stationary variance pattern and by the wave's consistent alignment with respect to tropical plumes. This latter feature implies that the wave is a causal factor in plume development. The wave aligns itself such that the weakest static stability is within the region of active plume development near initiation time. Diurnal variations of location, amplitude, and lateral structure are not completely explainable in terms of satellite radiance observations. Non-linear regression of both the composite and individual cases demonstrates robustness of both pattern and quantitative details of the tropical thermal wave.

ABSTRACT

Identification and Quantification of Synoptic Structure in Simulated TIROS N Radiance Soundings. (December 1988)

G. Anderson White, III, B.S., University of North Carolina at Chapel Hill;
M.S., Texas A&M University

Chair of Advisory Committee: Dr. James P. McGuirk

There has been continual improvement in the accuracy of retrieved atmospheric soundings from satellite radiance measurements; however, satellite data still provide an overly smooth product which is of limited use for synoptic scale analysis. Considerable smoothing occurs when information present in satellite radiance measurements is lost in the retrieval process. This research describes and develops techniques which (1) identify synoptic features and (2) quantify their fine structures directly from TIROS N satellite radiance data.

A series of nine, overlapping, synthetic temperature and moisture soundings is constructed which contains synoptic features representative of the tropical eastern Pacific Ocean. Each of the soundings in the series is perturbed randomly, within limits, to create a statistically meaningful training data set. The training data set is processed through a radiative transfer algorithm to generate equivalent TIROS N satellite observations.

The variance of the training set is partitioned into a portion accounting for synoptic class and a portion describing synoptic feature variation within a class. The variance structure of feature quantification differs strongly from that associated with classification.

In a two-step process, the training data observations first are separated according to synoptic feature, and, second, the fine structure of the synoptic feature is quantified. Three classification techniques are developed to partition the training data observations into synoptic groups and to classify new soundings: a subjective, graphical, interpretative procedure; canonical discriminant analysis; and, discriminant analysis. Accurate classification was accomplished until atmospheric sounding perturbations exceeded 12% of the observed temperatures of the synoptic class means.

Two experiments of feature quantification are described: a prediction of trade wind and frontal inversion height and strength using both synthetic and observed soundings; and, a prediction of frontal structure based on discriminant analysis of a training data set containing frontal inversion soundings. Positive skill, with some ambiguity, was demonstrated in both experiments.

ABSTRACT

A Comparison of Model-Generated and Satellite-Observed Radiances.

(May 1989)

Donna Ellen Woolley Smith, B.S., Texas A&M University

Chair of Advisory Committee: Dr. James P. McGuirk

The ECMWF operational IIIb analysis is verified against satellite observed radiances by converting the analyzed variables into synthetic radiances using a radiative transfer model. Observed satellite radiances are used as a ground truth because, over the data sparse tropical Pacific Ocean, these observed satellite radiances are the only observations that have synoptic scale resolution. It is assumed that if the analysis simulates atmospheric conditions correctly, the observed and modelled radiances will have comparable statistical structures.

Tropical mean soundings are simulated well: Only tropopause level and window channels exhibit biases in excess of one standard deviation (usually less than 3°C in absolute brightness temperature error). Simulated channel variability is slightly too large (less than 0.4 standard deviations) in most channels. The reanalysis reduced biases to less than 2°C, except in three window channels. Simulated biases were systematic, resulting in an estimated static stability that is too great; the reanalysis decreased this lapse rate bias.

Simulated temporal trends of area averaged means and variability (both signals of synoptic activity) are qualitatively correct, except they are weaker than observed trends and the area average persistence is too large. The

reanalysis improvement was restricted to the moisture channels. Even the reanalysis did not simulate the diurnal cycle.

Both the IIIb analysis and the reanalysis reproduced general patterns of synoptic variability but details and amplitudes are not simulated correctly. The IIIb analysis and the reanalysis reproduce the vertical structure of the observations. Reproduction of horizontal patterns is not as successful in the IIIb analysis, although the reanalysis improved the moisture fields. The inclusion of satellite humidity observations in the reanalysis resulted in improved simulation of observed moisture patterns. The reanalysis improved quality of simulation over the entire tropical domain and in regional patterns, such as the Subtropical High, the Intertropical Convergence Zone and the Pacific Dry Zone. Both the IIIb analysis and the reanalysis simulated conditions better in the Subtropical High. The models simulated the Pacific Dry Zone poorly.

ABSTRACT

Tropical Synoptic Scale Moisture Fields Observed

from the NIMBUS-7 SMMR. (May 1989)

Jeffrey David Fink, B.S., Texas A&M University

Chair of Advisory Committee: Dr. James P. McGuirk

Nimbus-7 SMMR brightness temperatures from 7 days in January 1979 and 3 days in May 1979 are used to estimate precipitable water and precipitation over the tropical eastern Pacific Ocean. These estimates are made from algorithms developed by Wilheit and Chang (1980) for precipitable water and by Katsaros and Lewis (1986) and Lipes (1981) for precipitation. The SMMR estimates are compared with moisture estimates from TIROS-N infrared moisture channels, TIROS-N outgoing longwave radiation, and the ECMWF model analysis. Comparisons are made within the context of five typical tropical synoptic scale features: Tropical plumes (TP) synoptic scale disturbances viewed in the cloud field, linking the tropics and midlatitudes; the Subtropical High (STH), the dry region extending along the northwest flank of a TP; the active Intertropical Convergence Zone (AITCZ), banded equatorial convection over the eastern Pacific Ocean; the quiescent Intertropical Convergence Zone (QITCZ), areas with no convective cloud tops present along the ITCZ; and the Equatorial Dry Zone (EDZ), an area along and south of the equator between 100°W and 120°W.

SMMR precipitable water estimates provide detailed information on the moisture structure in all areas of the tropics except in areas of heavy precipitation.

Most of the information present in the TIROS-N and ECMWF data identifies the synoptic feature and not variations within a feature. SMMR data identified TP precipitable water content as statistically identical to a QITCZ and the precipitation as statistically identical to AITCZ precipitation. Prediction of SMMR precipitable water using TIROS-N and ECMWF data explained 67% of the variance in SMMR data while ECMWF analysis alone explained 55% of the variance.

ABSTRACT

Synoptic-Scale East Asian Cold Surge-Induced Phenomena.

(August 1988)

David Carl Sautter, B.A., Grove City College

Co-Chairmen of Advisory Committee: Dr. James P. McGuirk
Dr. Aylmer H. Thompson

The East Asian cold surge (EACS) and its midlatitude and tropical responses were studied for several winters from 1979 to 1985. A climatology of surges was constructed based on an objective definition using surface and upper-air data. Each EACS initiated a midlatitude cyclone; these cyclones were tracked across the Pacific in outgoing longwave radiation (OLR) data and height and sea-level pressure analyses. The upper-level portion of the cyclone survived longer and propagated further eastward than the lower-level portion. Less than half of the associated troughs at 300 mb and less than one-third at 500 mb reached 120°W. The surface low usually dissipated at or west of the dateline. This low met criteria for "explosive cyclogenesis" in over one-third of all EACS events.

The OLR signature of each cyclone was identified and composited at 24-hour intervals; the composited cloud mass decelerated and then dissipated between 180° and 160°W. Only 2 of 26 tracked cloud masses survived all the way across the Pacific to regenerate near 120°W. Composite height fields in the vicinity of the cyclones indicated that changes in the longwave pattern over the Pacific accompanied the

shortwave midlatitude response. The east Pacific ridge amplified and a longwave trough deepened near the dateline as the shortwave dissipated. The weakening and disappearance of the cyclones is consistent with simple baroclinic wave theory.

The tropical response induced by the EACS was investigated using OLR anomaly data. Enhanced convection was noted south of the surge immediately after surge initiation. There was little evidence of eastward propagation of the tropical convection, even though recent research has mentioned the possibility of eastward propagation to the dateline. Therefore no tropical link was established between EACS and mid-Pacific tropical moisture bursts. A midlatitude link, however, was established between the EACS-induced cyclones and moisture bursts for at least 40% of all moisture bursts.

ABSTRACT

Active Modes of the Pacific ITCZ. (May 1988)

Patrick Michael Hayes, B.S., University of Wisconsin-Green Bay

Co-Chairmen of Advisory Committee: Dr. James P. McGuirk
Dr. Aylmer H.Thompson

Satellite-observed outgoing longwave radiation (OLR) data from eight six-month cool seasons were examined to find periods of active convection within the Pacific intertropical convergence zone (ITCZ). Descriptive statistics were used to define and describe the time-mean behavior of the Pacific ITCZ. Two seasons (76–77 and 82–83) showed distinctive El Nino-Southern Oscillation (ENSO) signatures in mean, standard deviation, and frequency distribution of OLR. Four other seasons (74–75, 75–76, 79–80, and 80–81) had "normal" OLR statistics. The remaining seasons preceded and followed the major 82–83 event and had intermediate seasonal-mean OLR fields.

Time series of an index measuring convective intensity in the ITCZ were analyzed to find active convection periods. Time-longitude diagrams of the intensity estimates showed how active modes develop, spread, and propagate across the Pacific. Three types of variability of the active modes were identified. The first type had small spatial scales (< 4000 km), short temporal scales (10–20 day durations), and occurred mostly in the eastern Pacific. The second type had longer spatial scales (5000–10,000 km), short temporal scales, and was found throughout the domain. The second type of variability also showed evidence of propagation. The third type had large temporal scales (greater than 30 days), medium spatial scales (2000–6000 km), and was a fixed feature. The third type of variability may be a result of combinations of two or more active periods of the first two types.

The eastern Pacific active modes (near 160°W) occurred approximately 10 times during each (non–ENSO) season, for an average period of 18 days. Active modes based on zonally–averaged intensities occurred less frequently, with a temporal scale between 22 and 28 days. Active convection in the eastern Pacific was not strongly related to active modes in the rest of the domain; strong east and west Pacific convection occurred simultaneously only four times during the normal seasons, for an average period between 30 and 60 days.

The intensity index was modified to estimate the latitudinal and longitudinal positions of active convection along the ITCZ. Time series of the zonal–average position and intensity showed that the ITCZ moved south as it intensifies.

Convective organization was described using composites of daily OLR from active days. Composites based on different active convection regions yielded different patterns: the zonally–averaged active days produced three zonally oriented cells of intense convection in the ITCZ region; requiring active convection at 160°W and in the zonal mean produced only two cells; this pattern also extended southeastward into the Southern Hemisphere.

ABSTRACT

Moisture Burst Structure in Satellite Water Vapor Imagery.

(May 1988)

David Joel Ulsh, B.S., Montana State University

Co-Chairmen of Advisory Committee: Dr. James P. McGuirk
Dr. Aylmer H. Thompson

The moisture burst is a tropical synoptic-scale weather event that typically originates along the ITCZ and has been defined previously in window-channel infrared imagery. This research uses 6.7-micrometer water vapor absorption band imagery to composite 35 moisture burst events during the North Pacific cool season of 1983-1984. Composite maps are constructed at four times, each 24 h apart, during the life cycle of the moisture burst. A comparative baseline is provided by an additional composite of 35 dates, constructed for times when moisture bursts were not active in the eastern North Pacific.

The evolution of the water vapor structure of a moisture burst is examined through the composites and a model is synthesized. The key features of the composited model are: 1) A 4000-km wave along the ITCZ at about 7°N, with moist regions to the east and west, separated by a drier area; 2) A 1500 km long dry area to the northwest of this wave, oriented along a SW-NE axis; and 3) A moist maximum northwest of the dry zone at about 30°N. These last two features appear at least 24 h before cloud development. During evolution the ITCZ wave

amplifies, and the dry axis and western ITCZ maximum intensify and extend northeastwards as the moisture burst, and the moist maximum to the northwest disappears. In contrast, the composite for inactive periods describes four zonally-oriented belts of alternating moist and dry regions.

The statistical composites and the resulting model are tested for robustness by: 1) Subjective comparison of the means against individual events from the dependent sample of moisture bursts, and an independent sample as well; 2) Comparison of anomalies against the inactive composite, using a paired t-test; and 3) Application of the model as a forecasting tool on an independent sample. In the forecast test the model correctly predicted 19 of 29 moisture bursts at least 24 h before cloud development. Forecast errors were found to be systematic.

ABSTRACT

Synoptic Scale Sensitivity of TIROS-N Moisture Channels in the Tropics. (December 1987)

Keith Gordon Blackwell, B.S., University of Wisconsin-Madison

Co-Chairmen of Advisory Committee: Dr. James P. McGuirk
Dr. Aylmer H. Thompson

Water vapor radiance data obtained from a satellite-borne radiometer were evaluated for synoptic information content and accuracy over the tropical eastern Pacific Ocean.

An upper moist layer was defined in terms of precipitable water by integrating sounding data downward from 300 mb. The varying pressure of this upper moist layer was correlated with collocated 6.7 and 7.3 μm water vapor brightness temperatures (BT)s.

A persistent cluster of elevated BTs was observed over the subtropical Pacific adjacent to the western flank of a series of moisture bursts. Collocated rawinsonde soundings and satellite BTs consistently showed excellent agreement within this region, indicating extreme dryness in the middle and upper troposphere. The anomalous lack of upper tropospheric moisture, the tight clustering of abnormally large BTs, and the close proximity to a large area of active convection suggests these elevated BTs occur only as an occasional synoptically induced feature.

Vertical motions were estimated through the temporal change of the upper moist layer "topography". Although high correlations were

obtained between satellite BTs and upper moist layer pressures, minute quantities of upper tropospheric moisture above 300 mb produced large changes in BTs. The inability of conventional rawinsondes to measure moisture in the cold, tropical upper troposphere often leads to discrepancies between rawinsonde-derived and satellite-inferred moisture profiles. These discrepancies were quantified and shown to result in an unsatisfactory estimation of vertical motion computed from the local change in BTs.

Estimation of the influence of horizontal moisture advection on local BT changes resulted in maximum values of the same order of magnitude as the maximum observed BT changes. However, comparisons of these magnitudes at individual grid points showed little similarity. Thus, vertical motion estimates had the potential to be strongly modulated by horizontal advection. However, the consistently weak correlations at individual grid points indicated uncertainty as to whether changes in channel 11 and 12 BTs were influenced more by horizontal rather than vertical advection of moisture.

Appendix B

Conference proceedings papers and extended abstracts.

Paper presented at: Fifth Conference on Satellite Meteorology and Oceanography, London, September 1990.

TOVS CHANNEL RADIANCES AS A "GROUND TRUTH" FOR ECMWF ANALYSIS

J.P. McGuirk & D.E.W. Smith
Texas A&M University
College Station TX 77843 (409-845-4431)

Operational synoptic scale analyses are less accurate in the tropics than they are in middle latitudes. Among the many reasons for this weakness is the lack of a "ground truth" verification. Verification of analysis based on subsequent forecast accuracy is flawed seriously: The forecast itself is used in future analysis cycles. In the absence of any observations, the analysis defaults to the forecast.

Alternatively, synoptic scale fields of satellite radiance observations exist throughout the tropics. They are poor ground truth for the analyses, however, because their meteorological interpretation is usually uncertain. They are, however, observations. It is possible to convert the analyses into equivalent satellite radiance observations by means of a radiative transfer model (RTM). The procedure is equivalent to "flying a satellite through the analysis." Although meteorological interpretation remains problematic, consistent, similar variables may be compared. A quantitative comparison, independent of model effects on the analysis, is then possible. This process was accomplished using a RTM (Susskind et al., 1982) for the ECMWF analysis and reanalysis during the winter and summer FGGE special observing periods over a region of the tropical eastern Pacific Ocean.

Descriptive statistics of observed and calculated radiances are computed over the whole domain and over synoptic scale sub-domains. Domain wide results are summarized by bias (mean differences) and sensitivity (spatial standard deviations) for each channel. Large biases with respect to satellite observations exist in the ECMWF estimated brightness temperatures (+2.5 to +5°C in upper tropospheric channels, and -4 to -5°C in window channels); thus the ECMWF analysis exhibits a larger static stability than do satellite observations. The reanalysis reduced the upper tropospheric bias to about +1.5 to 2.0°C, but did not correct the boundary layer bias. In winter, the analysis is too sensitive (noisy) in most tropospheric channels; for May, sensitivity differences are small. The sensitivity of many of the channels was improved in the reanalysis.

Moisture channel estimation was poor in the original analysis, but improved dramatically in the reanalysis. (The principal reasons for this improvement were probably both improved model physics and inclusion of satellite moisture observations.)

Within sub-domains, such as along the ITCZ or within the subtropical high, the analysis identified the mean spatial pattern but failed to provide synoptic detail. Although the reanalysis improves the detailed structure, synoptic scale resolution is still weak.

Other analysis problems are identified, such as poor persistence characteristics and problems with the diurnal cycle. The technique documents dramatic improvement in the reanalysis. Finally, "flying a satellite through analysis" is demonstrated to be a powerful validation tool.

Susskind, J., J. Rosenfield, D. Reuter and M.T. Chahine, 1982: The GLAS physical inversion method for analysis of HIRS2/MSU sounding data. NASA Tech. Memo. 84936, Goddard Space Flight Center, Greenbelt, MD, 101pp.

Paper presented at: Fifth Conference on Satellite Meteorology and Oceanography, London, September 1990.

USE OF SATELLITE-DERIVED SPATIAL PATTERNS IN SYNOPTIC-SCALE NUMERICAL FORECASTS

James P. McGuirk
Texas A&M University
College Station TX 77843 (409-845-4431)

McGuirk (1989) documented consistent, horizontal, spatial patterns associated with tropical, synoptic-scale systems in a variety of satellite observations (OLR, VAS vapor channel imagery, TOVS individual channel radiances). Many of these detectable signals do not appear in initializations of operational forecast models, both because certain observations are not used (OLR, VAS and TOVS vapor channels) and because the detectable signal is too small to exceed the noise level in satellite sounding retrievals. What is needed is a procedure to utilize the spatial coherence of these small amplitude signals to maintain their information content in model initializations. This paper describes forecasts made from a case study in which spatial patterns, derived from TOVS individual channel radiances but not present in the TOVS sounding retrievals, were added back into the operational model initializations.

The forecast events consist of a pair of tropical plumes (McGuirk, 1989) which developed south of Hawaii during January 1989. TOVS radiance observations (from both NOAA polar orbiters) were obtained from the NMC history tapes and horizontal spatial patterns were extracted statistically. These patterns, two tropical thermal waves and a moisture distribution, were used to perturb the temperature and moisture initializations of the NMC operational global spectral model for 00GMT January 16. Five 48-h forecasts were computed: A control with no satellite-based augmentation (this forecast repeated the operational suite); and two sets of satellite-perturbed forecasts, one set with temperature perturbations only and another set with both temperature and moisture perturbations; in these two sets, the perturbations were inserted, separately, before and after diabatic normal mode initialization.

Numerous diagnostics have been computed. The strong tropical plume, east of Hawaii, was slightly stronger, with stronger evolving moisture gradients (implying stronger vertical motion) and stronger jetstream, in the forecasts made with complete satellite data enhancements. The weak

tropical plume southwest of Hawaii did not develop at all in the forecasts without enhanced satellite data; significant synoptic evolution is observed in the forecasts using the added satellite signals. The similarity between forecasts made from pre- and post-initialization insertion demonstrates the robustness of the satellite signals. The model is insensitive to the lack of balance in the initial fields (no wind perturbations accompanied the mass field perturbations).

Further analysis of the forecasts and diagnosed products will be accomplished. Strong arguments can be made for the expanded use of available operational satellite observations. Specifically, modifications in the sounding retrieval algorithms can be suggested which incorporate these weak, but horizontally coherent, synoptic scale signals.

McGuirk, J. P., 1989: Tropical synoptic composites in VAS, OLR and TOVS radiance data, AMS 4th Conf. on Satellite Meteorology and Oceanography, San Diego, May 1989, 49-52.

Paper presented at the Conference on Probability and Statistics in the Atmospheric Sciences, Monterrey CA, October 1989.

EFFECTS OF SATELLITE OBSERVATIONAL CHARACTERISTICS ON EOF STRUCTURE

J.P. McGuirk, J.R. Schaefer, D.E.W. Smith and G.A. White III

Department of Meteorology
Texas A&M University
College Station Texas 77843 (409-845-4431)

1. INTRODUCTION

Empirical orthogonal function (EOF) analysis compresses a multivariate data set by taking advantage of the correlation among the individual elements of the observation vectors of the set. Because the eigen values of the correlation matrix give the percentage variance explained of each associated eigen function, the eigen functions can be ordered objectively. Interpretation may be enhanced by pre-processing (normalizing, weighting, filtering, or clustering are common) or by post-processing the analysis (orthogonal or oblique rotations and compositing are typical).

Although the basic technique is objective, certain of the more useful features also limit the utility of EOF analysis. By the very nature of eigen value computation, ordered functions will be selected from purely random data. This feature makes an objective determination of statistical confidence difficult. For certain approximate types of distributions, North et al. (1982) have described how to place confidence intervals on eigen values. When adjacent eigen values are not well separated, the associated eigen functions can be "mixed" (not well resolved); nevertheless, in many EOF analyses, sine/ cosine pairs of simple propagating features are resolved realistically. Preisendorfer and Barnett (1977) have described empirical techniques based on Monte Carlo permutation of the observation data set; this procedure cannot be generalized beyond the data set being evaluated. A rule of thumb is that, if an eigen function explains less variance than one of the elements of the observation vector, its significance is questionable; this rule is based more on the reality that little is gained in using a pattern that contains less information than a specific observation. Because of the orthogonal nature of the decomposition, all eigen functions are forced to be orthogonal to the "leading" eigen function, even if this orthogonality is not realistic physically.

Because of these properties, EOF analysis must be considered essentially exploratory. Both Richman (1986) and O'Lenic and Livezey (1988) discuss the "artistic" side of EOF analysis. Often simple analysis decisions or observation strategies severely limit or enhance the physical interpretation. In what follows, several examples are given in which the data structure itself modulates the interpretation of the EOF decompositions. The observational vectors are based on brightness temperature observations from the TIROS Operational Vertical Sounder (TOVS) over the tropical Pacific Ocean; in most cases the vectors are reduced sets of the 27 channels available operationally. Satellite radiance vectors and, surprisingly, tropical operational analysis as well are amenable to EOF analysis because the broad weighting functions of the individual channels lead to strong correlation between most of the channels. Observed brightness temperatures, brightness temperatures calculated from fabricated soundings by means of a radiative transfer model, and calculated brightness temperatures based on operational forecast model output are all examined. The radiative transfer model has been described by Susskind et al. (1983).

2. FINE-SCALE STRUCTURE

White and McGuirk (1989) describe an EOF decomposition of a large set of TOVS observation vectors generated from common (but fabricated) moisture and temperature soundings. The vertical eigen functions reveal only the three statistically and physically significant eigen patterns usually identified in tropical observational data sets (Anderson, 1986):

i. Tropospheric average temperature
ii. Tropospheric average moisture
iii. Tropospheric lapse rate.

However, if this EOF analysis is used as a basis for clustering sounding groups through canonical discriminant analysis or some other objective procedure, EOF decomposition can be reapplied to each of the resulting objectively formed sounding groups. Even though each group contains only a few per cent of the population variance, physically meaningful structures can be extracted from the EOF analysis. For example, in sounding groups dominated by frontal inversions or trade wind inversions, the group EOFs can be used to infer quantitative information regarding inversion height and strength. The generalized result is

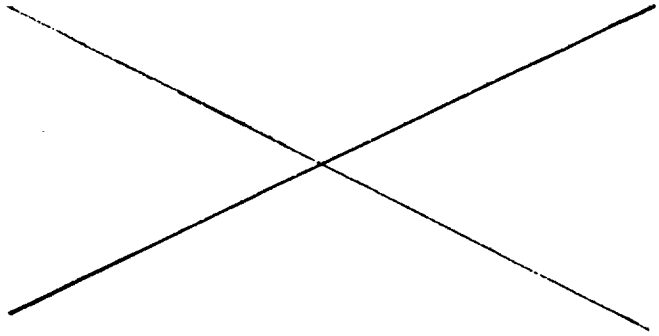

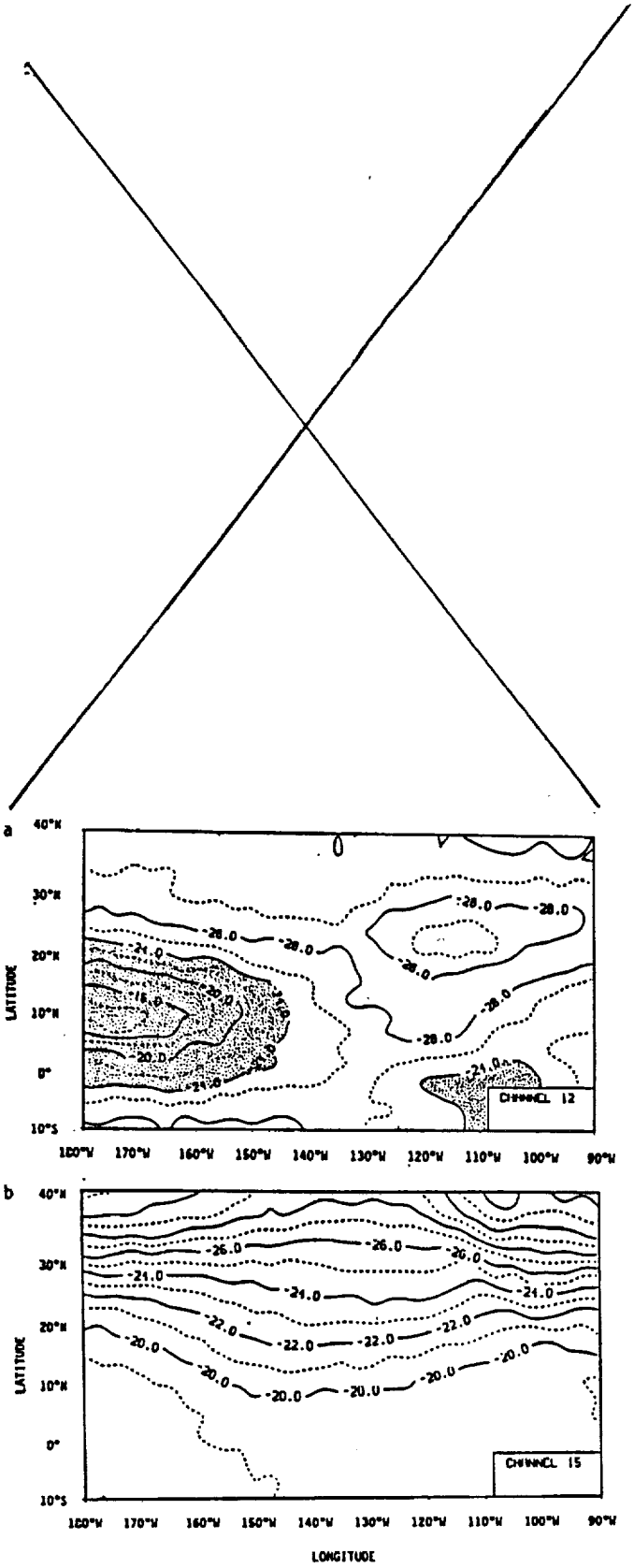

Fig. 1. Three month northern cool season mean brightness temperatures for a moisture channel (top, with warm-shaded dry), and a tropospheric temperature channel (bottom).

that physically meaningful patterns remain buried in eigen functions whose explained variance is less than that of a single brightness temperature channel; that is, eigen functions that cannot be demonstrated to be statistically significant.

3. OBSERVED SPATIAL PATTERNS

Figure 1 displays the typical spatial pattern of satellite temperature and moisture observations over the tropical east Pacific, as viewed through 3-month cool season means of two individual TOVS channels. The "temperature channel" is dominated by a meridional thermal contrast. The "moisture channel" is marked by three warm (dry) extrema. Only between 15 and 30°N do the two patterns share similar shape. The correlation structure of the individual signals themselves is not coherent throughout the domain. Figure 2 displays the horizontal structure functions (the autocorrelation as a function of the separation between observations) for these two channels; the structure functions were calculated separately for equatorial observations (0-15°N) and for subtropical observations (15-30°N). Horizontal variation of moisture is dominated by large scales, or correlation, along the equator (1300 km) and by much smaller scales in the subtropics (650 km); the temperature signal is just the opposite. The length scales are estimated objectively by the "integral length scale"; that is, the area under the structure function curve. Because of the narrowness of the latitude bands, the north south variation is sampled less than zonal variations. Two points are important: These differing temperature and moisture variations come from the same meteorological "weather systems"; and, given these definitive, broadscale patterns, it is difficult to use a method like EOF decomposition to extract meaningful synoptic scale patterns without removing some or all of the stationary spatial variance first.

To extract synoptic scale patterns, a 17-event subset of the TOVS observations was composited in such a manner to identify the mean structure of tropical plumes. Each observation

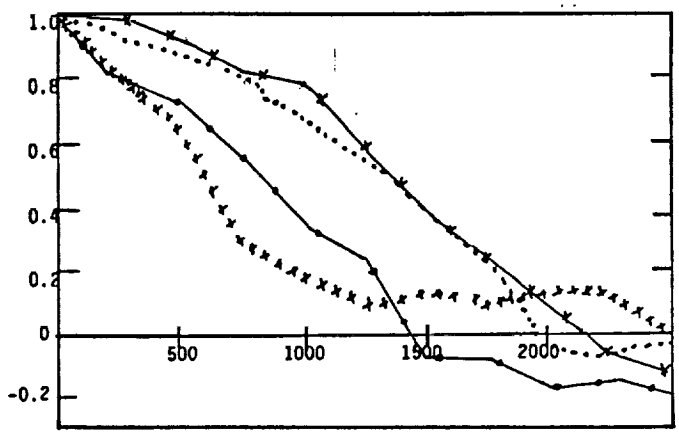

Fig. 2. Autocorrelation vs. observational separation (in km); that is, the horizontal structure function. Solid lines are for a moisture channel; broken lines are for a temperature channel. Dots are the subtropical band (15-30° N); x's are the tropical band (0-15° N).

vector consists of 19 channel brightness temperatures; thus, each channel carries approximately 5% of the variance in the normalized data set. The first 4 principal component patterns appear as Fig. 3; the eigen functions are inset to the right, arranged approximately by their theoretical weighting function peaks.

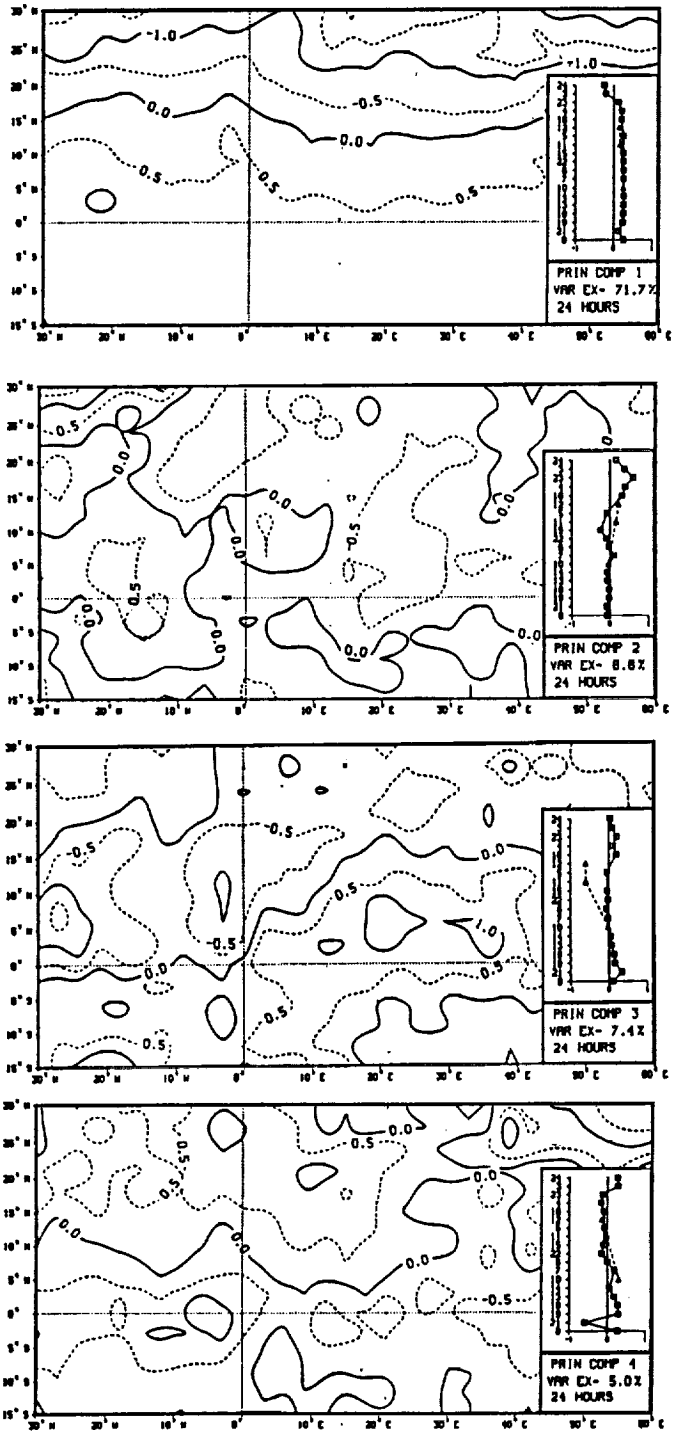

Fig. 3. First four principal components and associated eigen vectors and eigen values (inset at right) for TOVS brightness temperature vectors composited for 17 tropical plumes; the origin is centered on the plume and is approximately 7° N. The eigen vectors are stratified by weighting function peaks, with window channels at the bottom and tropopause channels at the top. Triangles are moisture channels.

A number of behaviors are typical. The first eigen function/principal component pair extracts a domain wide pattern, specifically the climatological thermal pattern of Fig. 2, and a vertical structure in which each channel is weighted nearly equally and of the same sign, except for the two channels reaching high into the stratosphere. Over 70% of the total spatial variance across these 17 events is explained in terms of a tropospheric mean temperature, an indication both of the high correlation among TOVS channels (even for moisture in the tropics), and of the weak tropical thermal variation. The two important moisture channels possess significant loadings in the first eigen function, although no hint of the actual moisture pattern, shown in Fig. 2, is evident. The reason that the moisture pattern is not present is due entirely to TOVS observational characteristics. Only two channels sense moisture primarily, whereas the remaining 17 channels respond primarily to temperature variation. The second and third eigen functions both possess strong loadings in the moisture channels. Unfortunately, the eigen values are nearly identical (between 7.5 and 9%); in this case, the danger of mixing of orthogonal modes, described by North et al. (1982), is a reality. Coupled with the moisture variation are two thermal signals, one in the upper troposphere and one in the boundary layer. Moist conditions are associated with a warm boundary layer, but the thermal pattern in the upper troposphere switches signs between the two eigen functions. Since the principal components are orthogonal to each other as well, differences in these patterns are apparent as well. Both patterns show common moistness in the tropical plume origin region; however, the third principal component emphasizes the north/south variation between the banded moistness of the ITCZ and the dryness of the subtropical high to the north, while the second pattern emphasizes the east/west moist/dry dipole.

The fourth eigen function (about 5% of the variance) possesses a weak boundary layer thermal signal. This signal is spread across three eigen functions. More significantly, this eigen function is dominated by a single channel, the microwave "window" channel. O'Lenic and Livezey (1988) have suggested that this behavior is a good way of identifying errors in the observations. In this case, the "offending" channel is responding to neither moisture nor temperature, but to surface and hydrometeor emissivity changes.

In instantaneous synoptic patterns, Anderson (1986) found that the three dominant signals separated nearly unambiguously, as described in the Introduction. He found no hint of the more detailed structure. To resolve synoptic scale signals in TOVS observations, preprocessing or postprocessing must accompany EOF analysis.

In sensitivity tests it was found that shrinking the horizontal domain, either zonally or meridionally about the tropical plume did nothing to improve the signal, even though the variance was reduced to strictly synoptic scale. Eliminating the microwave channel reduced noise only slightly. Eliminating the moisture channels allowed the upper tropospheric thermal wave to be isolated as the second eigen function (with about 10% of the variance) but this procedure was not the most efficient for depicting the wave's

structural properties. A final sensitivity test, in which the variance of the three moisture channels was artificially tripled, had the effect of identifying a single "moisture eigen function" which resembled strongly a tropical plume; this pattern represented 17% of the "variance". This pattern is displayed in Fig. 4.

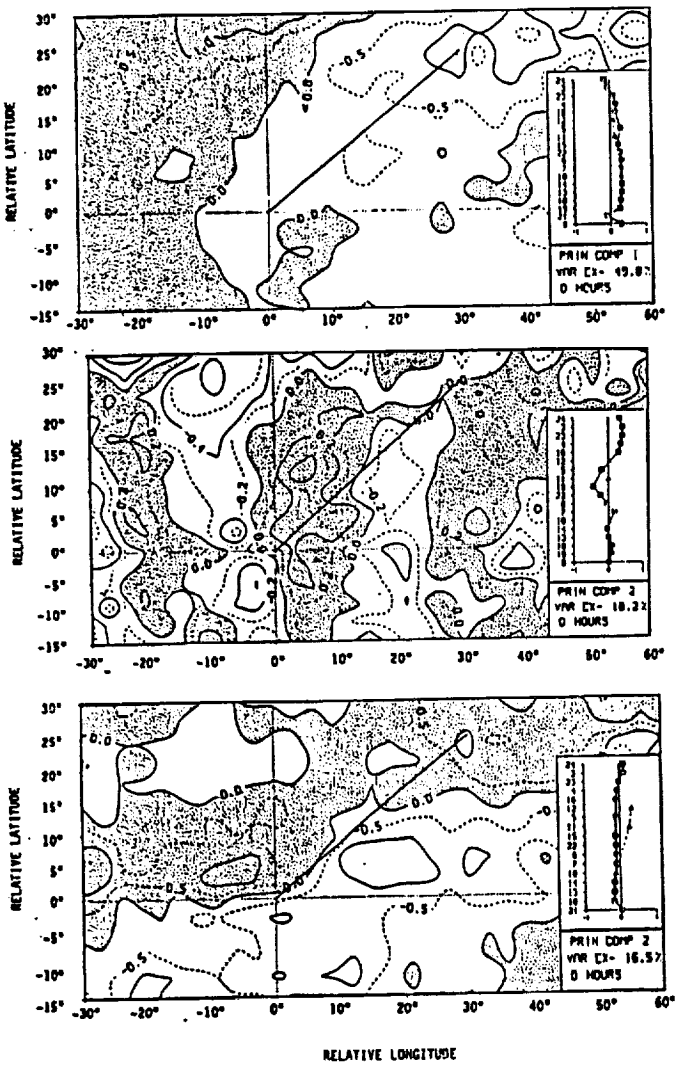

Fig. 4. Composited temperature EOFs resulting from removal of zonal means (top and middle). Moisture EOF resulting from weighting moisture variance by a factor of 3 (bottom, shading is dry).

The most useful preprocessing was the removal of the stationary pattern. When the zonal means were removed, the tropospheric average temperature function was still the leading pattern. The first two eigen function/principal component pairs appear as Fig. 4. They represent a planetary-scale, tropospheric deep thermal wave (warm to the west, cold to the east, 50% of the non-zonal variance) and an upper tropospheric thermal wave (warm over cold, or cold over warm; about 3000 km zonal wave length; 16% of the variance). The "moisture functions" are split into two patterns, which comprise the tropical portion of the plume, and a strong extension into mid latitudes, emphasizing a strong moisture gradient along the northwest flank of the plume. The patterns have been merged, as described above.

To summarize, EOF analysis selects only the dominant scale, usually the largest, and suppresses most other scales; important scales and patterns may be mixed or distorted because of the imposed orthogonality with the leading eigen functions. When eigen values are not well-separated, physical intuition must be used judiciously. The properties of the observation vectors may lead to misinterpretation of physical meanings. Most importantly, additional data preparation to isolate relevant scales can lead to physical interpretation that cannot be isolated otherwise.

4. MODELLED SPATIAL PATTERNS

Closer correspondence can be obtained between analysis and observations by processing the analysis through a radiative transfer model (Susskind et al, 1982), in a procedure equivalent approximately to "flying a satellite through the analysis." An example showing the breakdown of the synoptic analysis for small enough scales is shown in Fig. 5, which shows sample EOFs for regions of the ITCZ and subtropical highs. The first subtropical EOF (not shown) accurately reproduces the TOVS temperature signal, although the analysis includes moisture variates and the observations do not. For the second EOFs, although the spatial patterns are similar, the eigen functions are not; that is, the analysis is describing random variation, unrelated to what is occurring in the atmosphere. The situation is worse along the ITCZ, where the eigen values differ by 20% of the explained variance, the extrema of the spatial patterns are mislocated by over 1000 km, and the analysis includes a boundary layer signal not observed by TOVS.

To conclude, although careful data preparation can apparently minimize the differing views of analysis and satellite observations, statistical, structural differences appear even within the first and second EOFs.

5. ANALYZED SPATIAL PATTERNS

The EOF structure of ECMWF operational analysis is dissimilar to satellite structure, even when the decomposition is designed to mimic the satellite observational format. Figure 6 displays the first two EOFs from a typical tropical analysis; the moisture observations have been integrated vertically to two levels to simulate the TOVS measurements. Although the first EOF is similar to Fig. 3a, the moisture variables are weighted nearly equally to the temperature variables, and too much of the spatial variance is accounted for. The moisture EOF is primarily upper tropospheric and does not represent the synoptic structure well. Table 1 shows the reasons for the differences from observations. Fundamentally, the vertical correlation is too large in the temperature variables--in excess of 0.7 for nearly all tropospheric channels. The moisture loadings appear in all eigen functions (Table 1b); eigen vectors 3 and 5 are essentially nothing more than the upper and lower tropospheric moisture variables, respectively. Figure 7 is similar to Fig. 6, except the moisture variates are the mixing ratios at individual levels; only the second and third EOFs are shown. The upper tropospheric moisture function (Fig. 7a) is complex and noisy, but captures the moist ITCZ,

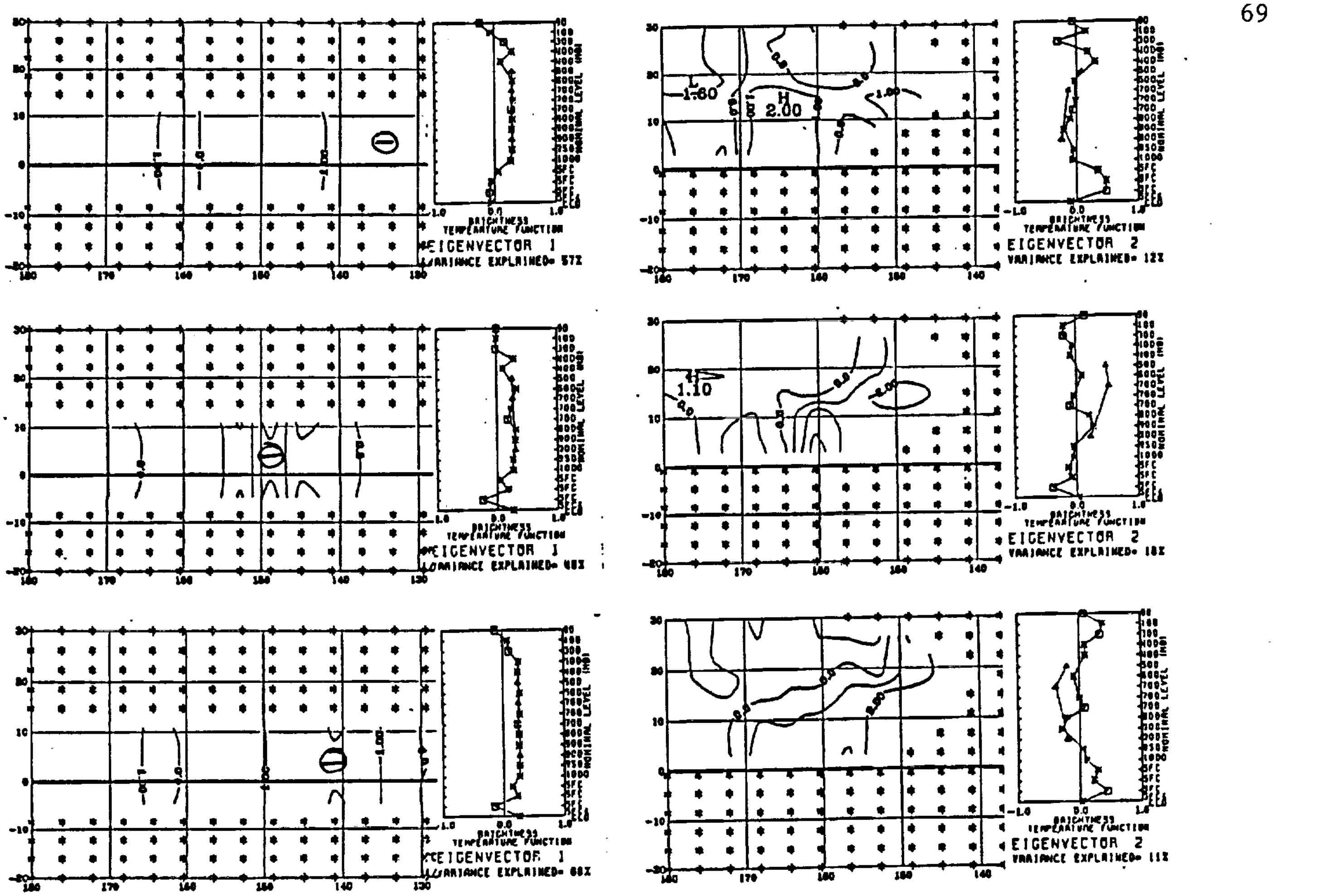

Fig. 5. Sample EOFs from regional decompositions (equatorial mode on the left; subtropical high mode on the right). Top panel is TOVS observations; middle panel is ECMWF IIIb analysis estimated brightness temperatures; bottom panel is ECMWF reanaylsis estimated brightness temperatures.

Table 1a. Vertical cross correlation matrix (index numbers in mb) for ECMWF temperatures (T) and precipitable water (P below, and above, 500 mb) analysis over the tropical Pacific Ocean.

	T100	T200	T300	T400	T500	T700	T850	T1000	P3T05	P5T010
T100	1.0000	-0.2558	-0.8717	-0.9148	-0.9222	-0.9182	-0.8838	-0.8385	0.0728	0.5350
T150	0.8753	0.1587	-0.7881	-0.9178	-0.8109	-0.8548	-0.8374	-0.7808	-0.0230	0.5117
T200	-0.2558	1.0000	0.2038	0.0348	0.0338	0.1157	0.1051	0.1853	-0.1761	-0.3044
T250	-0.7623	0.5770	0.8888	0.8342	0.6072	0.5885	0.5278	0.5211	-0.2085	-0.5286
T300	-0.8717	0.2038	1.0000	0.8802	0.8082	0.7285	0.8853	0.8342	-0.1412	-0.5508
T400	-0.9148	0.0348	0.8802	1.0000	0.9818	0.8741	0.8884	0.8114	-0.1048	-0.5102
T500	-0.9222	0.0338	0.8082	0.9818	1.0000	0.9325	0.8888	0.8408	-0.0475	-0.5807
T700	-0.9182	0.1157	0.7285	0.8741	0.9325	1.0000	0.9842	0.8705	-0.0337	-0.6042
T850	-0.8838	0.1051	0.8853	0.8884	0.8888	0.9842	1.0000	0.9438	-0.0788	-0.6356
T1000	-0.8385	0.1853	0.8342	0.8114	0.8408	0.8705	0.9438	1.0000	-0.1020	-0.6487
P3T05	0.0728	-0.1761	-0.1412	-0.1048	-0.0475	-0.0337	-0.0788	-0.1020	1.0000	0.6152
P5T010	0.5350	-0.3044	-0.5508	-0.5102	-0.5807	-0.6042	-0.6356	-0.6487	0.6152	1.0000

Table 1b. Frist six eigen vectors of the eigen values of Table 1a. The eigen values are (from left to right): 66, 14, 9, 5. 1 and 1 %.

	PRIN1	PRIN2	PRIN3	PRIN4	PRIN5	PRIN6
T100	-.325835	0.122380	0.094327	0.057779	0.172248	0.123188
T150	-.318528	0.025248	0.087398	0.218289	-.081180	0.174828
T200	0.142352	-.707868	0.314585	0.488073	-.210872	-.223182
T250	0.280411	-.380437	0.058588	-.087858	0.258408	0.421812
T300	0.314548	-.180758	-.047280	-.282278	0.230528	0.382885
T400	0.322381	-.044830	-.083331	-.324245	-.028348	-.181588
T500	0.323034	0.030758	-.142585	-.205079	-.088038	-.328833
T700	0.318807	0.173015	-.144873	0.120884	-.288148	-.248002
T850	0.308782	0.281701	-.148378	0.272288	-.258808	0.148015
T1000	0.284012	0.222812	-.184881	0.525848	0.008113	0.438408
P3T05	0.173257	0.287230	0.803842	-.218043	-.384288	0.218847
P5T010	0.263864	0.278083	0.353110	0.278011	0.705141	-.355387

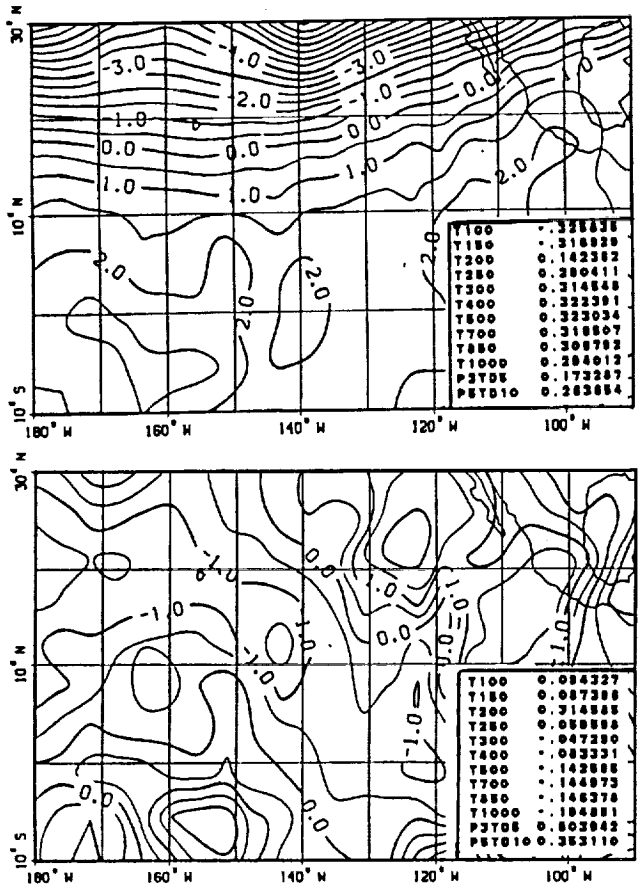

Fig. 6. First (74%) and third (17%) EOFs computed directly from ECMWF IIIb temperatures and precipitable water. The 1st EOF is a temperature function; the 3rd is a moisture function.

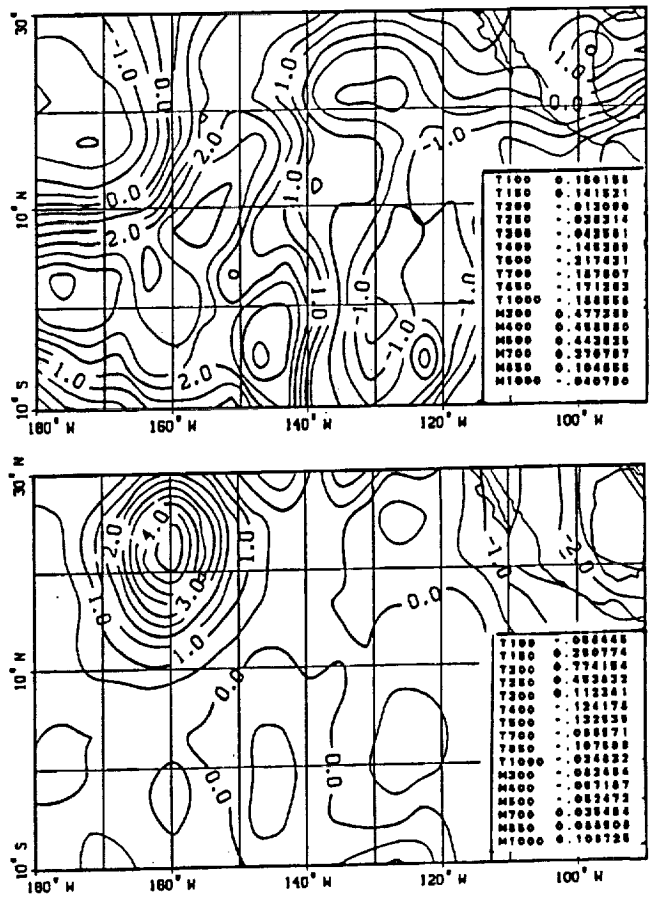

Fig. 7. Second (17%) and third (9%) EOFs computed directly from ECMWF IIIb temperatures and mixing ratios. The 2nd is a "moisture function"; the 3rd is an "error function" (see O'Lenic and Livezey, 1988).

tropical plume, and SPCZ. The third EOF identifies a likely analysis problem associated with observations over Hawaii. The signal in the center is nearly 4 standard deviations.

In summary, even data sets designed to be identical, and which appear to reproduce observations, can possess quite different statistical properties.

6. CONCLUDING REMARKS

EOF analysis is a powerful tool in the realm of data interpretation, but it will never supplant physical intuition. It should be used primarily as an exploratory technique, and should normally be accompanied by other signal processing techniques, such as filtering, clustering or rotation.

Acknowledgements. This research has been supported by the Global Scale Atmospheric Processes Program from NASA Headquarters and by the U.S. Air Force Institute of Technology.

7. REFERENCES

Anderson, L., 1986: Multispectral analysis of tropical raidiances from TOVS, PhD. dissertation, Texas A&M Univ., College Station TX.

North, G., T. Bell, R. Cahalan and F. Moeng, 1982: Sampling error in estimation of empirical orthogonal functions, Mon. Wea. Rev. 110, 699-706.

O'Lenic, E., and R. Livezey, 1988: Practical considerations in the use of rotated principal component analysis (RPCA) in diagnostic studies of upper air height fields, Mon. Wea. Rev. 116, 1682-1689.

Preisendorfer, R., and T. Barnett, 1977: Significance tests for EOFs. 5th Conf. on Probability and Statistics in the Atmospheric Sciences, Las Vegas, Amer. Meteor. Soc., 169-172.

Richman, M., 1986: Rotation of principal components, Intl. J. of Climate 6, 293-335.

Susskind, J., J. Rosenfield, D. Reuter and M. Chahine, 1982: The GLAS physical inversion method for anaysis of HIRS2/MSU sounding data, NASA Tech. Memo 84936.

White, G., and J. McGuirk, 1989: Unique signatures of synoptic features in TIROS N satellite data, 4th Conf. on Satellite Meteorology and Oceanography, San Diego, Amer. Meteor. Soc.

Paper presented at 18th Conference on Hurricanes and Tropical Meteorology, American Meteorological Society, San Diego, CA, May 1989.

ACTIVE MODES OF THE PACIFIC ITCZ

P. M. Hayes and J. P. McGuirk

Department of Meteorology, Texas A&M University
College Station, TX 77843 (409-845-4431)

1. INTRODUCTION

The three best documented large scale fluctuations along the Pacific ITCZ are small scale easterly waves (particularly over the summer western Pacific), tropical intraseasonal oscillations (TIO or the 30-60 d wave) and ENSO. The behavior of convection on intermediate synoptic scales has not been discussed. Outgoing longwave radiation (OLR) observations are used to define convectively active, synoptic scale, ITCZ regions in eight 6-month cool seasons along the Pacific ITCZ. The ITCZ is defined at each longitude as the minimum OLR observed between 30°N and 5°S; its intensity is defined as the spatially smoothed OLR amplitude (with a two dimensional binomial filter, r = 550 km) after the mean, annual and semi-annual cycles have been removed at each point. This definition emphasizes local activity; since local means are removed, east and west Pacific anomalies of the same amplitude do not imply euqivalent convection. Most subsequent analyses involved low-pass filtering (of either 10 or 20 d).

2. ITCZ VARIABILITY

2.1 Temporal and spatial scales

Figure 1 describes the 20-d filtered ITCZ evolution across the entire Pacific for a typical cool season. The horizontal heavy lines demark stationary convection; tilted lines imply propagation, east or west. Most years are marked by three prominent features:

i. Zonal bands of convective development (usually in excess of 5000 km and a time scale of 15 d; the filter clips the amplitude); these bands show no preference for stationarity or direction of propagation;

ii. Isolated patches of stronger convection (2-4000 km zonal scale, 15 d time scale) imbedded within the zonal bands; these features are normally stationary or retrograde;

iii. Several zonal bands often merge as a TIO event; although the TIO moves eastward, the bands within it may move retrograde.

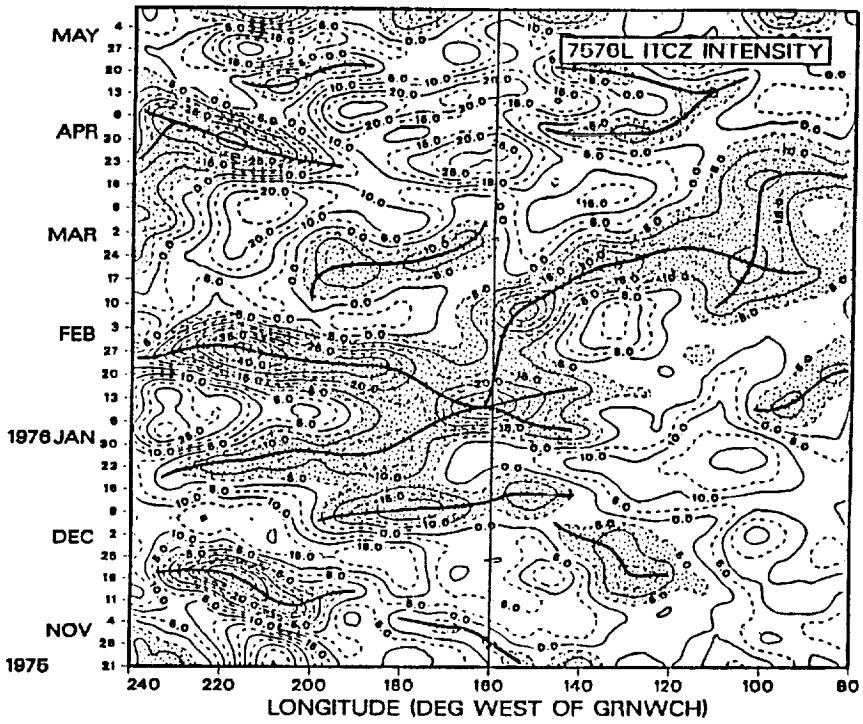

Fig. 1. Time-longitude section of ITCZ intensity (anomalies in Wm^{-2}) across the Pacific for 1975-76. Shading and heavy lines identify relative convective episodes.

During ENSO, the smaller scale features are suppressed, except on the eastern flank of the enhanced ITCZ region.

Figure 2 contrasts the ITCZ intensity at a single longitude (160°W) with the intensity averaged all the way across the Pacific. Fluctuations with 10-12 d time scales predominate. Amplitudes commonly exceed 25 Wm^{-2}; these oscillations are absent in the zonally averaged data, implying that the zonal scale is small. This feature also disappears during ENSO. Although active convection at 160°W normally is associated with a generally active ITCZ, there are occurrences of local activity not associated with an active ITCZ across the Pacific.

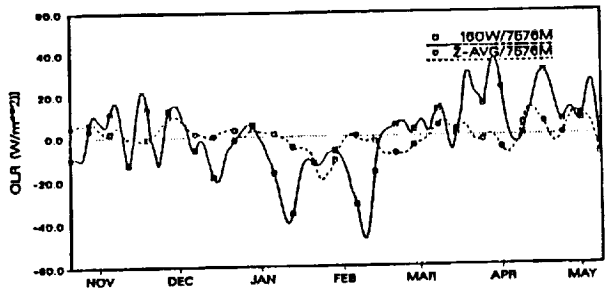

Fig. 2. ITCZ intensity for the 1975-76 cool season at 160°W (solid line) and zonally averaged across the Pacific (dashed line). Data are low pass filtered (10 d).

Further analysis demonstrates that when the zonally averaged ITCZ intensifies it moves southward, commonly in excess of 5° latitude. Latitudinal shifts with localized convection (160°W) cannot be generalized. The latitude of a locally active ITCZ is distributed bimodally: convective activity is centered at about 13°N, or somewhat south of 5°N; of course, many days of no discernable convection also are observed. The preferred northern zone disappears during ENSO. Bimodality of position is also observed in the zonally averaged data, but not in all years.

2.2 Patterns of active ITCZ

Figure 3 contrasts composites of OLR across the tropical Pacific basin for collections of days when i) the ITCZ was active at 160°W; ii) the ITCZ was active in a zonally averaged sense; and iii) the ITCZ was both locally active and zonally active. Significant pattern differences exist. Local convection is meridionally oriented. The rest of the Pacific ITCZ is relatively convection free. The zonally averaged active ITCZ is active nearly everywhere across the Pacific, and is bordered by convectively weak regions north and south, particularly over the latitudes of the SPCZ. Events involving both local and zonal convection possess a definite convective minimum between 140 and 120°W, with a convective extension southward of this cloud free region into the southern hemisphere.

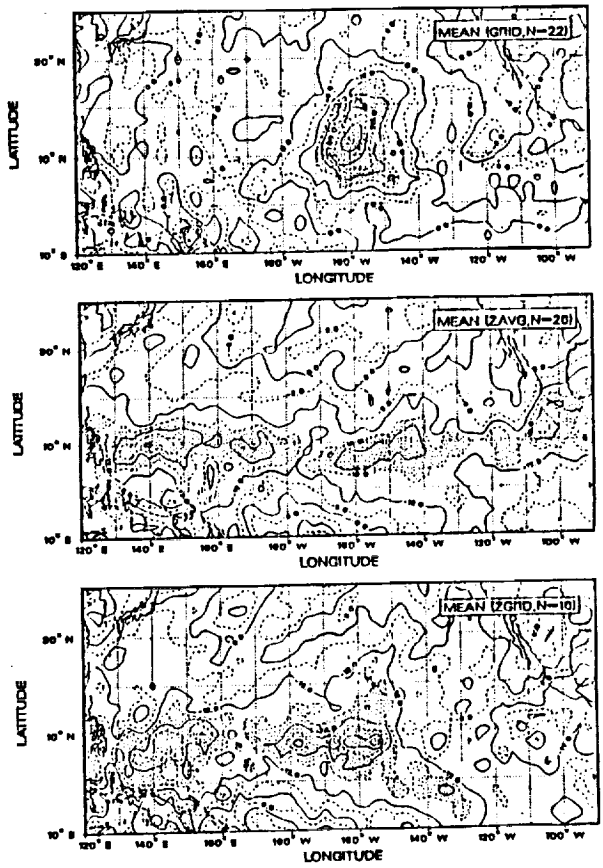

Fig. 3. Composite OLR anomaly maps for 22 d of local active ITCZ at 160°W (top), 26 d of zonally averaged active ITCZ (middle), and 16 d of both local and zonal active ITCZ. Shaded regions are relatively active. Isopleths at 6 Wm^{-2}.

3. SUMMARY

The relative intensity of the ITCZ is defined objectively. Organized convective episodes on several large synoptic time and space scales are identified. They typically occur in conjunction with each other and with the 30-60 d wave. The smaller scale features disappear during ENSO. Systematic, but different, patterns, movement and temporal behavior are associated with local and zonally extensive convection. Most importantly, intensifying zonal convection moves southward; local convection occurs at two preferential latitudes; local convection does not imply a generally active ITCZ, and vice versa.

4. ACKNOWLEDGEMENTS

This research is supported by NASA's George C. Marshall Space Flight Center. PMH acknowledges support by the U.S. Air Force Institute of Technology.

Paper presented at 18th Conference on Hurricanes and Tropical Meteorology, American Meteorological Society, San Diego, CA, May 1989.

DYNAMICAL CHARACTERISTICS OF TROPICAL PLUMES

C.A. Askue and J.P. McGuirk
Department of Meteorology

J.M. Klinck
Department of Oceanography

Texas A&M University
College Station, Texas 77843-3146

1. INTRODUCTION

1.1 Background

This paper describes the dynamical framework of tropical plumes; it tests the hypothesis that initial plume development can be described as the barotropic interaction of tropical waves.

The tropical plume is a common wave disturbance in equatorial regions. From satellite the plume appears as a continuous, narrow band of middle and high cloud, at least 2000 km in length, originating near the equator and extending into subtropical and middle latitudes. Many plumes develop in each northern hemisphere winter along the eastern Pacific ITCZ. The visible manifestation of the tropical plume (the cloud band) represents transport of tremendous amounts of energy, momentum, and moisture from equatorial regions to the midlatitudes (McGuirk et al., 1988).

Case studies reveal that the following dynamical features precede and accompany a tropical plume: a low-level synoptic-scale disturbance, an upper-level planetary-scale equatorial wave; a midlatitude trough that intrudes into the tropics; and an upper tropospheric equatorial wave approximately 3000 km in wavelength and essentially in phase with the midlatitude trough.

Previous studies have focused on development of the plume. This work seeks one or more mechanisms that may be important for plume initiation. Although the speed and consistency of plume formation suggest a common dynamic instability, simple barotropic or baroclinic wave instability of a zonal current is unlikely. The plume creates a more unstable flow as it evolves. In addition, the initial stages of a tropical plume appear to be detached from both CISK associated with the low-level disturbance and baroclinic effects of the midlatitude trough. Therefore, it is hypothesized that a barotropic instability of a longitudinally varying, basic current may be an important mechanism for initiating tropical plumes. Lorenz (1972) demonstrated such an instability in analytical studies of perturbations on Rossby wave basic states in quasi-geostrophic flow.

1.2 Case Study

In an attempt to identify reasonable basic states and possible perturbation structures, a tropical plume from January 1979 was chosen for a case study using FGGE data. The plume studied initiated about 0000 GMT 21 Jan 79 near 7.5°N. Figure 1 shows the wind field for 0000 GMT 22 Jan 79 (24 hours after initiation). The zonal wind, averaged zonally across the domain at each latitude, has been subtracted from the zonal wind components. The resulting picture suggests a great deal of influence from the southern hemisphere. In addition, the structure indicates that a reasonable basic state for a simple linear study may be formed from a sum of planetary-scale equatorial free modes, such as those identified by Matsuno (1966).

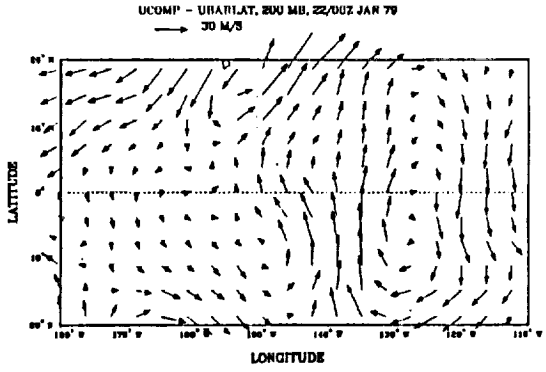

Fig. 1. ECMWF-analyzed winds for 00 GMT 22 January 1979 with zonal average for each latitude band subtracted from zonal wind component in that band.

Further evidence for a basic state containing planetary-scale features is shown in Fig. 2, a vertical cross-section of relative vorticity along 7.5°N at 0000 GMT 21 Jan 79, the latitude and time of origin for this case. Figure 2 reveals a disturbance with a well developed relative vorticity pattern centered near 300 mb and having a wavelength of about 9000 km, roughly twice the size of the domain shown. McGuirk (1989) describes a planetary scale wave in composited satellite thermal patterns consistent with the interpretation of this vorticity pattern as a Kelvin wave, with the convergence axis located at about 155°W.

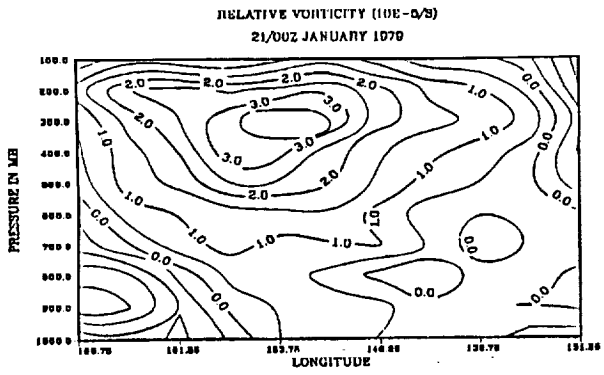

Fig. 2. Vertical cross-section of relative vorticity (10^{-5} s^{-1}) for 00 GMT 21 January 1979 along 7.5 °N, based on ECMWF wind data.

2. MODEL

The quantitative problem involves examining the stability of inviscid, horizontally-sheared, barotropic basic states with respect to a synoptic-scale perturbation. The investigation is developed numerically with a one-layer, shallow water, gridpoint model on an equatorial beta-plane. Sadourny (1975) proposed a finite differencing scheme for the shallow water equations that conserves potential enstrophy. Although the model was designed for long-term integrations, the particular scheme also proves useful for studies on shorter time scales. The model equations are as follows:

$$\frac{\partial u}{\partial t} - \eta V - fv + \frac{\partial H}{\partial x} = 0$$

$$\frac{\partial v}{\partial t} + \eta U + fu + \frac{\partial H}{\partial y} = 0$$

$$\frac{\partial P}{\partial t} + \frac{\partial U}{\partial x} + \frac{\partial V}{\partial y} = 0$$

where

$$P = gh = \textit{pressure/density}$$

$$\eta = \frac{v_x - u_y}{P} = \textit{potential vorticity}$$

$$H = P + \frac{1}{2}(u^2 + v^2)$$

$$U = Pu, \; V = Pv$$

The model includes a staggered C-grid centered on potential vorticity, a grid interval of 5o latitude and longitude between values of like variables, and a timestep of 90 seconds. Boundaries are periodic in the east-west direction and solid, free-slip walls north and south. The basic code used for this work was written by Paul Swarztrauber of NCAR and was modified from a doubly-periodic, non-rotating model to a periodic channel on an equatorial beta-plane.

3. DISCUSSION AND RESULTS

Model work at this point includes testing the model's stability and boundary conditions with respect to a variety of normal mode initial conditions. These states include uniform zonal winds, Gaussian jets, single equatorial modes, and full-domain, trigonometric stream function patterns. Testing has been done with both the linear and nonlinear set of equations.

An initial experiment consists of a linear superposition of equatorial modes, followed by integration with the nonlinear equation. Preliminary results indicate a localized strengthening of cross-equatorial flow in selected regions. Interpretation at this point is speculative. However, these early results provide encouragement for future work. This work will include perturbing a series of wavy, planetary-scale basic states with synoptic-scale perturbations. The goal is to identify possible instabilities which feed on the kinetic energy of the wavy basic state, and which may be likened to the initial stages of a tropical plume.

4. ACKNOWLEDGEMENTS

The research reported here is supported in part by NASA Contract NAS-37284. Maj Askue acknowledges the support of the United States Air Force Institute of Technology.

5. REFERENCES

Lorenz, E.N., 1972: Barotropic instability of Rossby wave motion. *J. Atmos. Sci., 29,* 259-264.

Matsuno, T., 1966: Quasi-geostrophic motions in the equatorial area. *J. Meteor. Soc. Japan, 44,* 25-42.

McGuirk, J.P., 1989: Tropical synoptic composites in VAS, OLR and TOVS radiance data, *Preprints, AMS 4th Conf. on Satellite Meteorology and Oceanography,* San Diego, May 1989.

McGuirk, J.P., A.H. Thompson, and J.R. Schaefer, 1988: An eastern Pacific tropical plume. *Mon. Wea. Rev., 116,* 2505-2521.

Sadourny, R., 1975: The dynamics of finite-difference models of the shallow-water equations. *J. Atmos. Sci., 32,* 680-689.

Paper presented at
4th Conference on Satellite Meteorology
and Oceanography, American Meteorological
Society, San Diego, CA, May 1989.

TROPICAL SYNOPTIC COMPOSITES IN VAS, OLR AND TOVS RADIANCE DATA

James P. McGuirk

Department of Meteorology
Texas A&M University
College Station, Texas 77843-3146

1. INTRODUCTION

1.1 Background

Understanding the transient structure of the tropical Pacific atmosphere is hampered by lack of data. Larger spatial and temporal scale features can be examined through smoothing of the data across the larger scales. This procedure fails for synoptic scale features over the Pacific because the resolution of the data normally exceeds the size of the system. A second problem is that the synoptic scale signal of satellite observations in the tropics is weak at best. Most operational techniques emphasize information associated with the vertical structure of the observations and the atmospheric systems themselves. It is curious that operational meteorologists turn first to the horizontal structure of satellite observations.

This paper contrasts the horizontal structure of specific tropical synoptic features with those of a zonal mean ITCZ. Two hypotheses are assumed:

I. The cool season Pacific ITCZ oscillates between two states: a zonally symmetric state, referred to as a quiescent state; and a locally convectively active, meridionally oriented state, referred to as a tropical plume. McGuirk et al. (1987) presented evidence substantiating this modal behavior in the ITCZ.

II. Satellite channel radiances possess signals sufficiently strong to reveal horizontal, as well as the vertical, structure of these synoptic ITCZ variations. Preliminary work (not reported herein) suggest that these horizontal signals are not captured well in modern analysis systems, even though the vertical structure often is specified accurately. These signals can be resolved by averaging over many events, or compositing, instead of smoothing temporal and spatial scales.

Conclusions are made regarding the two different appearances of the ITCZ--a weakly convective, zonally symmetric state and a locally, synoptically-active convective state. Of primary significance is how a number of different satellite systems view these distinctive states.

1.2 Data

The two ITCZ modes are contrasted in four different forms of satellite radiance data:

I. Daily, gridded (2.5°x2.5°) OLR, from which tropical convective cloud can be inferred;

II. Digitized, gridded (3.5°x3.5°) GOES VAS water vapor imagery (6.7 μm), which possesses a weighting function peak at approximately 500 mb for climatological moisture distributions.

III. Analyzed brightness temperatures (3.75°x3.75°) of TOVS water vapor channels from the NOAA 7 and 8 polar orbiters(6.7 μm [500 mb]; 7.3 μm [700 mb] is available but similar). Since this instrument is used for sounding reconstruction, data are absent in overcast regions.

Iv. Analyzed brightness temperature vectors, as in III, except for a nearly complete set of TOVS channels with weighting function peaks in the troposphere (HIRS and MSU); these channels are indicators of both thermal and moist structure.

In all cases the data are composited over many events to minimize the effects of missing data, sampling errors and variability of individual systems.

2. ZONAL ITCZ VS. SYNOPTIC PLUME

Hayes and McGuirk (1989) describe a procedure for identifying and quantifying periods of significant convection along the ITCZ. Figure 1 contrasts periods during which the ITCZ is active all the way across the Pacific with periods when the ITCZ is active at a single point (165°W) with no *a priori* knowledge of convective activity elsewhere. If attention is focused on active behavior at a point, the resultant pattern is strongly meridional and of synoptic scale. The pattern resembles a tropical plume. For strong zonally symmetric (at least across the Pacific) active convection, the signal is weaker and no significant synoptic detail is apparent. Correspondence between the two sets of days comprising these composites is not good; active convection at 165°W does not imply a strong or weak ITCZ. The zonally symmetric composite is the strong convection extreme of the quiescent mode; the quiescent mode typically is much weaker than that in Fig. 1. Even so, the convective maximum in the zonally symmetric ITCZ is significantly weaker (about 10 W/m²) than in the tropical plume mode. The dry subsidence region is also organized zonally, with comparable anomaly magnitudes in both composites.

Figure 2 compares OLR composites of many occurrences of synoptic scale tropical plumes with many days when no tropical plumes were observed. Days comprising composites in Fig. 2 are not the same as those composited in Fig. 1. The tropical plume composite is centered--in latitude, longitude and time--on the initiation of the plume and its intersection with the ITCZ; the pattern is similar to that generated by Lin and Mock (1986). Plume patterns are associated with locally active meridional overturning; that is, a local Hadley cell.

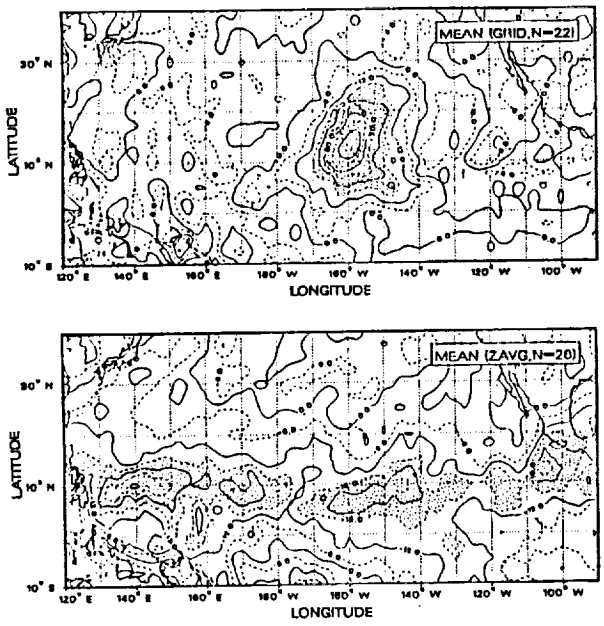

Fig. 1. (top) OLR composite anomaly map of 22 d of active convection at 165°W; (bottom) as in top, except 26 d with zonally averaged active convection. Contour interval is 6 W/m²; active convection regions are shaded.

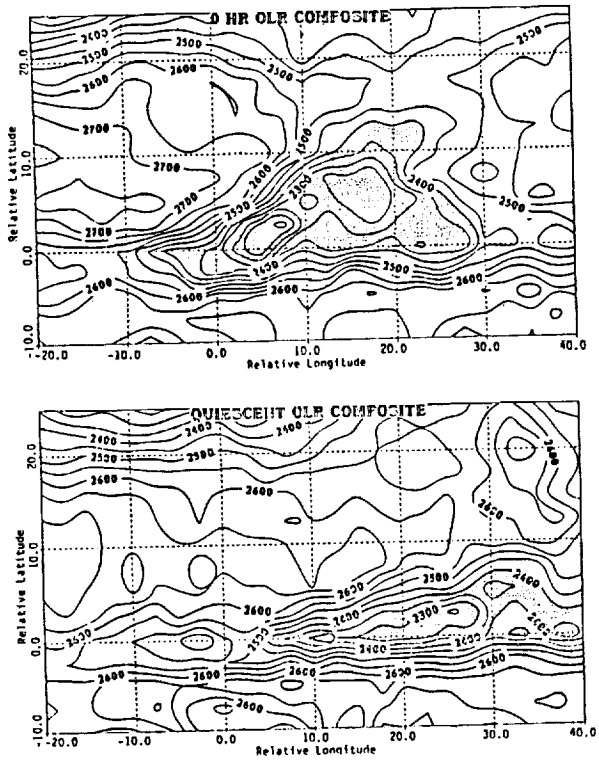

Fig. 2. (top) OLR composites of 35 tropical plumes, centered at the plume origin at 0° relative longitude and the ITCZ, and (bottom) 35 quiescent days. Units in 0.1 W/m²; high cloud regions are shaded.

When plumes are not active, the ITCZ is predominantly zonal and convectively weaker (10–15 W/m² warmer). The dry subsidence region poleward of the active convection (the subtropical high) is larger, more zonally oriented, and not as cloudy or warm (5–10 W/m² cooler). Thus, in the zonally symmetric mode, it can be inferred that the Hadley cell is weaker.

Figure 3 reproduces the composite events from Fig. 2, as viewed in VAS water vapor imagery. The patterns are similar but not identical. The wave nature of the plume and the contrast between zonally symmetric and plume states is stronger in the vapor imagery. Smaller scale details are different in the two views of the composite. A subset of the composite cases is shown in Fig. 4, as viewed in TOVS vapor channel data (6.7 μm). The plume composite has had the climatological brightness temperatures subtracted from it. The quiescent composite is apparently dissimilar to those in Figs. 2 and 3, only partly because of the larger domain represented; between 105° and 165°W the ITCZ is oriented more SW–NE and is displaced about 5° farther south. The subtropical high appears to be more of an east-west wave feature, rather than a zonally banded one because of its weakness in the eastern Pacific. The quiescent mode however more nearly resembles Figs. 2 and 3 than the climatological mean over which data were analyzed. The ITCZ is disappears east of 110°W. The plume composite of Fig. 4 implies a significant amplification of the climatological pattern and generally resembles the vapor imagery composite in Fig. 3. Within the plume region, all cloudy observations are absent in Fig. 4; therefore, Fig. 4 underestimates the plume signal.

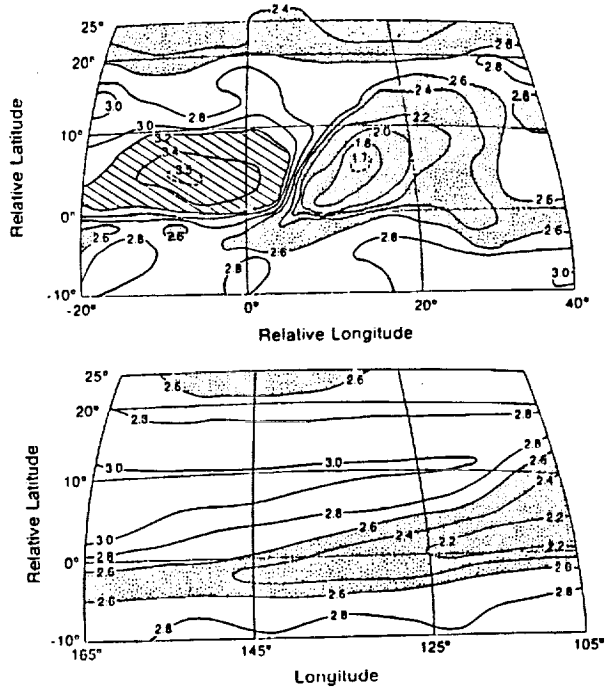

Fig. 3. As in Fig. 2, except for GOES VAS water vapor imagery composites. Units from 1–4 correspond to gray-scale from white (cloud) to black (clear); shading denote brightest clouds.

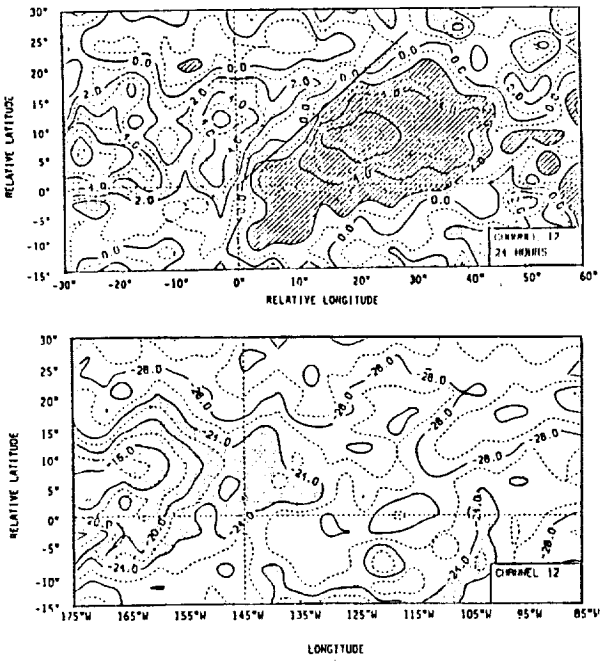

Fig. 4. (top) Anomalies of TOVS 6.7 μm water vapor brightness temperature composites of 17 plume events and (bottom) 17 "quiescent" days. Units in °C with shading dry and hatching/heavy line moist.

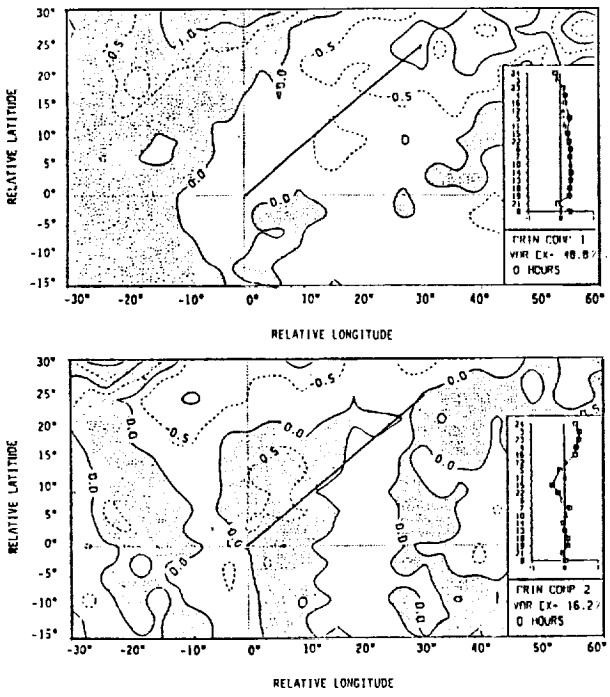

Fig. 5. EOF decompositions of TOVS tropospheric channel radiance observations for 17 plume events. Insets show approximate vertical structure and % eddy variance explained: (top) tropospheric average temperature and (bottom) tropospheric thermal wave--warm over cold; mappings give amplitudes with positive regions shaded.

Finally Fig. 5 presents two empirical orthogonal function decompositions of TOVS tropospheric channels for the Fig. 4 plume composites identifying two thermal patterns valid at the origin of the plumes. The insets show the approximate vertical thermal structure and the amount of total channel variance explained (the zonally symmetric structure has already been removed). The upper panel is a tropospheric average temperature signal, warm to the west of the plume, cold to the east. The lower panel depicts a synoptic scale, equivalent barotropic, upper tropospheric wave. Within the plume, the structure is warm air over cold, with the opposite to the west of the plume origin.

3. PRECURSOR SIGNALS

Figure 6 depicts composite maps of VAS imagery, OLR analysis, TOVS water vapor analysis and the EOF thermal wave 24 to 48 h before composite plume initiation; that is, mean precursor forecast signals. A strong (useful) wave signature appears in the vapor imagery, less strongly and a slightly different configuration in the TOVS vapor composite, not at all in the OLR analysis, and very strongly in the upper tropospheric thermal wave (TOVS). The OLR fails because, at times long before plume initiation, insufficient vertical motion has been generated to develop an organized cloud field; the OLR however does demonstrate the difference between the quiescent mode and the plume precursor phase--the quiescent case represents a relatively active, but zonally symmetric ITCZ. The discrepancies between TOVS and VAS vapor channels is unclear, but should be related to the overall discrepancy between the climatological patterns of the two systems. The TOVS thermal pattern demonstrates that dynamical disturbances exist already at this time in the deep tropics, even before any tropical development has occurred in conjunction with the mid latitude trough (a common feature associated with plumes and identified in the northwest corner of the VAS vapor composite of Fig. 6).

4. COMPARISON AND SUMMARY

The major differences between the observing systems deal with resolution and clouds. VAS imagery is continuous and interprets clouds simply as very wet regions. TOVS either corrects the observations to an equivalent no-cloud brightness temperature, or makes no observation at all in overcast cloud. OLR detects only cloud; moist unsaturated regions are equivalent to dry. Thus as tropical plumes evolve, they will be underestimated seriously by TOVS, which eliminates observations in the cloud plume region; the same problem exists in active ITCZ regions (like the quiescent mode). Resolution should not be a problem in these analyses because the compositing technique will minimize sampling errors. The discrepancy which exists between the vapor channels (TOVS and VAS), particularly in precursor stages when cloud contamination is minimized, is more difficult to understand. For pattern differentiation, vapor

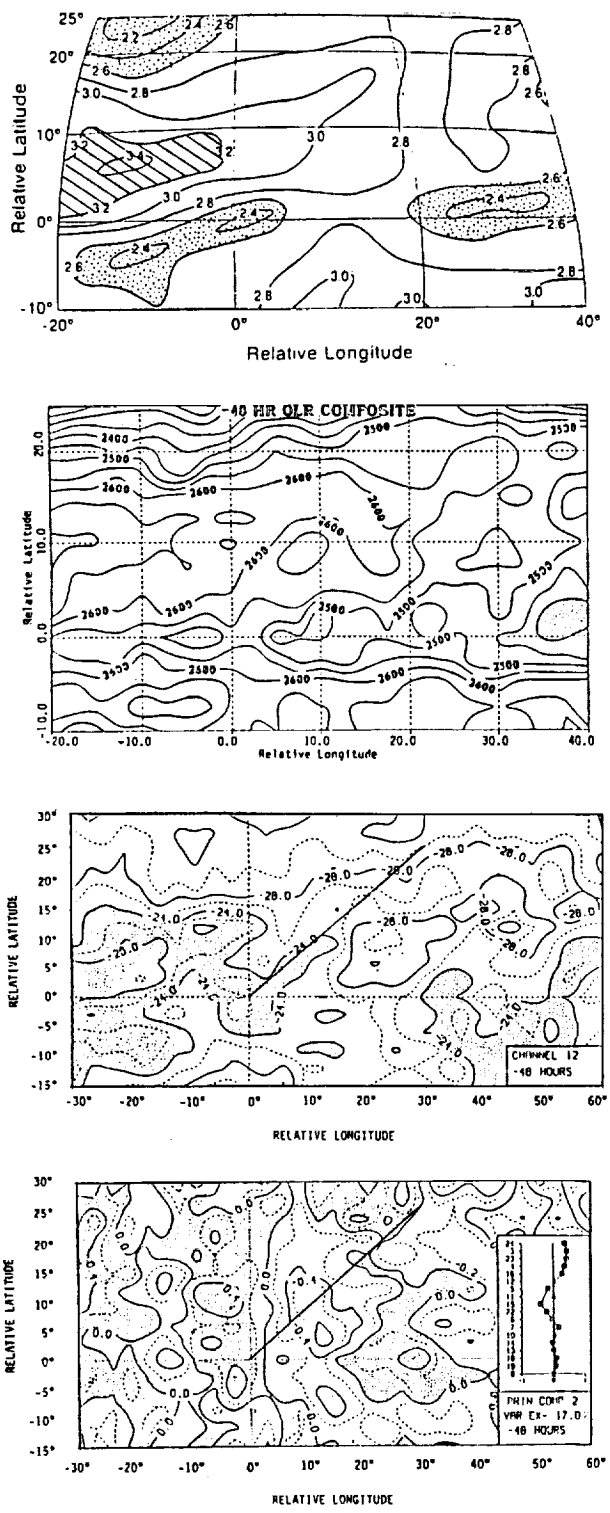

Fig. 6. Precursor composite signatures (24-48 h before plume initiation) for VAS imagery (top), OLR analysis (2nd), TOVS vapor channel (3rd), and TOVS thermal wave (bottom). Shading consistent with previous figures.

imagery may be superior to both vapor soundings channels and OLR because it senses meaningful information in both cloudy and cloud free regions.

The most significant results are:

I. All the satellite sensors detect similar and useful patterns;

II. The patterns are sufficiently different that independent synoptic information is available in each;

III. Cloud, vapor and temperature information each can be isolated;

iv. Tropical signatures are sufficiently strong that useful signatures can be detected in both moisture and thermal patterns both in the presence of clouds and even before their development;

v. The ITCZ exhibits a zonally symmetric convective phase and an enhanced regional convective phase (plumes), both of which can be differentiated from climatological mean behavior.

5. ACKNOWLEDGEMENTS

The research reported here is supported by NASA's George C. Marshall Space Flight Center, under Contract No. NAS-37284.

6. REFERENCES

Hayes, P.M., and J.P. McGuirk, 1989: Active modes of the Pacific ITCZ, *Preprints, AMS 18th Conf. on Hurricanes and Tropical Meteorology*, San Diego, May 1989.

Lin, R-Q., and D.K. Mock, 1986: A test of the ECMWF model in tropical synoptic-scale diagnosis. *Mon. Wea. Rev., 114*, 1519-1538.

McGuirk, J.P., A.H. Thompson and N.R. Smith, 1987: Moisture bursts over the tropical Pacific Ocean, *Mon. Wea. Rev., 115*, 787-798.

Paper presented at
4th Conference on Satellite Meteorology
and Oceanography, American Meteorological
Society, San Diego, CA, May 1989.

TROPICAL SYNOPTIC SCALE MOISTURE FIELDS OBSERVED FROM THE NIMBUS-7 SMMR

J. D. Fink and J. P. McGuirk

Department of Meteorology, Texas A&M University
College Station, TX 77843-3146 (409-845-4431)

1. INTRODUCTION

Nimbus-7 SMMR brightness temperatures from a 7 days in January 1979 and a 3 days in May 1979 are used to estimate precipitable water over the tropical eastern Pacific Ocean. The estimates are made from an algorithm developed by Wilheit and Chang (1980). The SMMR estimates are compared within the context of five typical tropical synoptic features: Tropical Plume (TP), a synoptic cloud system described by McGuirk et al. (1987); Subtropical High (STH); Active ITCZ (AITCZ); Quiescent ITCZ (QITCZ); Equatorial Dry Zone (EDZ), a subsidence region between 90° and 120° W.

Comparisons are made between the SMMR based precipitable water estimates and each of the following: TIROS-N 7.3 and 6.7 micrometer water vapor channels (TOVS 11 and TOVS 12, respectively), TIROS-N 10.5-12.5 micrometer Outgoing Longwave Radiation (OLR), and a model estimate from the European Center for Medium Range Weather Forecasts (ECMWF).

2. WATER VAPOR EVALUATION

SMMR estimates of precipitable water have a rms difference with respect to radiosondes of only 2.5 kg m^{-2} at a resolution of 60 km; therefore they will be treated as "ground truth".

2.1 Correlations and Mean Synoptic Structure

A set of 540 concurrent observations over the entire period are available for the five moisture estimators. Collocated cross correlations between the estimators are presented in Table 1a. Each estimator provides information about the moisture in the atmosphere when compared to SMMR; the best correlation is with the ECMWF analysis and then with TOVS 11. Though TOVS 11 and TOVS 12 are highly correlated, the SMMR and TOVS 11 correlation is superior because the TOVS 12 is too sensitive to insignificant upper tropospheric moisture; this sensitivity leads to serious errors in relatively dry atmospheres. The SMMR and OLR correlation of −0.56 is a precipitable water and cloud correlation; the correlation is not high because cloud cover (cirrus) does not guarantee a deep layer of moisture.

The data were separated geographically by feature and cross correlations were computed. Half of the correlations within the five synoptic features were not significantly different from zero, due only in part to the small sample sizes. Results are shown in Table 1b for TPs, with statistically insignificant correlations deleted. Table 1b is exceptional only in that most correlations are significant for TPs. The only insignificant correlations are those between ECMWF and infrared satellite observations. The interpretation of Table 1 is that (a) represents primarily interregional variation and (b) represents intrasystem variations associated with synoptic structure. Only small intrasystem signals exist, and these signals are largest in TPs and the AITCZ, where observed variability is largest.

Table 1a. Correlation of precipitable water estimates.

	TOVS 11	TOVS 12	OLR	ECMWF
SMMR	−.61	−.48	−.56	.70
TOVS 11	*	.89	.66	−.56
TOVS 12	*	*	.55	−.44
OLR	*	*	*	−.44

Table 1b. Correlation of precipitable water within TPs.

SMMR	−.35	−.36	−.28	.46
TOVS 11	*	.90	.60	
TOVS 12	*	*	.55	
OLR	*	*	*	

Comparisons of individual SMMR estimates with TOVS 11 and ECMWF estimates are shown in Fig. 1. Although correlations are good, scatter in the two plots is large. SMMR estimates span nearly the entire range for every ECMWF and TOVS 11 value.

Mean values and standard deviations within the five features showed that the TP and AITCZ had the highest moisture contents and standard deviations. SMMR and ECMWF possessed mean values within TPs and QITCZs that are statistically alike, implying that TPs resemble a QITCZs; the main difference is that TPs have a larger standard deviation than QITCZs.

2.2 Prediction of Precipitable Water

SMMR observation are estimated by multiple regression of TOVS 11, TOVS 12, OLR, and the ECMWF analysis, listed in order of decreasing importance. All four coefficients were statistically significant and the regression had a coefficient of determination $R^2 = 0.67$. Fig. 2 compares the resulting predicted and observed SMMR. The largest under predictions occurred within the AITCZ region, typically 15 kg m^{-2}. The largest overpredictions occurred within TPs and the EDZ, typically 10 kg m^{-2}. Inspite of the systematic nature of prediction errors, no statistically significant regressions were obtained within

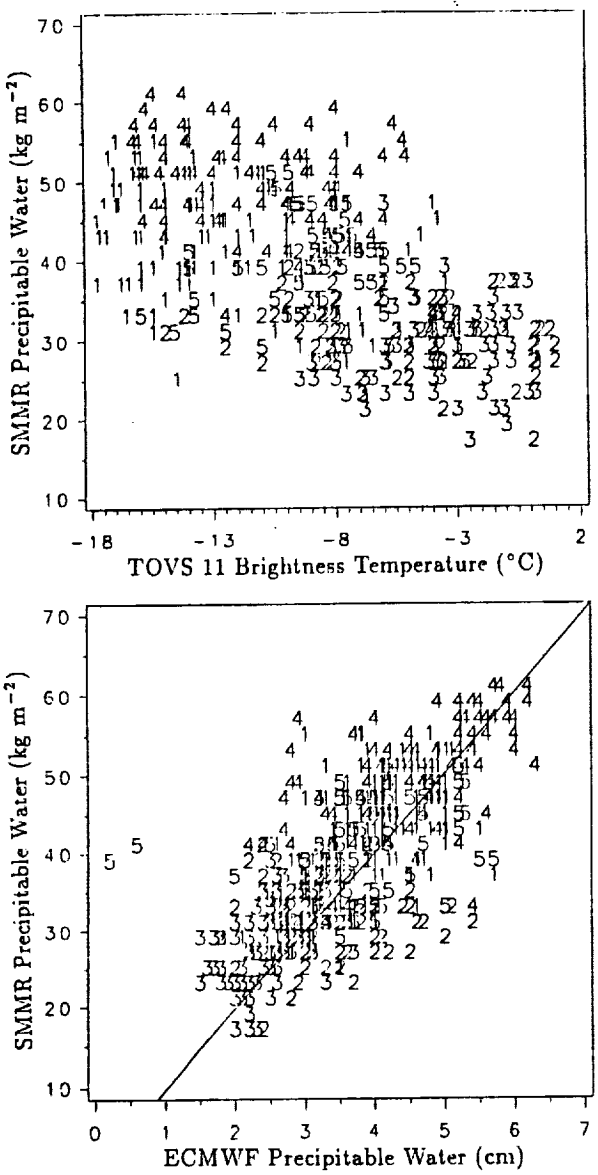

Fig. 1(top). Plot of SMMR precipitable water vs. TOVS 11 brightness temperature. (bottom) SMMR precipitable water vs. ECMWF. Data points 1=TP, 2=EDZ, 3=STH, 4=AITCZ, 5=QITCZ. The straight line would be a perfect fit.

synoptic features.

Figure 3 compares SMMR, ECMWF and predicted SMMR along the western edge of a single SMMR pass. The ECMWF estimates two maxima, at 3° N and 15° S, corresponding to an AITCZ and Southern Hemisphere convection; at 30° N is the dry STH. SMMR detects a similar pattern except the AITCZ is wetter. and the moist region is continuous into the southern hemisphere. The predicted SMMR nearly corrects for the ECMWF underprediction from 5 to 15° S; unfortunately it over predicts the moisture in the STH at 30° N.

3. SUMMARY

All five water vapor estimators are correlated; unfortunately most of the correlation is explained by regional differences, not by synoptic structures. Most of the geo-

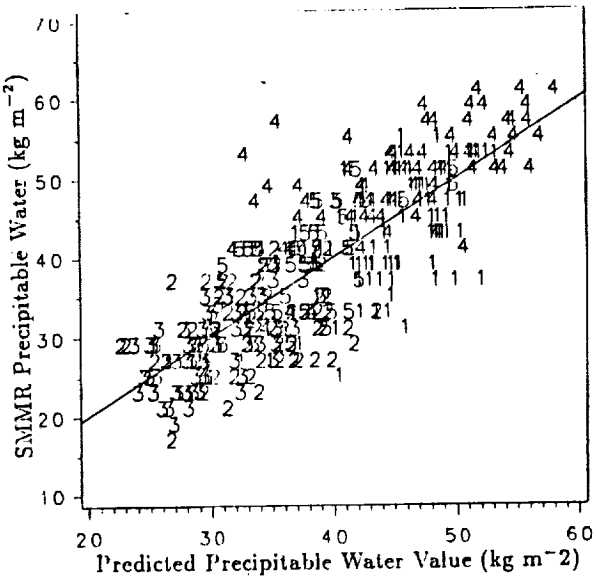

Fig. 2 Same as Fig. 1 except SMMR precipitable water vs. predicted SMMR precipitable water.

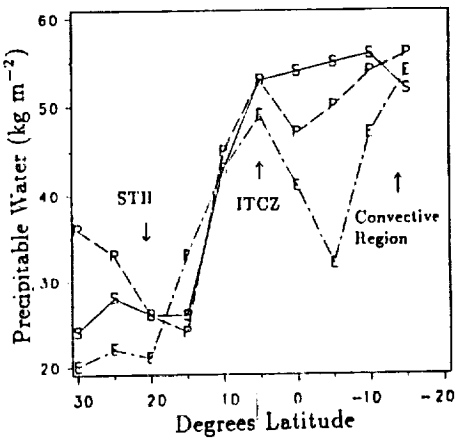

Fig. 3. Plot of SMMR (S), Predicted SMMR (P), and ECMWF (E) along the western edge of a SMMR pass at 160° W about 1200 GMT May 16, 1979.

graphical SMMR variation can be predicted from a model and infrared satellite observations. These predictions can differentiate between the TPs, EDZ, STH, AITCZ, and QITCZ.

4. ACKNOWLEDGMENTS

The research is sponsored by NASA's George C. Marshall Space Flight Center, under Contract No. NAS-37284. Jeffrey Fink acknowledges the support of the United States Air Force Institute of Technology.

5. REFERENCES

McGuirk, J.P., A.H. Thompson and N.R. Smith, 1987: Moisture bursts over the tropical Pacific Ocean, *Mon. Wea. Rev.*, *115*, 787–798.

Wilheit, T.T., and A.T.C. Chang, 1980: An algorithm for retrieval of ocean surface and atmospheric parameters from the observations of the Scanning Multichannel Microwave Radiometer, *Radio Science*, *15*, 525–544.

Paper presented at
4th Conference on Satellite Meteorology
and Oceanography, American Meteorological
Society, San Diego, CA, May 1989.

UNIQUE SIGNATURES OF SYNOPTIC FEATURES IN TIROS N SATELLITE DATA

G. A. White III and J. P. McGuirk

Department of Meteorology
Texas A&M University
College Station, Texas 77843-3146

1. INTRODUCTION

Observed tropical synoptic temperature variations are nearly absent from satellite derived temperature profiles. Enhanced information and increased resolution might be obtained through improved processing and analysis techniques using currently available data. White and McGuirk (1987) and White et al. (1988) described methods to extract meteorologically significant tropical synoptic features directly from satellite brightness temperatures. This research describes how these features can be quantified.

2. TECHNICAL CONSIDERATIONS

2.1 Radiative transfer model (RTM)

To develop analytical techniques a database of "satellite observed" synoptic features with known statistical properties was generated from a RTM. The RTM (Susskind et al., 1982) directly calculates satellite channel brightness temperatures that would have been measured from the TIROS N satellite had it viewed the atmosphere under study. The RTM supports 22 of the TIROS N's 27 channels.

2.2 Data

Nine tropical "seed" soundings of temperature and dew point, each containing a typical synoptic feature, were perturbed at each of 66 layers required by the RTM to generate a large set (50 each) of similar soundings. This random perturbation increased the sample size to one that is statistically meaningful given 22 satellite channels, while maintaining the integrity of the synoptic class. The perturbations of temperature and dew point in each sounding were introduced as white noise, highly correlated in the vertical, to simulate observed atmospheric variability. The nine seed soundings consisted of four inversions (frontal, radiation, turbulence and trade-wind), a warm-humid sounding, two observed island soundings, a warm anticyclone with a subsidence inversion, and the U.S. Standard Atmosphere to provide a baseline. The RTM produced 50 vectors of 22 brightness temperatures for each seed sounding.

2.3 Multivariate analysis

White and McGuirk (1987) demonstrated that such datasets can be partitioned, by variance, into two physically different portions: one explaining differences between synoptic sounding classes; the other detailing the fine structure within each sounding class. The former is described with canonical discriminant analysis (CDA); the latter, with rotated factor analysis (RFA).

3.0 ANALYSIS AND RESULTS

3.1 Sounding class (CDA)

CDA specifies the vertical structure functions by which the original soundings are sorted into their original classes. The first three structures are shown in Fig. 1. 58% of the between-class variance is contained in the first canonical variable. This variate senses tropospheric average temperature, even though the seeds possessed nearly identical mean temperatures. CAN2 explains 26% of the between-class variance, primarily in moisture and window channels. CAN3 accounts for 10% of the variance and is sensitive to mid tropospheric temperatures and surface temperatures of opposing signs. CAN2 and CAN3 together resemble a lapse rate signal with 2 being a moisture sensitive part and 3 being a moisture insensitive part. Rarely are more than three canonical variables required to explain most of the variance structure of satellite soundings.

3.2 Synoptic structure (RFA)

After classification, the synoptic characteristics of individual classes were quantified through their within-class variance. Factor analysis differentiates soundings from the same seed; the factors are rotated orthogonally to simplify structural information. Details of trade wind and frontal inversions are presented.

3.3 Specific inversion structures

Trade wind inversions are described by three factors (Fig. 2) explaining almost 90% of the total within-class variance. The first factor can be interpreted as a boundary layer lapse rate and average tropospheric temperature. Factor 2 contains the mid tropospheric water vapor channel and the near-surface temperature channels. Factor 3 shows surface contributions and a weak water vapor signal. Together they specify variations among trade wind inversions.

The frontal inversion is described by four factors (Fig. 3) which account for 94% of the variance within frontal soundings. Factor 1 describes lower tropospheric average temperature. Factor 2 relates temperature and moisture in the mid and upper troposphere. Factor 3 is a weak tropopause signal and is not shown. Factor 4 is a lapse rate signal.

4. CONCLUSIONS

The utility of satellite data depends, in part, on analysis methodology. This research describes splitting the variance of satellite observations into a portion which characterizes gross synoptic conditions, and a portion which quantifies details of the gross conditions. Factors identifying sounding types are different than those quantifying structural detail; structural factors vary between sounding types. Multivariate statistical techniques potentially can extend the use and information content of currently available satellite observations.

5. ACKNOWLEDGEMENTS

This research is supported by NASA's George C. Marshall Space Flight Center. GAW acknowledges the support of the U.S. Air Force Institute of Technology. Susskind and Reuter of the NASA Goddard Laboratory for Atmospheres provided the RTM.

6. REFERENCES

Susskind, J., J. Rosenfield, D. Reuter and M. T. Chahine, 1982: The GLAS physical inversion method for analysis of HIRS2/MSU sounding data. NASA Tech. Memo. 84936, Goddard Space Flight Center, Greenbelt, MD, 101 pp.

White, G. A. and J. P. McGuirk, 1987: Canonical discriminant analysis of synoptic signatures in satellite brightness temperature. Preprint from Tenth Conference on Probability and Statistics in Atmospheric Sciences, Edmonton, Alberta, Canada, Amer. Meteor. Soc.

_____, _____ and A. H. Thompson, 1988: Identification and recovery of discontinuous synoptic features in satellite-retrieved brightness temperatures using a radiative transfer model. Preprint from Third Conference on Satellite Meteorology and Oceanography, Anaheim, CA, Amer. Meteor. Soc.

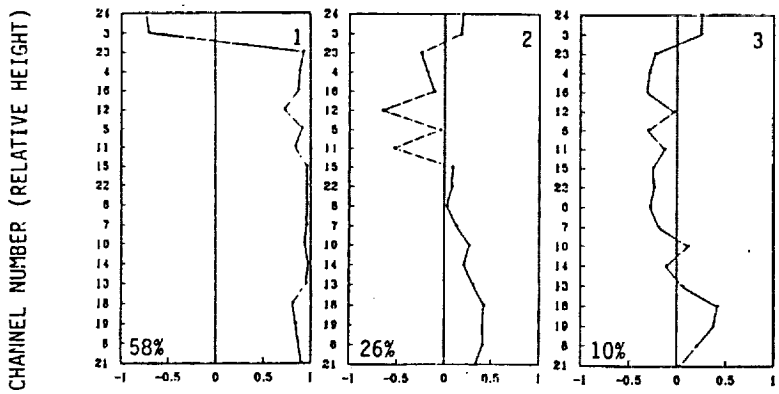

Fig. 1. Canonical variables identifying classes based on nine seed soundings. Channel numbers appear as the vertical axis according to each channel's weighting function maximum. Horizontal axis is the normalized channel amplitude. CAN1 represents tropospheric temperature; CAN2 represents water-vapor and surface window channels; CAN3 represents mid-tropospheric temperature and lapse rate. Per cent of explained <u>between</u>-class variance is given.

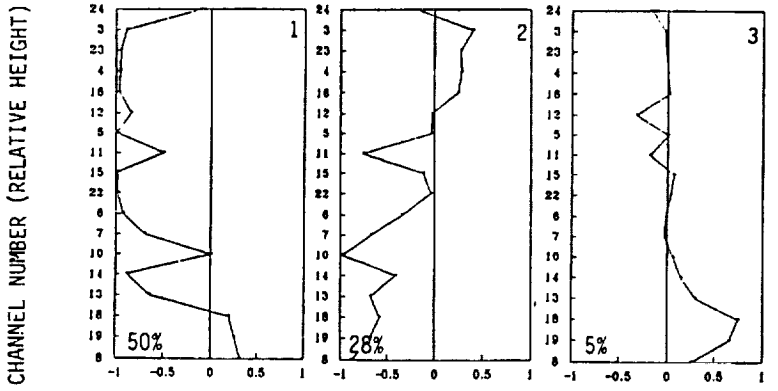

Fig. 2. Rotated factor loadings from a set of trade wind inversions. Axes as in Fig. 1. Factor 1 describes a near-surface inversion and tropospheric average temperature; factor 2 quantifies the amplitude of the trade wind inversion; factor 3 identifies low level moisture. Per cent of explained <u>within</u>-class variance is given.

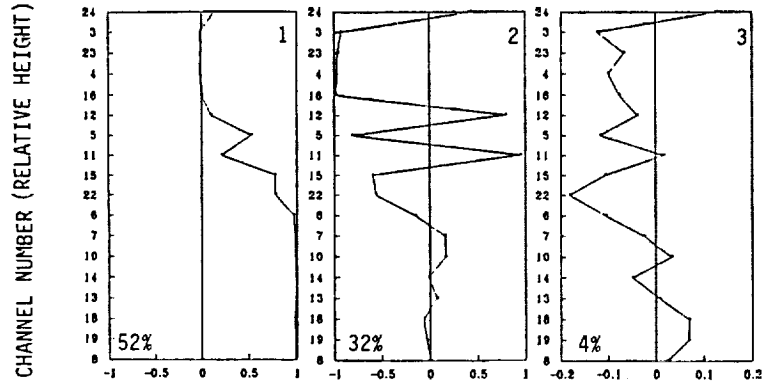

Fig. 3. As in Fig. 2, except for frontal inversions. Factor 1 quantifies lower tropospheric temperature; factor 2 is a mid and upper tropospheric temperature/moisture signal; factor 4 is a lapse rate signal (Note expanded scale).

Barotropic Mechanisms Associated With Tropical Plume Formation

C.A. Askue and J.P. McGuirk
Department of Meteorology
Texas A&M University
College Station, TX 77843-3146
(409-845-4431)

Paper presented at:
Seventh Conference on Atmospheric Waves and Stability, American Meteorological Society, San Francisco, Marcy, 1989.

This paper describes the dynamical framework of tropical plumes and preliminary investigation of the barotropic wave interactions accompanying their evolution. The tropical plume is a common wave disturbance in equatorial regions. From satellite the plume appears as a continuous, narrow band of middle and high cloud, at least 2000 km in length, originating near the equator and extending into subtropical and middle latitudes. Many plumes develop each season along the Pacific ITCZ.

Case studies reveal that the following dynamic features precede and accompany a tropical plume: a low-level synoptic-scale disturbance, an upper-level planetary-scale equatorial wave; a midlatitude trough that intrudes into the tropics; and an upper tropospheric equatorial wave (approximately 3000 km in wavelength and essentially in phase with the midlatitude trough.)

Although the speed and consistency of plume development suggest a common dynamic instability, simple barotropic or baroclinic wave instability of a zonal current is unlikely. The plume creates a more unstable zonal flow as it evolves. In addition, the initial stages of a tropical plume appear to be detached from both CISK associated with the low-level disturbance and baroclinic effects of the midlatitude trough. Therefore, it is hypothesized that barotropic instability, but not necessarily of the zonal current alone, may be an important mechanism for initiating tropical plumes.

The method of investigation involves examining the stability of inviscid, horizontally-sheared, barotropic basic states with respect to a series of perturbations. In particular, the stabilities of Rossby wave and Kelvin wave basic states are considered. The investigation is handled numerically with a one-layer, shallow water, gridpoint model on an equatorial β-plane. Boundaries are periodic in the east-west direction and solid, free-slip walls north and south. Model-generated fields of zonal and meridional winds, relative vorticity, and momentum flux are interpreted with respect to observed fields. The interaction of synoptic-scale and planetary-scale waves is described. The capability of this interaction to generate synoptic-scale waves by quasi-linear barotropic processes is evaluated.

CIRA Satellite Research Workshop,
Colorado State University, Sept.
1988.

James P. McGuirk
Texas A&M University
College Station, TX 77843

HORIZONTAL AND VERTICAL PATTERN RECOGNITION IN SATELLITE RADIANCE DATA

The following figures present examples of two types of signal extraction technique which show merit for analysis and interpretation of satellite observations. They both start from the premise that signal content may be maximized if satellite data are analyzed in their own right, by techniques designed to utilize the strength of the satellite data. This premise is in opposition to an operational approach to satellite analysis which attempts to transform the satellite observations into an "equivalent" more conventional. It is assumed that information is lost when satellite radiance data are converted into equivalent soundings. Although this procedure is adequate in an operational context, more information is available in satellite observations.

What the satellite does best is to measure and display patterns. This feature is what operational meteorologists find most useful.

Vertical Structure

The first technique is essentially a vertical pattern recognition procedure by which TOVS (Tiros Operational Vertical Sounder) observations are utilized to improve the first guess in a typical sounding retrieval scheme. In a procedure similar to empirical orthogonal function analysis (EOF), a set of satellite radiance soundings are split into a set of generic synoptic soundings, each dominated by a specific feature. This partitioning is determined by the structure of the satellite observations themselves. Then each synoptic sub-group is reanalyzed, excluding the information that determines the group and looking instead at the information which determines variability of the specific synoptic feature within the group. These signals are used to quantify properties of the synoptic feature.

Figure 1 summarizes the procedure. A set of many (450) overlapping soundings are generated synthetically from statistical permutation of nine similar seed soundings, each containing a distinct tropical synoptic feature: trade wind inversion, lower tropospheric subsidence inversion, warm-humid sounding, etc. These soundings are passed through a radiative transfer model to produce equivalent synthetic satellite soundings. **Then canonical discriminant analysis is applied to split the variance into a part that determines sounding class (Fig. 1, upper right) and a part that determines the quantitative details of the specific sounding feature (Fig. 1, lower left).** Finally, new soundings can be split similarly, classified and quantified within an operational context.

Figure 2 displays the splitting of the 450 soundings into 9 discrete groups, as functions of the first three canonical variables. Each group contains soundings which fall within an envelope of $\pm$ 30°C, which is an extremely severe test of the procedure. At this large spread, several of the sounding groups are beginning to merge and become indistinguishable. More importantly, two sets of canonical variables are displayed as Fig. 3. The top three represent the distribution of signal among the TOVS channels which explains what separates the sounding groups. They represent, from left to right, tropospheric temperature, moisture/boundary layer temperature, and tropospheric lapse rate signals. They resemble closely eigenvectors in observed sounding retrievals. The bottom three variables display the signal of the first three canonical discriminants associated with variation within soundings distinguished by trade wind inversions. All three describe different aspects of lower tropospheric sounding structure. Most significantly, they are different than the variables accounting for the splitting into groups; that is, those structures normally detected in observations. Thus the technique identifies the existence of signal not typically incorporated into satellite derived soundings. This signal has been identified by isolating the variance associated with specific sounding features. This procedure is equivalent to specifying the first guess sounding more accurately.

Horizontal Compositing

The second technique is pattern recognition in the horizontal domain, simply a mapping or filtering of channel radiance data. The filtering is accomplished by compositing events. All synoptic variations which are not essential to the composited feature are filtered by smoothing; only the features that are common to most cases of a composited synoptic event remain in the composite mapping. Several examples follow.

Figure 4 displays patterns associated with periods of active ITCZ convection as observed in gridded OLR data (shaded areas are cold/convective regions). In the top panel, 22 d with active convection at 160°W were averaged; in the middle panel, 26 d with active convection averaged across the Pacific; and, in the bottom panel, 16 d with both. The important point is that all three convective patterns are different, with convection at a point dominated by meridional scales, and convection at a point coupled with general ITCZ activity dominated by a complex wave structure.

Figure 5 displays a composite of the time sequence of a synoptic feature known as a tropical plume; the data are VAS water vapor imagery, digitized and analyzed, with low values cold/wet and high values warm/dry. This sequence (each separated by 24 h) possesses a sufficiently strong signal 48 h before the plume matures as to allow predictive skill. Figure 6 (top) contrasts the conditions in Fig. 5 to a quiescent period during which no plume activity is occurring; the middle and bottom panels represent the same conditions as the precursor and quiescent panels in the VAS imagery, except these are composites of OLR data. Although the quiescent panels are similar, no signal

is apparent in the OLR precursor composite; therefore, the precursor signal is due to a moisture pattern not observed by a cloud sensing instrument.

The last example is a multivariate TOVS composite of 17 tropical plumes; the compositing is accomplished through EOF analysis, necessitated by the relative absence of data in the broad overcast cloud regions. Insets to panels display the vertical structure of the signal across the TOVS channels (channels are ordered in relative height, and triangles/dashed lines give moisture channels). The patterns display the amplitude of the vertical structure. The origin at 0/0 is the origin point of the plume along the ITCZ, with the heavy diagonal line giving the mean plume cloud axis The top panel displays the leading eigenvector after the zonal average steady field had been removed. It portrays a large amplitude thermal wave with tropospheric warmth over and east of the plume and coolness to the west. The middle panel emphasizes moisture signals, with excessive dryness west of the plume and moistness south of the plume cloud axis. This moisture displacement is due, in part, to sampling properties of different satellites. The bottom panel portrays a low amplitude, upper tropospheric thermal wave which is always associated with plume development. It is tropical wave that propagates upper tropospheric warmth and lower tropospheric instability into the plume origin region just as the plume initiates.

Most of these signals fail to appear in operational analyses until late in a system's development for a variety of reasons. They represent the synoptic state of the tropical atmosphere and satellites observe them.

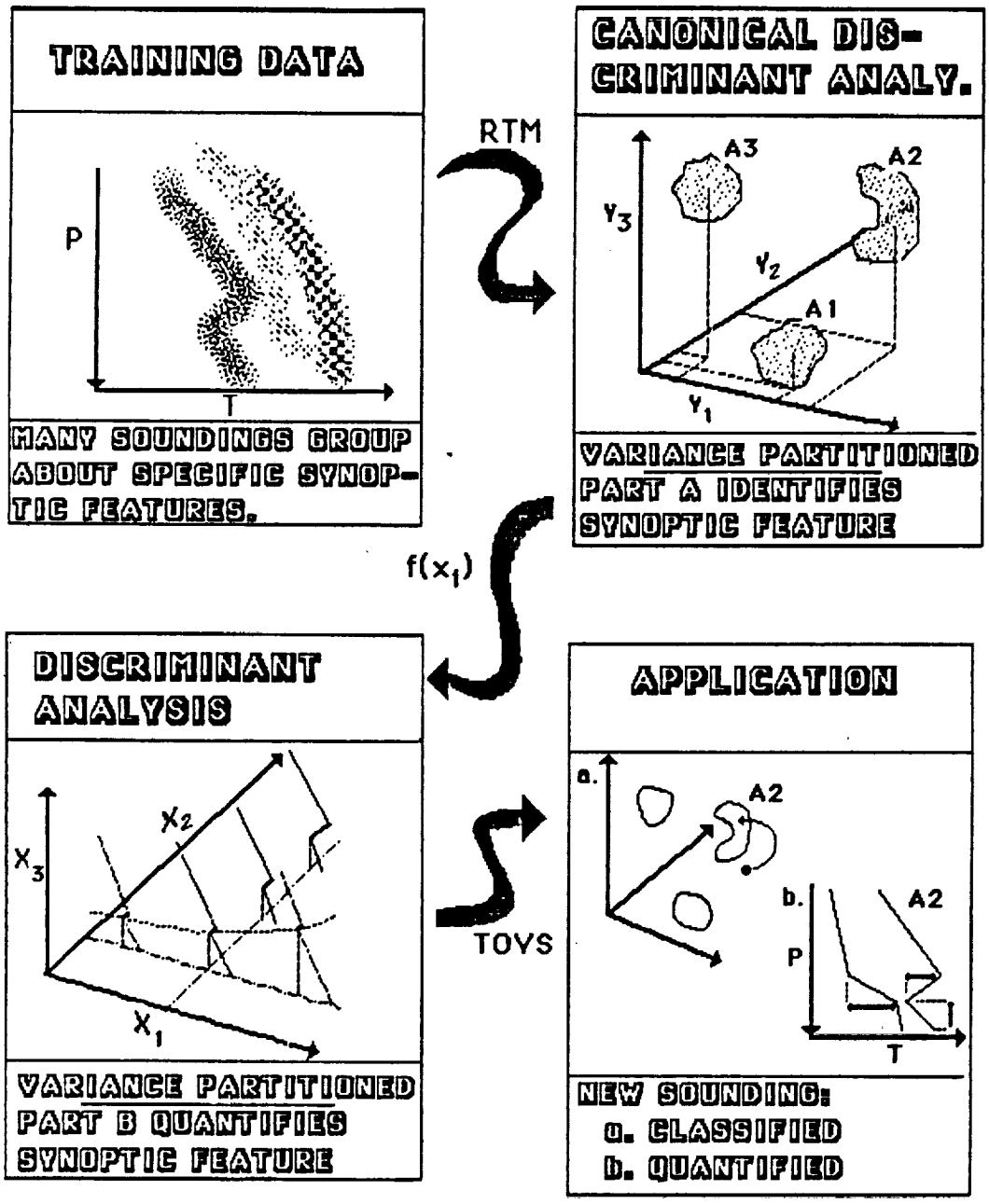

FIG.1 Schematic of statistical technique to identify and quantify synoptic features in TOVS radiance data.

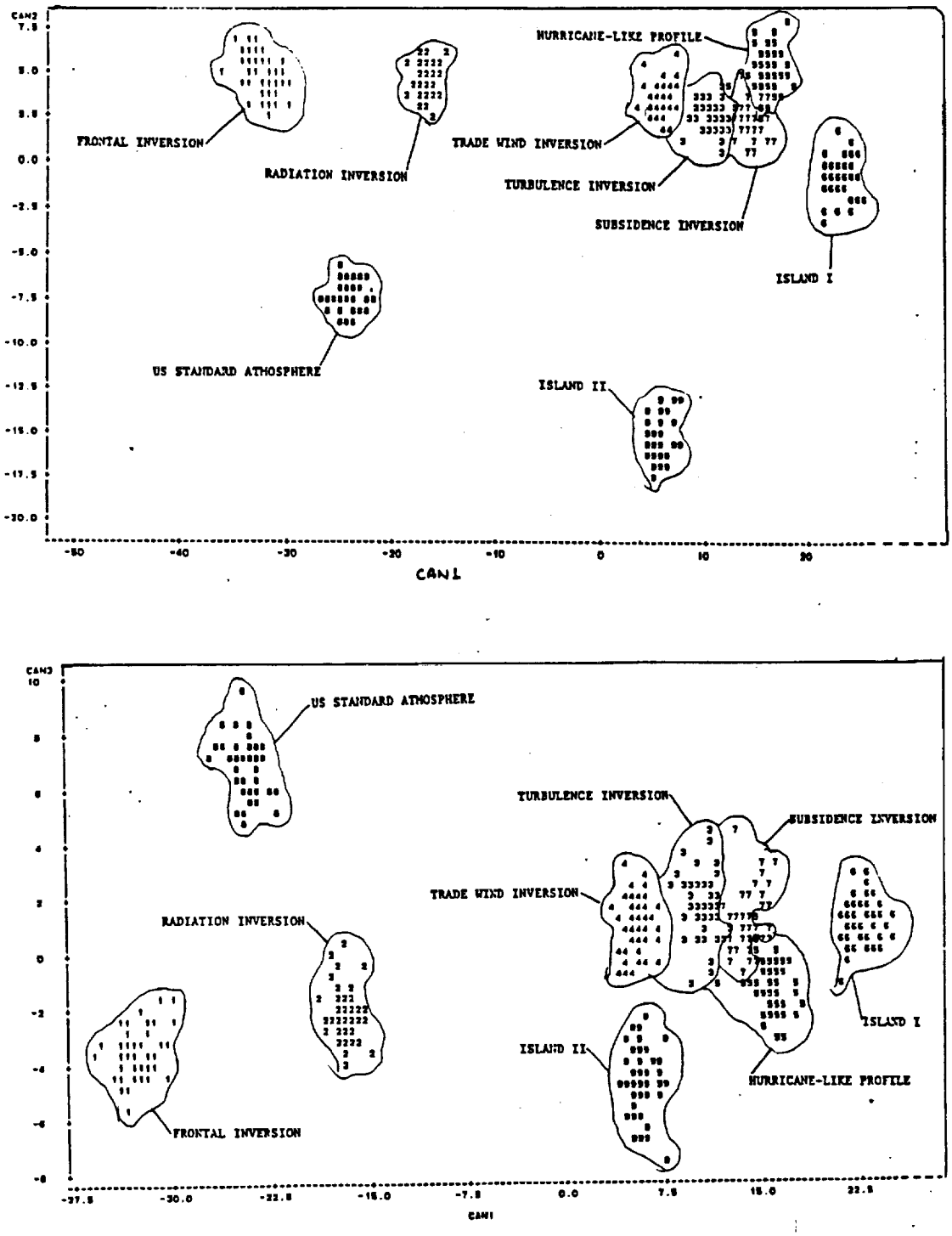

FIG. 2. Separation of sounding groups as a function of canonical variables for a sounding temperature envelope of ± 30°C.

TRADE WIND INVERSIONS

CLASSIFY

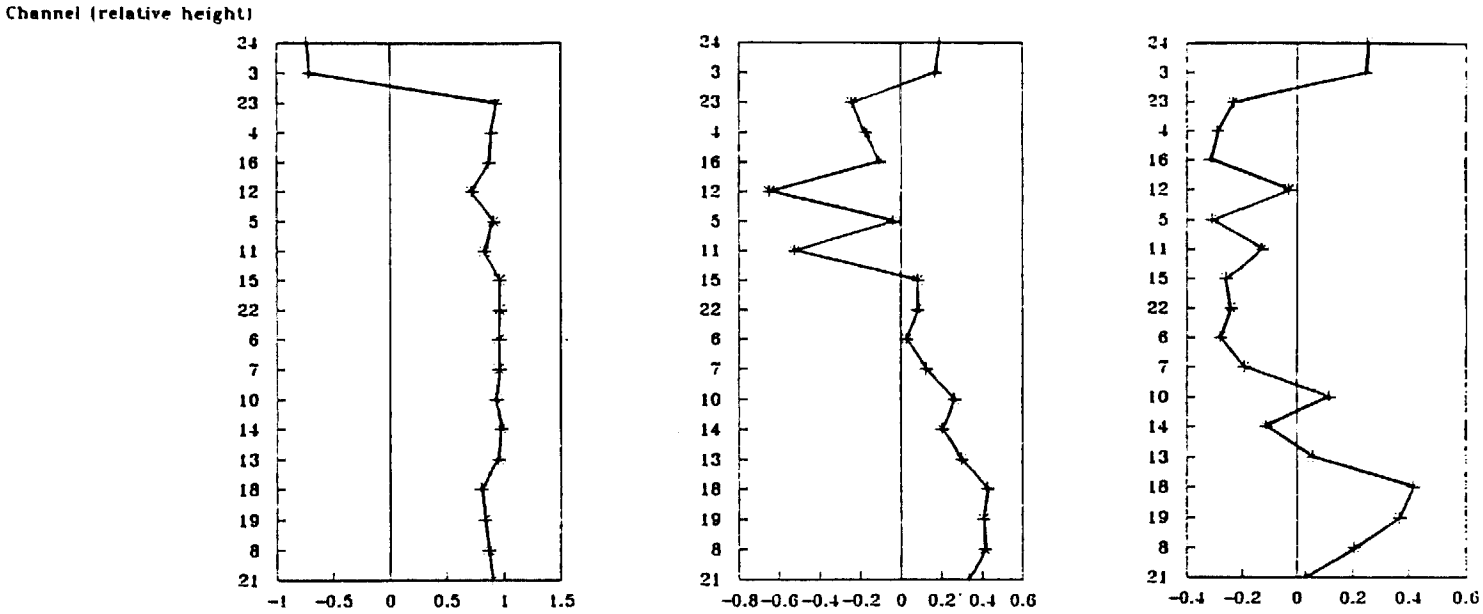

QUANTIFY

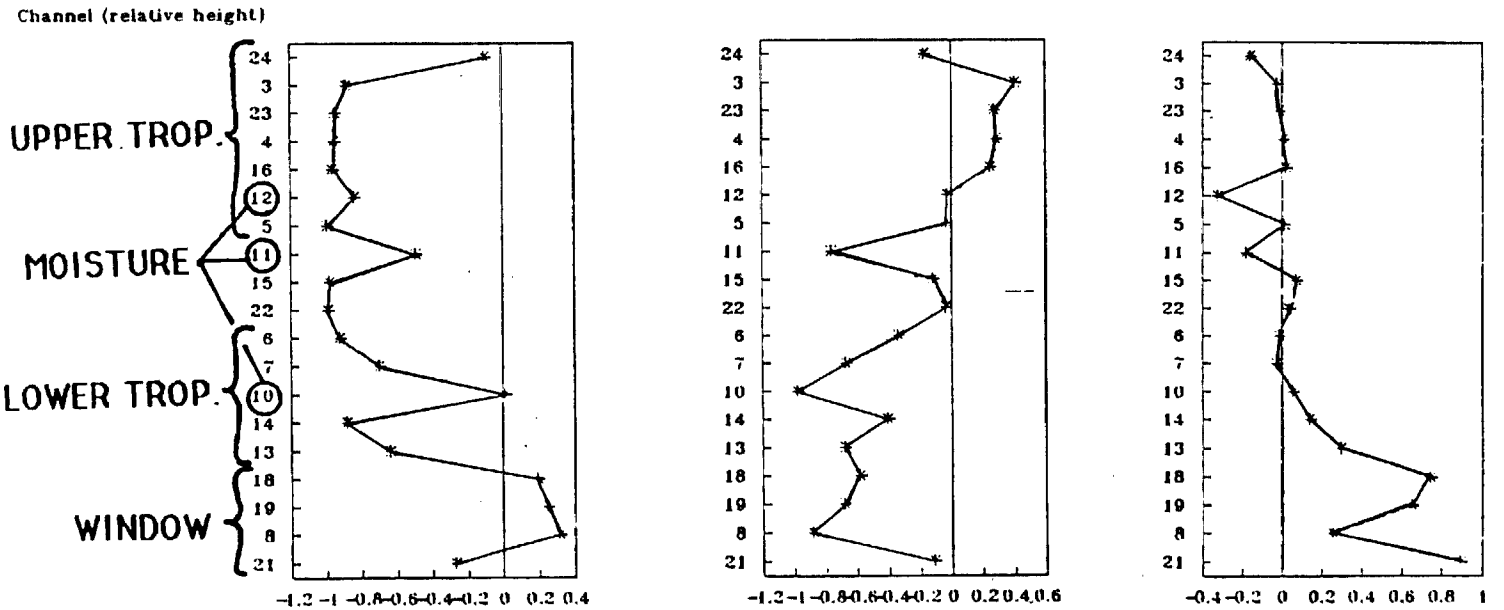

NORMALIZED BRIGHTNESS TEMPERATURE

ACTIVE ITCZ COMPOSITES

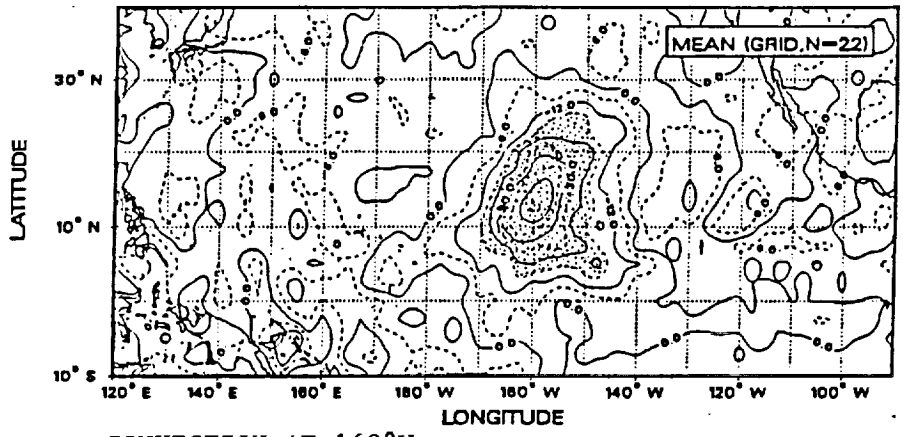

CONVECTION AT 160°W

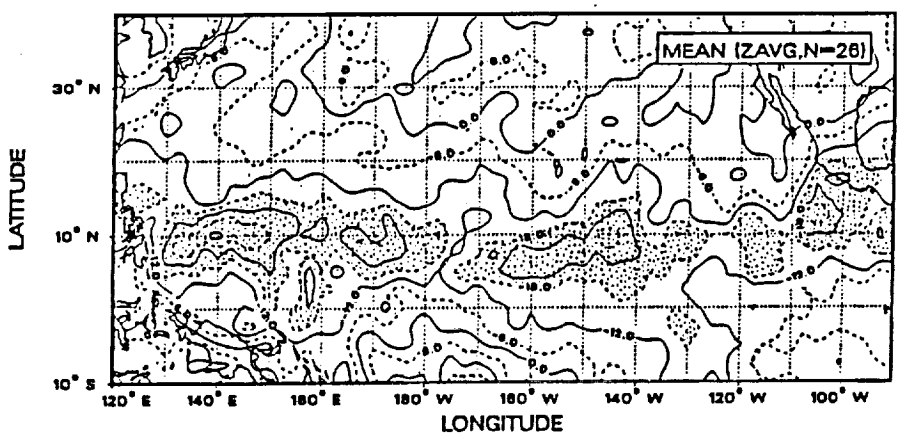

ZONALLY AVERAGED CONVECTION

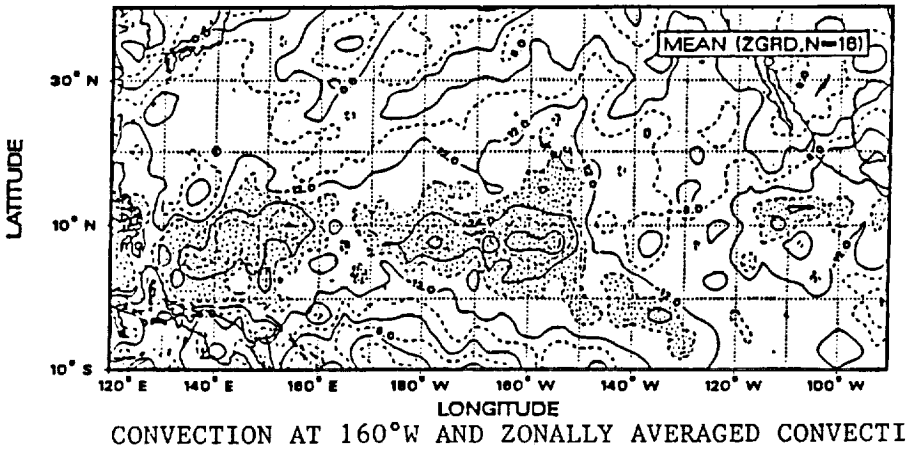

CONVECTION AT 160°W AND ZONALLY AVERAGED CONVECTION

FIG. 4. Example of composites of active ITCZ convection, viewed in OLR data. Negative anomalies (active convection) are shaded.

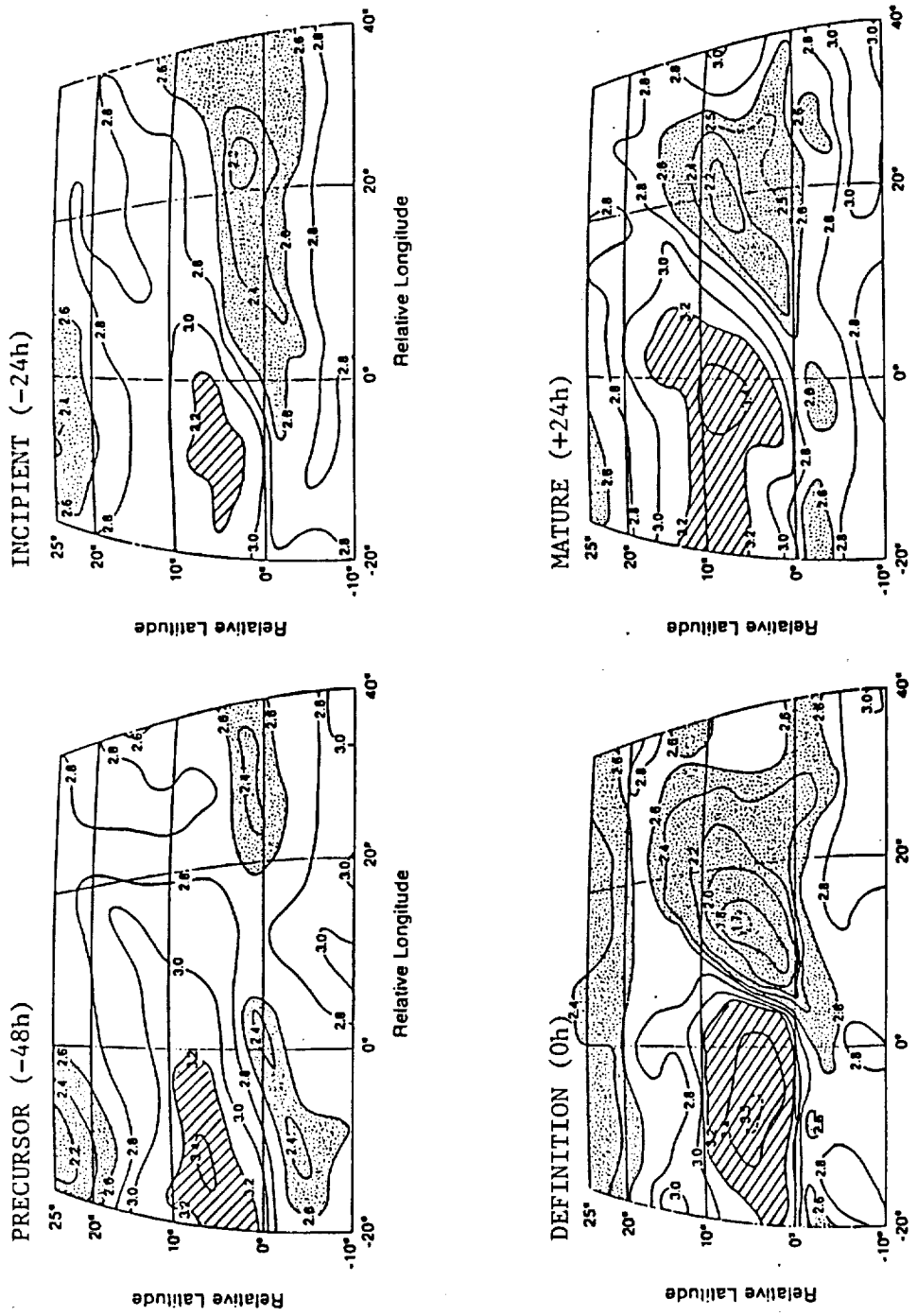

FIG. 5. Example of composited evolution of tropical plume in digitized VAS water vapor imagery. Shaded areas are moist; hatched areas are dry.

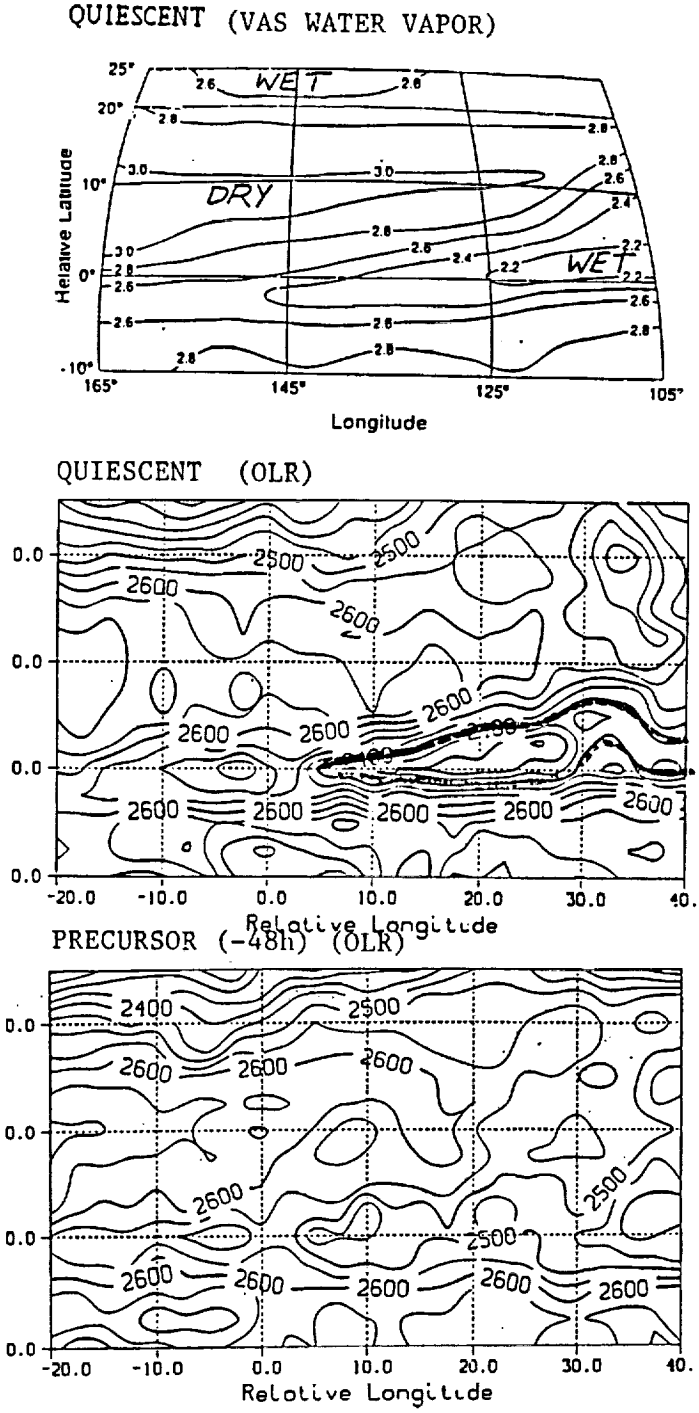

FIG. 6. Comparison of tropical plume composites and precursors in VAS water vapor imagery and gridded OLR observations. See also Fig. 5.

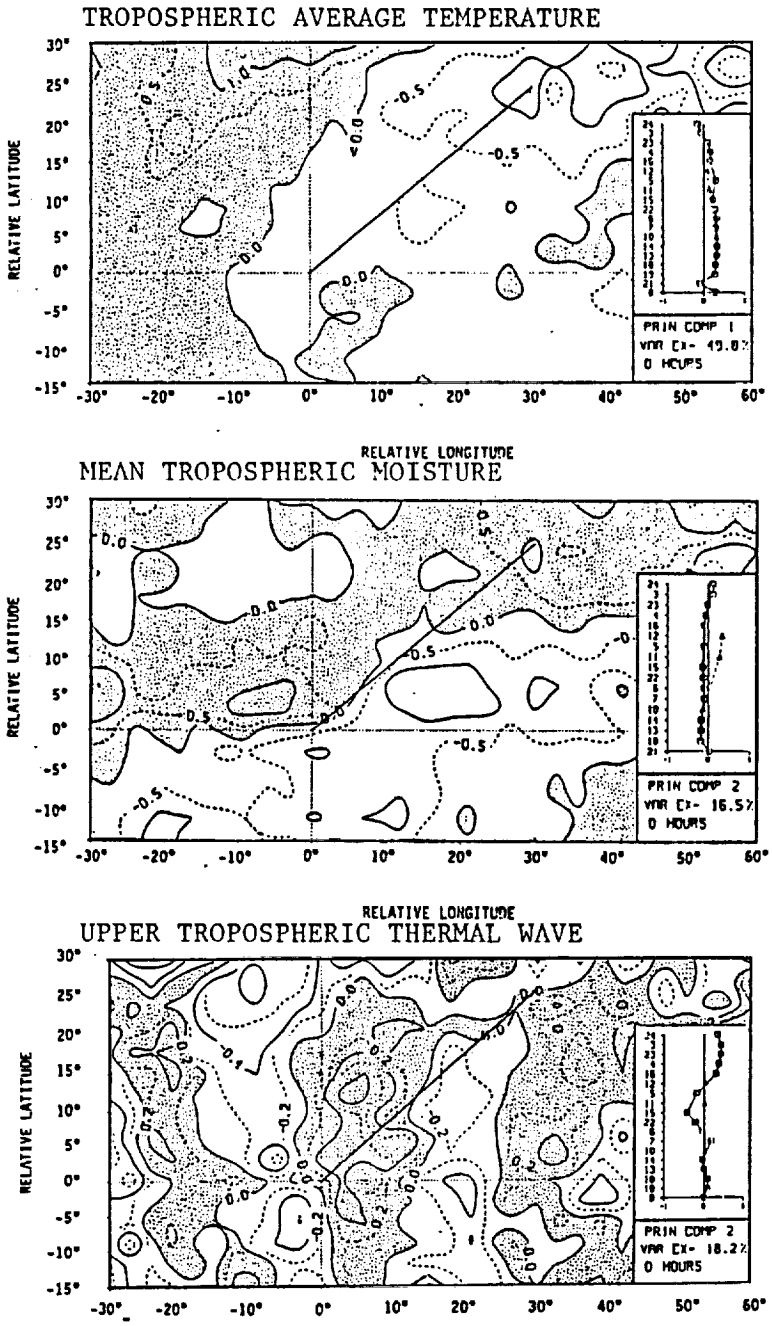

FIG. 7. Examples of composited tropical plume features in TOVS radiance data. Eigenfunctions of vertical structure appear in insets, with channels ordered approximately vertically. Triangles are moisture channels. Positive amplitudes are shaded.

Paper presented at:
Third Conference on Satellite Meteorology and Oceanography, American Meteorological Society, Anaheim CA, February 1988.

TROPICAL SYNOPTIC SIGNATURES IN COMPOSITED 6.7 MICROMETER WATER VAPOR IMAGERY

A. H. Thompson, J. P. McGuirk and D. J. Ulsh

Department of Meteorology
Texas A&M University
College Station, TX 77843-3146

1. INTRODUCTION AND OBJECTIVE

Long plumes or bands of air with above-average moisture content, indicated by extensive cirrus and mixed high and middle clouds, frequently develop near the intertropical convergence zone (ITCZ). These plumes, which we call "moisture bursts," grow rapidly poleward and eastward. These moisture bursts are clearly evident in satellite-derived visual (VIS) and window channel infrared (IR) imagery. The high moisture content of the bursts probably extends beyond the boundaries of the visible cloud mass and provides early indications of the developments.

The objective of this study is to determine the signature and behavior of the moisture bursts as presented in satellite-derived imagery of the 6.7 micrometer water vapor channel (WV) imagery of the GOES system. This is accomplished by constructing composite models from a large number of individual cases of the distribution of 6.7 micrometer brightness temperature from about 48 h before to some 24 h after definition of the burst. The characteristics revealed in these composites are discussed and compared with the signatures of the moisture bursts as seen in VIS and IR imagery.

2. PREVIOUS WORK

Plumes of high clouds originating in the equatorial regions over the eastern and central Pacific Ocean and extending to and across the coasts of Baja California and California were noted frequently in the satellite imagery of the 1960s (Anderson and Oliver, 1970). The first systematic investigation, by Thepenier and Cruette (1981), showed that these tongues of cloud were quite frequent and occurred over other oceans as well.

McGuirk et al. (1987) coined the expression "moisture burst" for these cloud bands. They also carried out an extensive investigation of the frequency and distribution of occurrence over the North Pacific Ocean east of longitude 180°. They define a moisture burst as a band of high clouds or high and middle clouds (oriented roughly NE-SW) at least 2000 km long and extending across latitude 15°N. Their definition also included criteria on beginning and ending times. This definition is objective, but moisture bursts are defined only in terms of the cloud appearance in unenhanced IR imagery from GOES. The studies show that the bursts tend to be phenomena of the northern hemisphere cool season, with about ten bursts occurring each month. Frequency is significantly less during summer and apparently during years of El Nino.

Thepenier and Cruette mention frequent midlatitude cyclogenesis downstream of the moisture bursts. McGuirk et al. also mention such events, while Schroeder (1983) found that about three quarters of the local severe weather outbreaks over North America were related to the interaction of a moisture burst with an extratropical system.

3. DATA AND ANALYSIS TECHNIQUE

The primary satellite data consist of 6.7 micrometer WV imagery from GOES-West and the paired IR imagery, both sets usually available at 6-h intervals. The data period covers 200 days beginning 15 October 1983, thus for the Northern Hemisphere winter season. Use of the 6.7 micrometer data from GOES-West restricts the area of analysis to the eastern Pacific.

Selection of events was based on the tabulation of moisture bursts prepared as part of the study reported by McGuirk et al. These events were defined in terms of their IR signature. Thirty-five events were identified and used in preparation of the composite model. For each event, a "zero time" was established as the time of the satellite imagery nearest the time when the moisture burst first attained a length of 2000 km while extending across latitude 15°N. At this time, the system satisfied the moisture burst definition; for purposes of compositing, this time is termed "definition" time. Additional reference times were established at 48 h and 24 h before, and 24 h after, the definition time. Composite models were synthesized for each of the four reference times. The intent of the earliest composite is to identify the water vapor structure that exists prior to development of the clouds associated with the moisture burst; the -48 h composite is designated "precursor." The composite at -24 h depicts early development moisture structure. Cloud development and initial poleward progression typically commence within a few hours of this composite; it is thus designated as "initiation" time. The +24-h composite is designated as the "mature" stage, and is nominally associated with maximum length of the cloud band.

Another 35 cases without occurrence of a

moisture burst were used to construct a "quiescent" composite model. These cases were selected from the same 200-day period as were the moisture burst cases.

A grid with dimensions of 35° latitude by 60° longitude was used to develop the composites. This grid was divided into squares 5° on a side. Each square was further divided by a NE-SW diagonal, roughly parallel to the axis of the moisture burst; thus, the resulting data appear, effectively, on a staggered grid. The grid is movable, with the origin located with respect to the main cloud mass of the moisture burst. The specific origin, fixed objectively for each individual case, was the northwest "corner" of the main cloud mass as seen in the IR imagery at definition time (the zero time). The origin point of the grid is not the origin point of the moisture burst as defined by McGuirk et al., but rather it was chosen to minimize smoothing of the frequently-seen strong gradient of brightness temperature (in both IR and WV imagery) along the northwest boundary of the burst. The grid's latitude lines were always placed parallel to actual latitude. Once the grid origin was fixed at definition time of a given case, it remained at that point for the other three times of that case.

The grid used for the quiescent cases also was movable, but only with respect to latitude. The zero of relative latitude was positioned at the instantaneous zonal mean latitude of the ITCZ cloud band through the longitudinal extent (165°W to 105°W) of the grid domain.

The displayed gray shades located above the water vapor image were grouped into four gray-shade categories or "brightness temperature indices" (BTI), roughly equally divided across the range of possible gray shades. Category 1, the lowest brightness temperatures, represents deep convective cloudiness. Category 2 is associated with thin or multi-layered cloudiness in the middle or upper troposphere. Categories 3 and 4 are associated with increasing dryness of the middle and upper troposphere. These last two categories represent regions devoid of middle and upper clouds.

Gridding was performed by selecting for each example at the definition time the category (1 through 4) which best matches the gray shade of the small triangular area represented by each grid point. This was repeated for each of the 35 events. Composites were constructed by averaging the BTI at each grid point. Averaged gridded data were contoured. The BTI varies between values of 1 (convective cloud at a gridpoint for nearly every case) and 4 (nearly dry above the boundary layer for nearly every case). Composites were constructed for each of the other times (-48 h, -24 h, and +24 h, and for the quiescent events). The resulting set of five maps represents the composite pattern of the developmental stages of a moisture burst, as seen in WV imagery, and a composite of quiescent conditions in the same imagery. These composite mappings of the WV structure of a moisture burst as shown by the BTI pattern are discussed in the next section.

4. THE WATER VAPOR STRUCTURE OF MOISTURE BURSTS

McGuirk et al. discussed the limitations of describing moisture bursts solely in terms of the appearance in IR imagery. The resulting picture and understanding of moisture bursts is preconditioned by, and limited to, the cloud patterns viewed by IR pictures. Significant modification to our understanding results when moisture bursts are seen from a different point of view -- WV imagery. Weaker systems, precursor signals developing before the clouds appear, and lower tropospheric features are all important examples.

4.1 Quiescent Composite

The quiescent composite represents the water vapor field when there is no defined moisture burst active in the eastern North Pacific area for at least 24 h both before and after the time of each of the 35 cases used in construction. The intent of the quiescent composite is to provide a means for evaluation of the uniqueness and relative strengths of the moisture burst as seen in the four WV composite charts, especially in the water vapor precursor pattern when patterns are not prominent. Note that this composite is "quiet" only in the sense that there are no identifiable moisture bursts occurring in the grid domain within a period of about two days.

The pattern of BTI in the WV channel for the quiescent composite is shown in Fig. 1. In general, the BTI pattern shows a nearly E-W orientation. The general features are of alternating zonal bands of warmer, drier (higher BTI) and colder, wetter features. The moist feature near 0° relative latitude represents the mean position of the ITCZ. It is more moist (lower BTI, suggesting a more active ITCZ in this area) and displaced slightly poleward on the east side of the domain. The dry features north and south appear to be evidence of the mean location of the subsiding branch of the Hadley Cell circulation. On the northern side, the Hadley circulation appears asymmetric, with the ascending branch stronger to the east and the descending branch stronger to the west; of course, this is not a closed circulation. The moist feature on the northern edge of the composite is likely the southern edge of the climatological position of an upper-level, difluent trough in the westerlies (Palmén and Newton, 1969), and the generally more moist

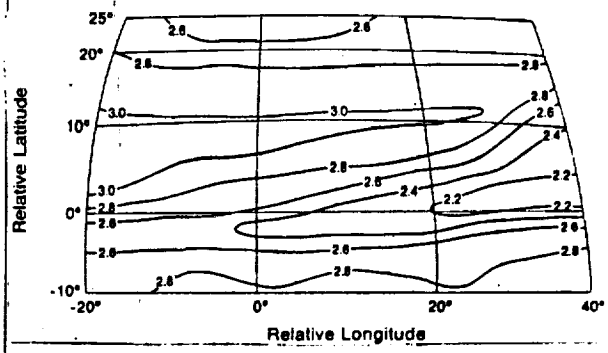

Fig. 1. Composite water vapor mapping for the quiescent (non-moisture burst) events. Isopleths are brightness temperature index, with low being moist.

atmosphere to the north of the subtropical highs of the northern hemisphere.

4.2 Precursor Composite (48 h before definition)

McGuirk et al. (1987) state that the first distinct poleward advance, seen in VIS and/or IR imagery, of the clouds of a developing moisture burst begin some 12 to 24 h before the burst reaches initial maturity. Figure 2, a composite of the distribution of BTI 48 h before the burst reaches maturity, suggests that WV imagery provides useful information much earlier. Three features are worthy of note. The ITCZ contains two active, or moist, regions separated by a drier region between relative longitudes +5° and +20°. A line drawn along the axis of the low BTI region suggests a wave pattern along the ITCZ with a crest near relative latitude +1° and relative longitude +6°. The distribution of variance of the BTI suggests that the dry (high BTI values) region is a realistic and statistically significant feature, as is the wave-like pattern.

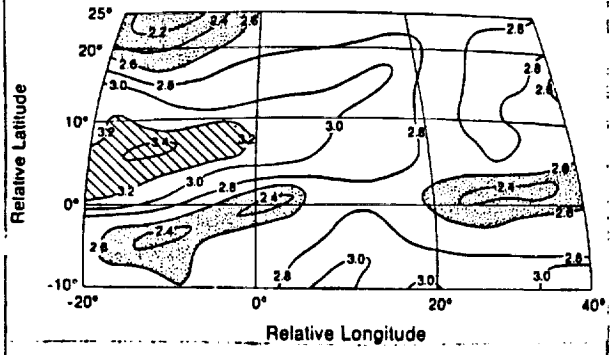

Fig. 2. As in Fig. 1, except for precursor composite, 48 h before moisture burst definition. In this and later diagrams, stippled areas are relatively moist; hatched areas are dry.

The second feature is the ENE-WSW axis of high BTIs parallel to, and some 1300 km to the NNW of, the moist belt. A similar, but weaker, feature is seen south of the ITCZ band. The gradient of BTI is a maximum between the ITCZ and the high BTIs to the NNW.

The third feature is the region of low BITs in the northwest corner of the grid to the north of the dry center. It has the appearance and position suggesting a middle-latitude wave in the polar westerlies (the absolute latitude of the northern boundary of the composite chart is near 35°N). A check of individual cases shows that over three-fourths have a cloud mass in this position which fits the description of a cold-frontal band in IR imagery.

A graphical subtraction (Fig. 3) of the quiescent composite from the composite of 48 h before moisture burst maturity emphasizes the features and anomalies in the precursor composite. Note for example the increase of BTI east of the grid origin and the decrease near and southwest of the origin. Also, note the indication of strengthening of the BTI gradient north

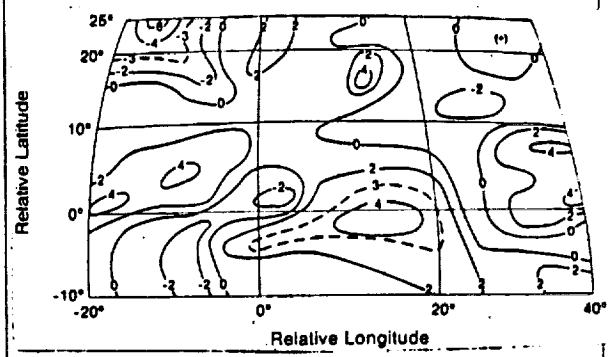

Fig. 3, Graphical subtraction of the quiescent composite (Fig. 1) from the precursor composite (Fig. 2). Contours are BTI values multiplied by 10, with positive signifying drier than quiescent.

of the ITCZ west of the origin and the large drop in BTI in the NW corner of the chart. The spacing of anomaly centers along the ITCZ suggests a wave of length near 4000 km.

4.3 Initiation Composite (24 h before definition)

The composite constructed for 24 h before burst definition (Fig. 4) reveals features similar to those of Fig. 2, though with significant differences. The moist area along the ITCZ is no longer split, and the BTI values indicate that there is less convective activity than earlier west of the grid origin, while the BTI values east of the grid origin have decreased (moistened); the 2.6 BTI contour has expanded significantly meridionally. The maximum decrease occurs about 1500 km east of the origin, suggesting the probability of maximum convective activity there. However, there is little evidence of a moist axis developing extensively to the NE in advance of the developing moisture burst; northeastward cloud progression commences within 12 h after the initiation composite of Fig. 4. Both the dry region to the NW of the origin and the strong gradient of BTI continue as dominant features;

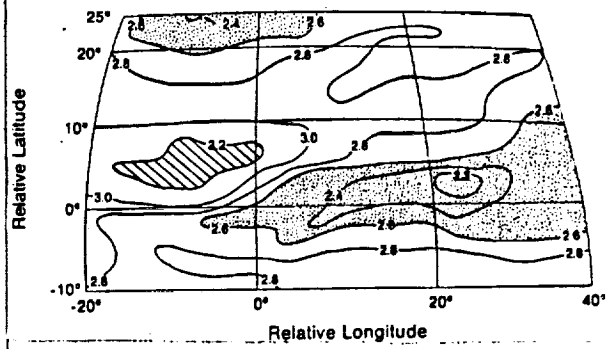

Fig. 4. As in Fig. 1, except for initiation composite 24 h before definition.

the counterclockwise turning of the strong-gradient axis is the principal indicator of the evolving burst. The axis has extended all the way to the northeast corner of the domain, although the strong gradient is confined to within about 5° of the ITCZ. The moist middle latitude feature in the NW portion of the composite shows significant drying (increase in BTI) and spreading with decreasing gradient of BTI during the 24-h interval before Fig. 4. This indicates either a weakening of the dynamic mechanism associated with this feature or a rapid movement or both. Recall that the origin of the composite is effectively fixed in position, so eastward propagation of the feature nearer the westerly belt is expected. 24-h changes from precursor to initiation composite are shown quantitatively in Fig. 5, which is the graphical subtraction of the pattern of Fig. 2 from that of Fig. 4. The pattern reflects intensification of the ITCZ wave, a narrow warming/drying band on the north side of the ITCZ, a broader moistening band further north, and another drying band on the northern border of the domain.

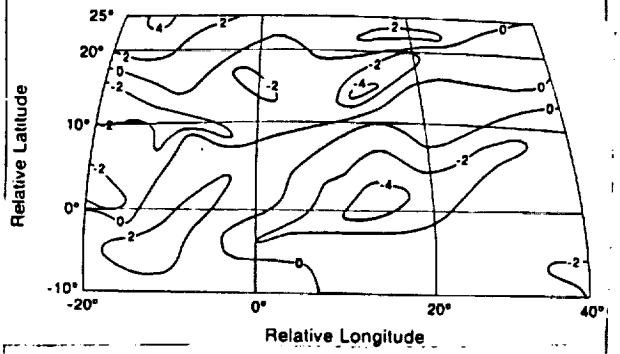

Fig. 5. 24-h BTI change from the composites 48 h and 24 h before definition computed by graphically subtracting Fig. 2 from Fig. 4. Contours as in Fig. 3.

4.4 Definition Composite (zero time)

During the 24 h following initiation (Fig. 4), the moisture burst grows from no indication in VIS or window channel imagery to an extensive plume of visible cloud at least 2000 km in length and crossing 15°N (absolute latitude). By this burst definition time ("zero time"), the corresponding WV composite (Fig. 6) presents a very distinct pattern of a mature burst:

* An elliptical area of low BTI oriented NE-SW and centered some 1600 km to the ENE of the origin point.
* A region of quite high BTI with long axis E-W centered some 800 km NW of the origin point.
* A strong gradient of BTI on the south side and especially on the west side of the burst.

In addition, indications of the ITCZ extend both east and west along 0° relative latitude, with an indication that the western part is slightly south of and considerably weaker than, the eastern part. As in the earlier composites, a

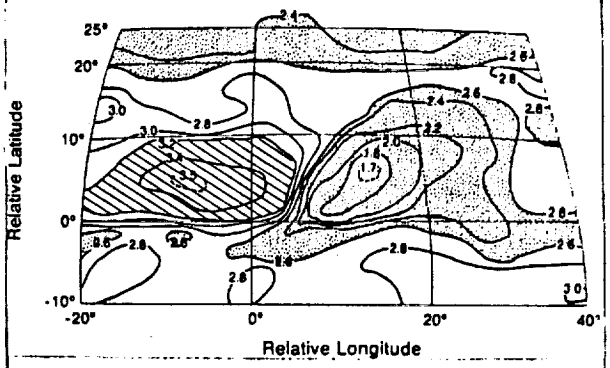

Fig. 6. As in Fig. 1, except for definition time.

wave pattern along the ITCZ is visible, and appears to have amplified. The northern edge of the composite shows weak indications of two moist pockets spaced about 3000 km apart.

The extent of the moisture burst cloud band at this time exceeded 4000 km from the 2.6 BTI line near the grid origin to the same line at the leading edge of the burst. The minimum value of BTI of 1.7 suggests significant deep convection. The signature for the definition stage of the burst as displayed in the WV channel data is very like that displayed in window channel and/or visible imagery.

The 24-h change chart for the period ending at definition time (Fig. 7) supports the concept of the near explosive development of the moist area northeast of the grid origin, and continued wave intensification. Note the drop of BTI of a full unit some 1400 km ENE of the origin and the significant rise of BTI north and northwest of the origin. Along with the cloud generation along the moisture burst axis there was significant drying immediately west of the moisture burst. However, this dry area seems to develop well before definition time; the BTI increases in this area appear to be associated mainly with eastward movement of the moisture burst system through the grid.

Comparison (not pictured) of the quiescent stage (Fig. 1) with the definition composite (Fig. 6) shows that the moisture burst exhibits a coherent pattern of anomalies over a

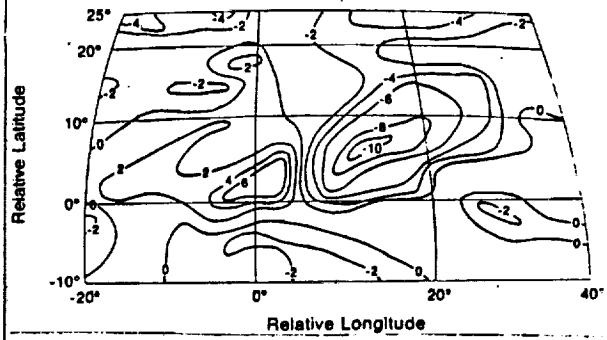

Fig. 7. As in Fig. 5, except for the composites 24 h before and at the definition time.

significant portion of the eastern Pacific environment.

4.5 Mature Composite (24 h after definition)

The final moisture burst composite in Fig. 8, constructed for 24 h after the initial maturity time, shows features similar to those at definition (Fig. 6) except that the burst has had time to spread further NE and gradients and sharpness of the features have decreased. The low BTI center associated with the burst also has shown a significant increase in value (a drying). This drying is probably a combination of weakening of the moisture burst dynamics and variation in the orientation of the burst from case to case. The variation is likely the less significant of these factors since the area of the 2.6 BTI isoline has shown little change from the definition composite.

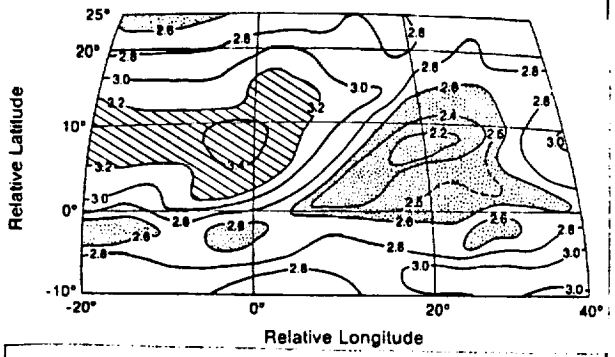

Fig. 8. As in Fig. 1, except mature composite, 24 h after definition.

The dry area to the west of the burst has shown only slight weakening (moistening) as contrasted with the pronounced change in the moist area. There also is slight indication of rejuvenation of convective activity along the ITCZ, away from the moisture burst.

5. A MODEL OF DEVELOPMENT IN WATER VAPOR IMAGERY

The composites described in the preceding section contain sufficient consistency and continuity to allow construction of a model describing the development of the synoptic entity which we call a "moisture burst" in terms of its characteristics in 6.7 micrometer imagery. The model contains four stages, based on the four composites:

a) Precursor: about 48 h before definition.
b) Initiation: about 24 h before definition.
c) Definition stage: Identified moisture burst.
d) Mature stage: 24 h after definition.

In some cases, the system may not begin actual dissipation until much longer than 24 h after initially reaching maturity -- bursts have lasted as long as 10 d.

Examination of the composites, of the water vapor imagery themselves, and of the corresponding window channel imagery, indicated a relationship between the BTI contours and the existence of middle and upper tropospheric clouds on window channel imagery. The 2.6 BTI contour seems to be the average cloud/no cloud cutoff value for middle/upper troposphere. Similarly, the 3.2 BTI contour is assumed to be the boundary of the region of enhanced subsidence to the west of the (incipient) burst region. This value represents an area that is somewhat drier than the normal background signal of the quiescent composite.

Three separate signals are recognizable in the composites and are transferred to the model (Fig. 9). The first is the wetter (lower BTI) values of the ITCZ, labelled A in the model. This signal later becomes the moisture burst. The signal labelled B is the encroaching mid-latitude trough to the NW. C is the region of enhanced dryness associated with subsidence west of the burst origin region. These signals are represented by the appropriately-labelled stippled areas in Fig. 9.

Fig. 9a represents the precursor stage, when the ITCZ (with its axis represented by the dashed line) has a section of relative minimum convective activity a short distance downstream from the origin of the burst-to-be and between the two active areas A. The approaching middle-latitude trough (B) and the dry region of suppressed activity (C) are shown at the upper left and left center, respectively. The solid lines with directional indications suggest the upper tropospheric flow pattern of the precursor stage: the intensifying middle latitude trough in the northwest and the cross-equatorial flow into a speed maximum immediately west of the burst origin and thus directly over the region of maximum gradient of BTI. These wind fields were determined by use of the individual wind analyses of the European Centre for Medium Range Weather Forecasting.

Fig. 9b represents the initiation stage some 24 h before burst definition, and usually shortly before the burst is apparent in window channel imagery. By this time, convective activity, signal A, has decreased along the western portion of the ITCZ and increased in the central section where the wave crest is located. Signal B shows some spreading eastward, while signal C also moves to the east. The flow from northwest associated with signal B has moved equatorward and shows strong confluence and an associated speed maximum near the burst origin in association with the cross-equatorial flow. The visual manifestations of the moisture burst are not yet present. Nonetheless, the indications of burst development are definite in terms of evolving wind pattern.

Fig. 9c shows signal C near maximum extent and signal A showing extensive development to the NE as the winds east of the origin back, and the ITCZ wave continues to intensify.

The continued maintenance or gradual dissipation of the burst is shown in Fig. 9d, with the upper trough retreating poleward and the convection of the ITCZ reestablishing itself. The gradient between signals A and C shows distinct weakening by this time.

6. CONCLUSIONS

A model of the signatures of a synoptic development as seen in 6.7 micrometer water

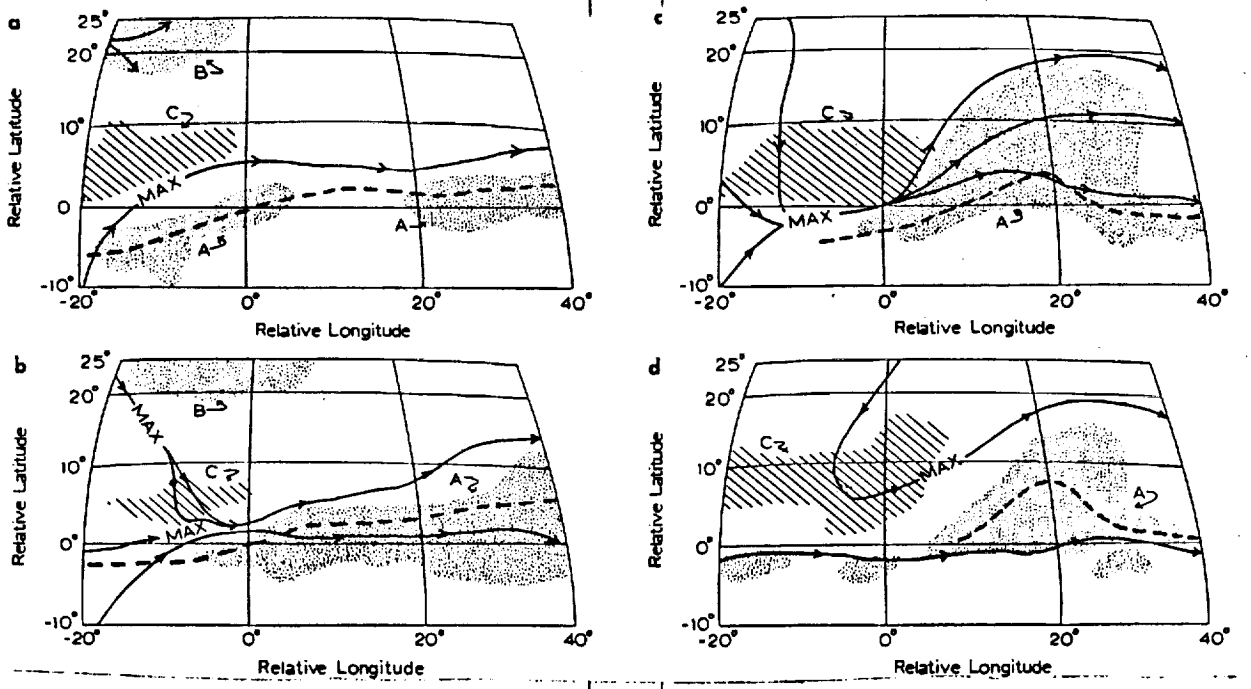

Fig. 9. A model of moisture burst development as seen in 6.7 micrometer water vapor imagery. a. Precursor stage. b. Initiation stage. c. Definition stage. d. Mature stage. Symbols are explained in text.

vapor channel imagery is constructed easily from a composite of cases, in this example a moisture burst over the eastern Pacific Ocean. Some of the signatures appear in the water vapor imagery before appearance in the window channel or visible imagery.

One of the advantages, not previously discussed, of using this form of satellite imagery is that it uniquely clarifies the role of the tropics in the evolution of moisture bursts. Previous studies (Anderson and Oliver, 1970) focus on the important mid-latitude aspects to the near exclusion of any active tropical role. The WV imagery, particularly the 24-h change maps, focus on important tropical development, almost to the exclusion of mid-latitude features. This emphasis has been an unexpected benefit of WV images.

Finally, a test of the forecast capability of the model was performed on 120 consecutive days including 29 moisture bursts. A meteorologist given 2 h of training with the models was able successfully to forecast 19 (65%) of the bursts at least 24 h in advance of definition. In only 6 cases were bursts forecast when none occurred. Forecast failures were dominated by situations of multiple synoptic systems in the Pacific domain. This preliminary test suggests that the precursor signals in 6.7 micrometer water vapor imagery are sufficiently robust to allow significant forecasting skill over 24 to 48 h.

Acknowledgements. This study was supported partially by the Marshall Space Flight Center, NASA, under Contracts NAS8-35182 and NAS8-37284. Conclusions are those of the authors.

References

Anderson, R., and V. Oliver, 1970: Some examples of the use of synchronous satellite pictures for studying changes in tropical cloudiness. Proc. Symposium on Tropical Meteorology, Honolulu, Amer. Meteor. Soc., E XII 1-6.

McGuirk, J., A. Thompson and N. Smith, 1987: Moisture bursts over the tropical Pacific Ocean. Mon. Wea. Rev., 115, 787-798.

Palmén, E., and C. Newton, 1969: Atmospheric Circulation Systems, Academic Press, 603 pp.

Schroeder, T., 1983: The subtropical jet stream and severe local storms - a view from the tropics. Preprints 13th Conf. on Severe Local Storms, Tulsa, OK, Amer. Meteor. Soc., 161-162.

Thepenier, R., and D. Cruette, 1981: Formation of cloud bands associated with the American subtropical jet stream and their interaction with midlatitude synoptic disturbances reaching Europe. Mon. Wea. Rev., 109, 2209-2220.

TEMPORAL AND SPATIAL VARIABILITY AND CONTAMINATION OF 6.7 AND 7.3 MICROMETER WATER VAPOR RADIANCES

Paper presented at:
Third Conference on Satellite Meteorology and Oceanography,
American Meteorological Society,
Anaheim CA, February 1988.

Keith G. Blackwell, James P. McGuirk and Aylmer H. Thompson

Department of Meteorology
Texas A&M University
College Station, TX 77843-3146 (409-845-4431)

1. INTRODUCTION

Accurate evaluation of the spatial and temporal distribution of atmospheric water vapor (WV) remains a problem over data-sparse areas. Rawinsonde measurements are by far the most reliable (Timchalk, 1986); yet rawinsonde information is virtually nonexistent over oceanic areas. Similarly, the eastern tropical Pacific Ocean is plagued by a scarcity of data; however, this data limitation became less of a problem during the FGGE year of 1979. FGGE's Special Observing Period 1 (SOP 1) provided an increase of meteorological observational data including additional land/ship launched rawinsondes reports and satellite-measured radiances.

Of the various wave bands sensed by the satellite-borne radiometers, the 6.7 μm and 7.3 μm wavelengths are very close and moderately close, respectively, to the wavelength which experiences the maximum absorption by (water vapor) WV in the troposphere. Therefore, 6.7 μm radiances (channel 12) are highly moisture sensitive, and the 7.3 μm band (channel 11) is moderately sensitive to moisture content of the troposphere. As a result of this sensitivity, these two wavelengths are used widely to detect variations of atmospheric moisture in time and space.

2. OBJECTIVE

The objective of this research is to evaluate the accuracy and synoptic information content of quantitative WV radiance data in a tropical area bounded by latitudes 10°S and 30°N and longitudes 90°W and 180°. The period of study is 21-29 January, 1979. Special attention is focused on the relationship between the moisture-sensitive radiances (6.7 μm and 7.3 μm channels) and the changes in the topography of a moist layer as measured by conventional "ground truth" rawinsondes.

3. BACKGROUND

Several studies (Chesters et al., 1982, Stout et al., 1984, Weldon and Holmes,[1] and Stewart et al., 1985) have focused on the vertical resolution of moisture sensitive satellite channels, especially the 6.7 μm band. Most of these studies indicate a potential relationship between the variation in the height of mid- or upper-tropospheric moist layers and the changes observed in WV brightness temperatures (BTs). In addition, Ramond et al. (1981), Stewart et al. (1985), Stewart and Fuelberg (1986) and Peterson et al. (1984), among others, associate high BTs with deep subsidence in the middle and/or upper troposphere. Roulleau (1978), Rodgers et al. (1976) and Steranka et al. (1973) concluded that WV imagery may be used as a tracer to delineate tropospheric dynamics, including mid-tropospheric vertical motions.

4. DATA

The data from FGGE SOP 1 consist of traditional observations, satellite information, and computer-generated analyses based on these data. The data set includes aircraft dropsondes, ship- and surface-launched rawinsondes, and satellite-derived BTs. The BTs used in this investigation were the moisture-sensitive channel 11 and 12 infrared (IR) radiances from the TIROS-N polar orbiting satellite.

The computer-derived ECMWF analyses are labeled FGGE IIIb. They include pressure surface wind fields which are available on a 1 7/8° by 1 7/8° gridded field, modified to a 3 3/4° by 3 3/4° gridded field of zonal (u) and meridional (v) components for 21-29 January 1979.

In addition to the FGGE data sets, infrared satellite imagery was used. This imagery was obtained from the GOES West satellite located above the equator near 130°W.

Dropsondes were not used because of their inaccuracy in measuring mid-tropospheric moisture (Velden et al., 1984). Dropsondes examined within the area of interest for this study possessed errors similar to those found by Velden, et al.

5. OBSERVED BRIGHTNESS TEMPERATURE SIGNATURES

The satellite BTs available within the analysis area over the 9-day period of study were located over the ocean and the adjacent land over the southwest United States, Mexico and Central America. Possible adverse terrain

[1]From a manuscript titled: "Characteristics of Water Vapor Imagery." Manuscript available from NOAA/NESDIS, Washington, D.C. 20233.

influences on the WV imagery were checked by testing the mean of 145 "continental" BTs from each channel with the mean of 180 adjacent "oceanic" BTs from each channel. Statistical tests detected no significant difference in BT means between ocean and land in either channel; therefore, high terrain was not significantly influencing the BTs over Mexico and the southwest United States. This conclusion was anticipated because both IR satellite imagery and rawinsondes indicated an extensive layer of mid- and upper-tropospheric moisture associated with an active synoptic cloud system blanketing this region. For drier conditions, topography may be a problem in this region.

A distribution of frequency of occurrence of channel 12 BTs as a function of observed temperatures is shown in Fig. 1. Constructed from 3330 TIROS-N 6.7 μm BTs recorded during the 9-day study period over the eastern Pacific, this distribution shows a skewed pattern in the direction of larger BTs. This skewness was nearly 10 times larger than the expected standard deviation of the skewness for a typical sample of this size taken from a true normal distribution. This pattern suggests a bimodal distribution in frequency of occurrence of BTs. Most BTs approximate a normal distribution about a mode of -17°C; a smaller group of higher BTs is clustered around -12.5°C.

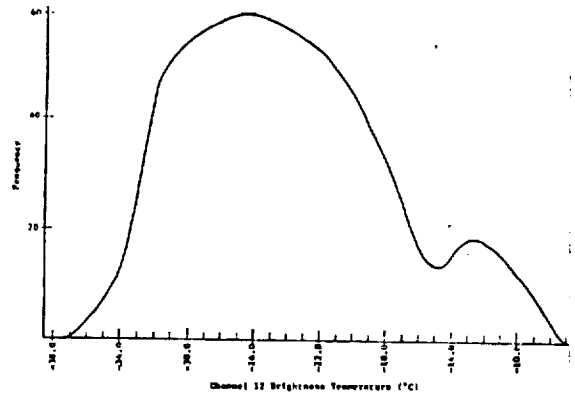

Fig. 1. Channel 12 brightness temperature (BT) frequency distribution. Frequency is given as the number of occurrences per 0.3°C interval out of 3330 observations.

The majority of the BTs in the frequency distribution were lower than -15°C. Although these lower BTs are distributed nearly normally, the peak was broad between -20°C and -32°C. The smaller group of BTs higher than -15°C appeared to show evidence of another frequency maximum between -11°C and -13°C.

Unlike the channel 12 BTs, the frequency distribution for 3330 TIROS-N 7.3 μm channel 11 BTs during the same period of time showed a pattern approximating a normal distribution with very little evidence of skewness toward higher BTs.

Evidence of a secondary frequency maximum in channel 12 BTs and the apparent absence of a secondary maximum in the frequency of occurrence of channel 11 BTs may be significant. Since the peak weighting of channel 12 typically occurs near the 500 mb level (Fig. 2), this secondary maximum of high BTs observed in Fig. 1 may be the signature of a synoptic feature in the upper troposphere.

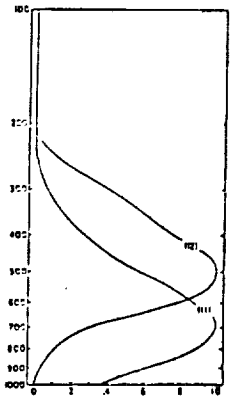

Fig. 2. TOVS weighting functions (normalized) for channel 11 (7.3 μm) and channel 12 (6.7 μm). After Smith et al. (1979).

Figure 3 shows the unenhanced window channel GOES West IR satellite imagery of the eastern Pacific at 0615 UTC 24 January 1979; the hatched region southwest of Hawaii displays the corresponding geographical distribution of channel 12 BTs observed on 24 January which were higher than -15°C. All of the BTs observed in this persistent cluster (hatched region in Fig. 3) fell within the smaller frequency maximum in Fig. 1, and also fell within a near cloud-free region southwest of Hawaii in Fig. 3. Without exception, this same pattern was observed each day throughout the period. From the 21st through 25th, these high BTs were clustered south and west of Hawaii and corresponded to large, mostly clear regions in the window channel imagery. Especially interesting was the location of these BTs directly adjacent to the western flank of a developing moisture burst (McGuirk et al., 1987). The region of high BTs elongated eastward and diminished during the last few days of the period as the moisture burst moved toward the east and weakened (Schaefer, 1985).

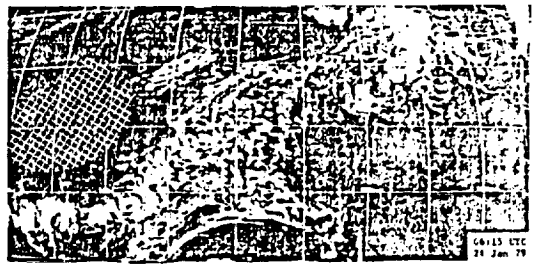

Fig. 3. Unenhanced window channel GOES West satellite image for 0615 UTC 24 January 1987. Hatched region southwest of Hawaii represents the geographical distribution of channel 12 BTs higher than -15°C for 24 January 1979.

The region southwest of Mexico (known as the Pacific dry zone) looked very similar in GOES West window channel imagery to the high BT region southwest of Hawaii; however, there was a noticeable lack of high BTs within this dry zone. This region south of Mexico remained free of any synoptic cloud systems throughout the

entire 9-day period and also remained virtually free of any BTs higher than -15°C which would be contained within the smaller channel 12 BT frequency maximum (see Fig. 1).

These findings suggest that the broad peak of the bimodal distribution in Fig. 1 may be related to the typical occurrence of low BTs associated with a normal to very wet mid and upper troposphere in the tropics; the smaller frequency peak of high BTs may be associated with an extremely dry mid- and upper-tropical troposphere. These extremely dry mid- and upper-tropospheric regions have been verified below 300 mb by rawinsondes. Moisture profiles above this level were generally not available from conventional rawinsonde soundings. This small set of high BTs seems to be related exclusively to certain synoptic disturbances over the eastern Pacific.

Similar to the sounding profiles southwest of Hawaii, rawinsonde soundings south of Mexico in the Pacific dry zone indicated very dry mid-tropospheres. However, the upper tropospheric profiles near the 300 mb level in the dry zone were moister.

It is hypothesized that the large area of extremely high channel 12 BTs observed near and south of Hawaii may be associated with deep tropospheric subsidence as previously suggested by several researchers. Furthermore, it is hypothesized that the movement and concentrated nature of these large channel 12 BTs relative to the active convection associated with a moisture burst may denote the subsidence branch of an intense, direct synoptic-scale circulation. This hypothesis is further substantiated by the observed shrinking of this BT area as the moisture burst weakens. Since channel 11 is more sensitive to moisture in the lower troposphere (see Fig. 2), the absence of a small secondary frequency peak in the higher BT region of the channel 11 distribution suggests that phenomena producing the secondary channel 12 peak may be an anomaly restricted to the upper troposphere. This absence of a secondary channel 11 peak also suggests that the subsidence of dry air does not extend into the tropical boundary layer. This lack of subsidence into the boundary layer was further evidenced by numerous soundings within the high BT region which indicated a moist surface layer overlain by dry air, separated by a pronounced inversion.

6. ESTIMATING TROPICAL SYNOPTIC VERTICAL MOTIONS

Initially, a procedure described by Stout et al. (1984) was used to estimate vertical motion; however, results were extremely discouraging. A relationship was developed between mid-tropospheric precipitable water (PW) thicknesses calculated from over 100 soundings, and collocated 6.7 μm and 7.3 μm water vapor BTs sensed by satellite.

The distribution of the upper 5 mm of PW for each sounding was calculated as a function of pressure by integrating the specific humidity downward from 300 mb at each reported sounding level. The pressure level associated with each 0.1 mm PW increment was referred to as a PW thickness pressure (PWTP). Although strong correlations (0.81 at the 0.6 mm PW thickness and 0.84 at the 0.9 mm PW thickness for channels 12 and 11, respectively) were obtained between these PWTPs and BTs (essentially a correlation between pressure and BT), a large root mean square (RMS) error was also observed.

Comparison of estimated vertical motions with adiabatically derived estimates, with velocity potential fields, and with outgoing longwave radiation fields demonstrated the failure of the technique in its current configuration. Therefore, the correspondence between mid- to upper-tropospheric moisture measured directly by rawinsonde with that sensed indirectly by satellite is questioned. It is hypothesized that the two moisture-sensitive satellite channels used in this study may have sensed moisture undetectable by conventional rawinsondes.

7. MOISTURE SAMPLING ERRORS

7.1 Comparisons of PWTP, BT and Sounding Profiles

If rawinsonde and satellite were actually sensing the same moist layers, then the rawinsonde/satellite plots of PWTP versus BT for each sounding location should fit closely to the composite linear regression curve for all sounding locations. Fig. 4 shows the 0.6 mm PWTP/channel 12 BT scatter plot for Johnston Island. Points marked "B" in this figure represent very dry soundings with most having less than 0.6 mm of PW above the 550 mb surface. Also shown is the distribution of "Bs" with respect to the linear regression curve for all the data shown in Fig. 9. The slope of the best fit curve for the data represented by the "B"s is different from the slope of the composite regression line. The nearly horizontal orientation of a best-fit line through this data plot suggests that the moisture profiles, as determined by rawinsonde for all 12 Johnston Island soundings, were very closely related. The 0.6 mm PWTPs for all the Johnston Island soundings varied by only 41 mb in range (12% of the total PWTP range shown in Fig. 9); however, the collocated channel 12 BTs differed up to 14°C (56% of the total BT range in Fig. 9).

Results for channel 11 are similar, but with less variation than in channel 12 BTs. This reduced variation suggests that the Johnston Island soundings may have closely resembled one another in channel 11 imagery. In contrast to channel 12 data, this smaller variation of channel 11 BTs also implied that channel 11 BTs may have recognized mean-profile similarities in soundings better than channel 12.

Similar Johnston Island soundings are shown for 0000 UTC on 23 January 1979 (Fig. 5a) and for 1200 UTC on 28 January 1979 (Fig. 5b). The 24°C wet-bulb potential temperature curve is shown on both soundings as a reference. On the 23rd, a strong inversion existed near 700 mb; on the 28th the inversion appeared near 800 mb. Both soundings were moist below and very dry (dew point depression defaulted to 30°C) above the inversion. Due to instrument limitations,

dew point depressions, as measured by rawinsonde, which were greater than or equal to 30°C were recorded as 30°C. Therefore, actual dew point depressions likely were greater than 30°C. More evidence of sounding similarity was shown by the rather insignificant 4 mb difference between their 0.6 mm PWTPs of 578 mb and 582 mb. Given these nearly identical rawinsonde soundings, one would expect only a small difference in collocated channel 12 BTs. Rather, the channel 12 BT difference between soundings was 12°C (46% of the BT range observed in Fig. 10). Although the sounding on the 28th was colder in the 400-300 mb layer, the absence of detectable moisture in this layer significantly lessened the layer's influence on the collocated channel 12 BT. Smaller, but significant, discrepancies were detected with channel 11 BTs as well.

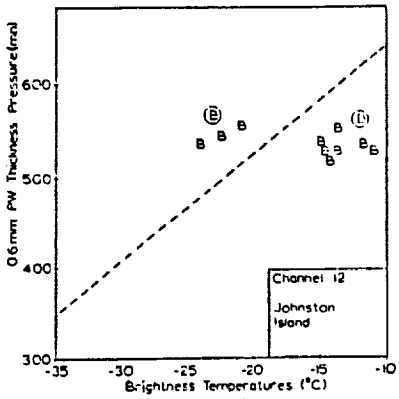

Fig. 4. Scatter plot of 0.6 mm PWTPs versus channel 12 BTs for Johnston Island (B = 91275). Circled letters correspond to the two soundings discussed.

7.2 Calculated versus Observed BTs

The potential of PW in the cold upper troposphere to affect channel 12 and 11 BTs was explored by comparing observed BTs to model-derived BTs. BTs were calculated from actual soundings by means of the GLAS Physical Inversion radiative transfer model (RTM) (Susskind et al., 1982). The RTM produced channel 12 weighting function curves from the Johnston Island soundings shown in Fig. 5. These weighting function curves are shown in Fig. 6. In layers where the sounding dew point depression defaulted to 30°C and moisture was systematically overestimated. This overestimation occurred between 750 mb and 300 mb in the two Johnston Island soundings. Moisture at pressures less than 300 mb was set to zero since rawinsonde moisture readings terminated at heights just above this level. Analogous to the soundings, the weighting function curves were similar, with both curves peaking near 500 mb. The collocated RTM and observed BTs at 0000 UTC on the 23rd were -10°C and -11°C, respectively; thus the correlation was excellent. However, the comparison at 1200 UTC on the 28th was extremely poor. As expected due to sounding similarity, the RTM BT remained high (-9°C) while the observed BT was -23°C, suggesting significant moisture in the atmosphere above 300 mb.

A more conclusive BT/sounding test was constructed using the detailed moisture information available from a limited number of special rawinsondes launched from scientific ships in the eastern Pacific. RTM channel 12 and channel 11 BTs were first computed from 1000-300 mb moisture profiles obtained from the ship-launched rawinsondes and these RTM BTs were compared to observed BTs. BTs also were calculated from the 1000-100 mb moisture profile available from the special soundings.

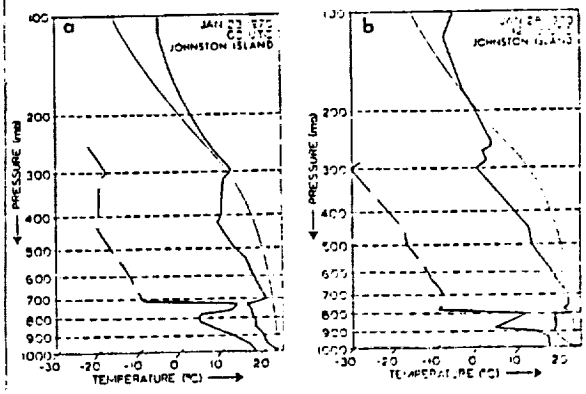

Fig. 5. Johnston Island Soundings for 0000 UTC 23 January 1979 (a) and 1200 UTC 28 January 1979 (b). The smooth curve in this skew-T log p plot represents the 24°C wet-bulb potential temperature. The jagged line on the right represents the temperature. The jagged line on the left represents the dew point. Dashed regions on the dew point curve represent dew point depressions ≥ 30°C.

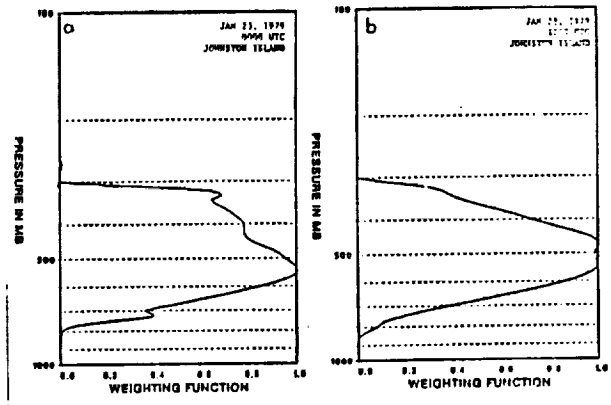

Fig. 6. RTM channel 12 weighting function profiles for the Johnston Island soundings at 0000 UTC 23 January 1979 (a) and 1200 UTC 28 January 1979 (b). Moisture has been deleted at heights above 300 mb. The slight weighting above 300 mb is not due to the influence of moisture on the RTM.

The Matamoros sounding from 2100 UTC on 26 January (Fig. 7a) is given as an example. For channel 12, the observed BT was -10°C; the RTM-calculated BT for moisture between 1000 and 300 mb was -8°C; and the RTM estimate including moisture between 300 and 100 mb (equivalent to 0.038 mm of PW) was -15°C.

The special sounding from 2100 UTC on 26 January (Fig. 7b) from the ship Pariz provides a second graphic example. Although the total PW contained in the 300-100 mb layer was only 0.187 mm, the channel 12 weighting function curves for the 1000-300 mb (Fig. 8a) and 1000-100 mb (Fig.

8b) moisture profiles were extremely different. The profile with moisture extending to the 100 mb level indicated nearly half the total area encompassed by this weighting curve occurred at heights above the 300-mb level. This large discrepancy in weighting function profiles produced correspondingly large differences in the RTM BTs: -15°C for the RTM computation, dry above 300 mb; -31°C for the RTM computation with moisture to 100 mb; and -35°C observed by the satellite over Pariz.

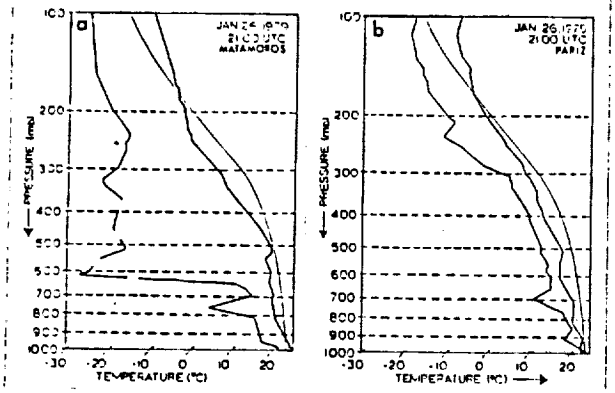

Fig. 7. As in Figure 5, except for 2100 UTC 26 January 1979 soundings for Matamoros ship at 7°N/91°W (a) and Pariz ship at 1°N/150°W (b).

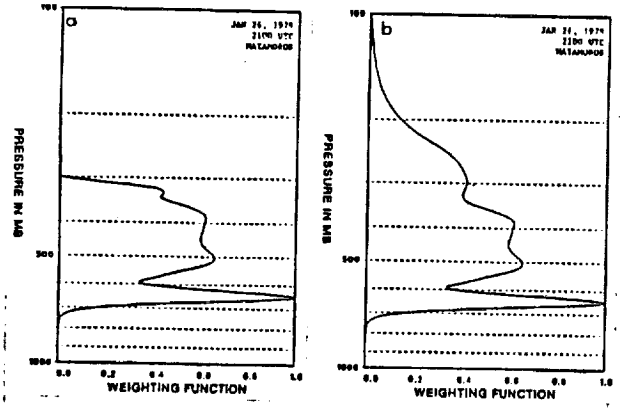

Fig. 8. RTM channel 12 weighting function profiles for the Matamoros ship sounding at 2100 UTC 26 January 1979. Moisture deleted at heights above the 300 mb level (a) and moisture deleted at heights above the 100 mb level (b). The slight weighting above 300 mb in (a) is not due to the influence of moisture on the RTM.

Finally, RTM BTs were calculated from all 111 rawinsondes, with moisture above 300 mb not included. These RTM BTs were compared to the collocated observed BTs and the discrepancies were analyzed on the scatter plot shown in Fig. 9. The drier soundings, associated with higher channel 12 BTs, produced better agreement with the RTM; the wetter soundings, coupled with lower BTs, produced poorer agreement. Special significance was given to the BTs in the upper right corner of the plot. Without exception, BTs higher than -14°C closely matched the BTs produced by the RTM. These were the same BTs encompassed within the very high channel 12 BT region observed in the subtropical Pacific to the northwest of the moisture bursts (see Fig. 3) and falling within the secondary frequency maximum observed in channel 12 BTs (see Fig. 1).

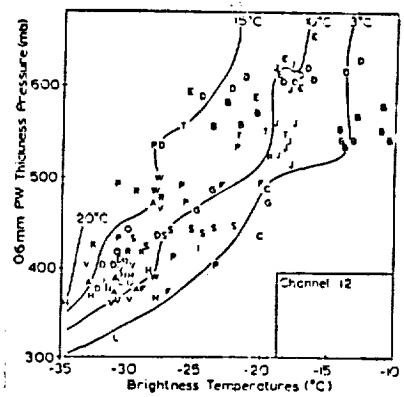

Fig. 9. Scatter plot of 0.6 mm PWTPs versus channel 12 BTs with overlaid observed-BT/RTM-BT difference contours. Each rawinsonde station is represented by a letter (A = 91700, B = 91275, C = 91066, D = 91165, E = 91285, F = 91487, G = CROMW, H = PARIZ, I = DISCO, J = MATAM, K = 76723, L = 76225, M = 76612, N = 72561, O = 76394, P = 76679, Q = 72255, R = 72250, S = 76692, T = 78641, U = 76256, V = 76458, W = 76654).

A less defined pattern was displayed in the channel 11 analysis (Fig. 10). In addition, the magnitudes of the differences between observed BTs and RTM BTs for channel 11 were significantly smaller than those for channel 12. Channel 11 seemed to be much less sensitive to the contaminating influence of upper tropospheric moisture than channel 12.

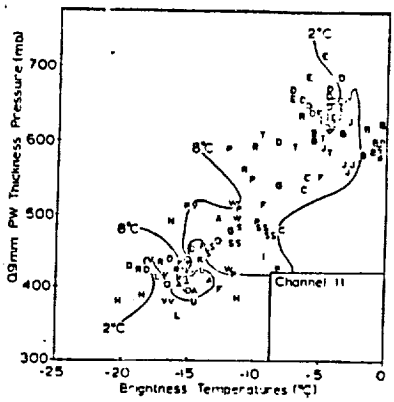

Fig. 10. As in Fig. 9 except for 0.9 mm PWTPs versus channel 11 BTs.

8. SUMMARY AND DISCUSSION

Initially, the high correlations obtained between moisture sensitive BTs (derived by satellite) and the upper few tenths of a millimeter of PW (derived from rawinsonde) measured at heights below the 300-mb level implied that the moist layers sensed by satellite were nearly identical to the ones measured by rawinsonde. However, the large RMS errors obtained when linear and polynomial curves were fitted to the satellite/rawinsonde comparisons suggested a more complex relationship. Minute quantities of upper tropospheric moisture, not detectable by conventional rawinsondes, significantly modulate the radiation signature emanat-

ing from lower levels. This upper moisture acts to mask the moisture profile in the middle and lower troposphere. Channel 11 was less affected by this upper tropospheric moisture than channel 12; yet, both channels were significantly influenced. Thus, evidence in this study indicates that satellites significantly sense the upper moist layer in the tropical troposphere while, in most situations, rawinsondes do not.

This discrepancy in sensing capability was observed over the vast majority of the eastern Pacific Ocean; therefore, an extensive layer of high tropospheric moisture, possibly concentrated just beneath the tropical tropopause, may be the rule rather than the exception. Indeed, all measurements reported by Kley et al. (1982) indicated saturated conditions in the vicinity of the tropical tropopause.

The concentrated area of very high BTs in the subtropical Pacific appears to have been the only region observed during this study where both satellite and rawinsonde consistently and correctly evaluated the top layer of tropospheric moisture actually present. Therefore, through some process, this upper moist layer must have been eliminated. As mentioned in several studies, very high channel 12 BTs have been associated with deep tropospheric subsidence; yet, these high BTs occurred in the tropical eastern Pacific only in a localized, nearly cloudless region south of Hawaii. From IR satellite pictures, a subsidence-dominated troposphere is also expected in the cloudless eastern Pacific dry zone to the south of Mexico; however, very few of the high channel 12 BTs were found there, and certainly not the highest. This discrepancy appears to be associated with the presence of upper tropospheric moisture over the eastern Pacific dry zone.

Finally, the observed closeness of the high BT region to the western flank of a moisture burst, the eastward movement of this BT region as the moisture burst moved eastward, and the areal shrinking of these high BTs concurrent with the weakening of the moisture burst indicate these BTs may be the descending branch of an intense, direct, synoptic-scale circulation. Furthermore, this deep subsidence may originate in the stratosphere and extend into the mid or lower troposphere.

9. REFERENCES

Chesters, D., L. W. Uccellini, and A. Mostek, 1982: VISSR Atmospheric Sounder (VAS) simulation experiment for a severe storm environment. Mon. Wea. Rev., 110, 198-216.

Kley, D., A. L. Schmeltekoph, K. Kelly, R. H. Winkler, T. L. Thompson, and M. McFarland, 1982: Transport of water through the tropical tropopause. Geophys. Res. Lett., 9, 617-620.

McGuirk, J. P., A. H. Thompson, and N. R. Smith, 1987: Moisture bursts over the tropical Pacific Ocean. Mon. Wea. Rev., 115, 787-798.

Petersen, R. A., L. W. Uccellini, A. Mostek, and D. A. Keyser, 1984: Delineating mid- and low-level water vapor patterns in pre-convective environments using VAS moisture channels. Mon. Wea. Rev., 112, 2178-2198.

Ramond, D., H. Corbin, M. Desbois, G. Szejwach, and P. Waldteufel, 1981: The dynamics of polar jet streams as depicted by the Meteosat WV channel radiance field. Mon. Wea. Rev., 109, 2164-2176.

Rodgers, E. B., V. V. Salmonson, and H. L. Kyle, 1976: Upper tropospheric dynamics as reflected in Nimbus 4 THIR 6.7 μm data. J. Geophys. Res., 81, 5749-5758.

Roulleau, M., 1978: Remote Sensing of the Atmosphere: Inversion Methods and Applications. Elsevier, 149-159.

Schaefer, J. R., 1985: Observing the synoptic structure of two moisture bursts. Masters Thesis, Texas A&M University, College Station, TX, 145 pp. (see pp. 38-66).

Smith, W. L., H. M. Woolf, C. M. Hayden, D. Q. Wark, and L. M. McMillin, 1979: The TIROS-N Operational Vertical Sounder. Bull. Amer. Meteor. Soc., 60, 1177-1187.

Steranka, J., L. J. Allison, and V. V. Salmonson, 1973: Applications of Nimbus-4 THIR 6.7 μm observations to regional and global moisture and wind field analysis. J. Appl. Meteor., 12, 386-395.

Stewart, M. R., and H. E. Fuelberg, 1986: Relationships between 6.7 micrometer imagery and radiosonde-derived parameters. Preprints, Second Conference on Satellite Meteorology/Remote Sensing and Applications, Amer. Meteor. Soc., Williamsburg, VA, May 13-16, 1986, 67-72.

Stewart, T. R., C. M. Hayden, and W. L. Smith, 1985: A note on water-vapor wind tracking using VAS data on McIDAS. Bull. Amer. Meteor. Soc., 66, 1111-1115.

Stout, J., J. Steranka, and R. A. Petersen, 1984: Vertical displacements of the mid-tropospheric water vapor boundary in the tropics derived from the VISSR Atmospheric Sounder (VAS) 6.7 μm channel. Preprints, Conference on Satellite/Remote Sensing and Applications, Amer. Meteor. Soc., Clearwater Beach, FL, Jun. 25-29, 1984, 86-89.

Susskind, J., J. Rosenfield, D. Reuter, and M. T. Chahine, 1982: The GLAS physical inversion method for analysis of HIRS2/MSU sounding data. Tech. Memo. No. 84936, NASA, Goddard Space Flight Center, Greenbelt, Maryland 29771.

Timchalk, A., 1986: Satellite derived moisture profiles. Preprints, Second Conference on Satellite Meteorology/Remote Sensing and Applications, Amer. Meteor. Soc., Williamsburg, VA, May 13-16, 1986, 64-66.

Velden, C. S., W. L. Smith, and M. Mayfield, 1984: Application of VAS and TOVS to tropical cyclones. Bull. Amer. Meteor. Soc., 65, 1059-1067.

IDENTIFICATION AND RECOVERY OF DISCONTINUOUS SYNOPTIC FEATURES IN SATELLITE-RETRIEVED BRIGHTNESS TEMPERATURES USING A RADIATIVE TRANSFER MODEL

Paper presented at:
Third Conference on Satellite Meteorology and Oceanography,
American Meteorological Society,
Anaheim CA, February 1988.

G. A. White, III, J. P. McGuirk and A. H. Thompson

Department of Meteorology
Texas A&M University
College Station, Texas 77843-3146

1. INTRODUCTION

Meteorological analysis over critically data sparse areas, such as tropical oceans, is dependent, in part, on remotely sensed data from satellites. In the classic retrieval method, a portion of the satellite channel brightness temperature data and a knowledge of the climatological conditions of the region and season are used in algorithms to reconstruct atmospheric vertical temperature profiles. Despite the success of conventional retrieval methods, additional unused information may be present in the satellite channel data.

McGuirk et al. (1985, 1986) used empirical orthogonal function (EOF) analysis of satellite data to explore the structural detail of the atmosphere. They found that individual channel brightness temperatures may be preferable to reconstructed temperature and moisture profiles because the reconstructions are smoothed both horizontally and vertically.

The objective of this study is to recover and identify discontinuous synoptic features directly from satellite-retrieved brightness temperatures. Of special interest are the meteorologically important elements of an atmospheric sounding; namely, the near discontinuities in temperature and moisture found typically in fronts and inversions. The techniques used to create conventional reconstructed temperature and moisture profiles from satellite data unavoidably smear these discontinuities and contaminate their signatures. In pursuit of the objective, this study poses two main questions: can vectors of satellite channel brightness temperatures be classified by synoptic source (e.g., fronts, inversions, etc.), and can these sources be quantified?

To answer these questions, a synthetic climatology of atmospheric temperature and moisture soundings was chosen, containing well-defined synoptic features representative of those found over the tropical eastern Pacific Ocean. The temperature and water vapor variables in each of a set of "seed soundings" were perturbed randomly, within narrow limits, to create a statistically meaningful training data set of 60 soundings for each seed sounding. Each sounding was transformed by a non-linear radiative transfer model (RTM) to a vector of 22 of the 24 individual satellite channel brightness temperatures which would have been observed had TIROS N satellite sensors viewed that vertical section of the atmosphere. (Two channels were omitted because they contain no relevant information for this study.)

The brightness temperature vectors arising from the training data sounding groups were classified and labeled as to their known synoptic features using two methods: (1) *a priori* through knowledge of the initial seed sounding and (2) objectively through cluster analysis (Johnson and Wichern, 1982). Both methods led to nearly identical results.

Finally, to test the ability of the system to associate unknown soundings with recognizable synoptic features, temperature and dewpoint temperature profiles containing synoptic features not originally part of the sounding climatology were evaluated by the RTM. The resulting satellite channel brightness temperature vectors were added to the sounding climatology which was then evaluated by canonical discriminant analysis (CDA).

CDA serves three purposes: first, it confirms (or refutes) the initial classifications of the sounding climatology; second, it quantifies the basis for synoptic classification (Johnson and Wichern, 1982); and finally, it places the unknown brightness temperature vectors in the physically most similar family in the sounding climatology. Identification of the synoptic features found in brightness temperature vectors is accomplished in a relative sense by comparison rather than by iterative solution of the radiative transfer equation.

2. METHOD

2.1 Radiative transfer model

As in similar studies, the need for collocated satellite observations and upper air data was evident. However, since this work focuses on the development of statistical techniques, the use of synthetic atmospheric temperature and moisture soundings and a RTM to produce satellite channel brightness temperature vectors provided a simplified approach. The combination of soundings and RTM posed two distinct advantages: first, it allowed the flexibility to study any synoptic feature for which atmospheric vertical profiles could be drawn, and second, the complex signals found in real soundings were eliminated.

The RTM was developed at NASA Space Flight Center's Laboratory for the Atmospheres

and is documented by Susskind et al. (1982). It is a non-linear 66-layer (surface to 1 mb) rapid transmission algorithm which directly calculates brightness temperatures for HIRS and MSU channels on board TIROS N. Because of its non-linearity, the model slightly increases the variability of the atmospheric temperature and dewpoint temperature information.

2.2 Sounding classification

Vertical soundings of temperature and dewpoint temperature were created to represent typical synoptic conditions found over the tropical eastern Pacific Ocean. The soundings were coded according to their synoptic origin. Natural variation in the soundings was introduced by modifying randomly the seed sounding temperature and mixing ratio by as much as ± 2 percent in each of the 66 layers of the RTM. The variability was distributed as white noise. Fifty perturbation iterations were calculated from each seed to create a statistically meaningful sounding climatology each containing a synoptic signature.

2.3 Retrieval vs classification

Direct reconstruction of vertical atmospheric profiles from satellite sounding data is not possible (Chahine, 1970). The retrieval of blackbody radiation requires inversion of the radiative transfer equation. No stable solution can be obtained by simultaneous integral equations for each satellite channel because of the redundancy resulting from overlap of channel weighting functions. A stable solution normally is obtained by introducing another condition—an average observed temperature profile appropriate to the location and season. The brightness temperatures are used to find small deviations from the climatological mean profile. There is some bias toward the mean sounding, and the method works best for small deviations from the main sounding. Further, this successive approximation method produces a profile of temperature only; moisture retrievals rely on other approaches.

The method described here is similar to conventional temperature retrieval techniques in that it requires statistical comparison of satellite data products to known soundings. However, there are two distinct advantages: (1) moisture, as well as temperature, retrieval is possible; and (2) smoothing that takes place in the conventional retrieval process is minimized.

2.4 Canonical discriminant analysis (CDA)

Canonical correlation analysis is a generalization of regressing one variable on another; i.e., regressing one vector on another vector. CDA extends this concept by regressing the random variables of satellite channel brightness temperatures on dummy variables (class of atmospheric sounding, in this case). CDA is related to EOF analysis; the main difference is that EOF analysis seeks to interpret total variance while CDA attempts to explain primarily between-class variance. Thus CDA accounts for within-class means and serves to discriminate among groups by responding to between-class variance.

Analyzing the satellite channel brightness temperature vectors with CDA has two purposes. The first is to confirm the classification of individual soundings by noting clustering of canonical variates. The second is to find sets of linear combinations of variables that best describe the physical differences of the synoptic features as represented by the various clusters (Smith and Woolf, 1976).

2.5 Physical interpretation of CDA

The brightness temperature vectors resulting from RTM analysis of the perturbations of the original seed soundings and their synoptic classifications constitute a training data set. When evaluated by CDA, the training data become separated according to between-sounding-class variance. The greatest variance is explained by the first canonical variable and successively smaller amounts of variance are explained by additional canonical variables. In this fashion, CDA reveals a physical basis for the sounding group separation and thus suggests synoptic signatures which are present in the channel brightness temperature vectors.

A physical representation of the canonical variables is seen in the correlation coefficients of satellite channel brightness temperatures. A large coefficient (absolute value) indicates that a channel is a significant contributor to the variance for a given canonical variable. With a knowledge of the atmospheric variables to which a channel is sensitive (Smith et al., 1979) and a summary of between-class canonical correlation coefficients, each brightness temperature channel is assigned membership in appropriate canonical variables. Since most of the between class variance is associated with the first canonical variable (CAN 1), the greatest separation of sounding groups is revealed by the amplitude of this canonical variable. Lesser variance is carried by, and hence lesser separation is shown by, subsequent canonical variables. Normally, the first three canonical variables account for most of the variance. For example, if HIRS channels 10 and 11 (the water vapor channels) constitute the major contribution to the first canonical variable, then CAN 1 derives the variance it represents from lower tropospheric water vapor fluctuations. Similar inferences may be drawn from interpretation of the correlation matrices and assignment of additional TIROS N channels to the remaining canonical variables.

3. DATA

A small data base was constructed using seven seed soundings representative of conditions often found over the tropical Pacific Ocean. The soundings were perturbed randomly to create the training data set as described above. Two additional test soundings, depicting similar but distinctly different synoptic features than contained in the training data set were introduced in the analysis procedure.

3.1 Training data set

While seven soundings are not a complete representation of conditions found over the tropical Pacific Ocean, they present an adequate group for testing the method described here. The seed soundings are shown in Fig. 1. The envelope of perturbed temperature and moisture soundings for sounding class 1 is shown in Fig. 2.

The synoptic conditions in the lower troposphere are of most interest, and oftentimes upper tropospheric moisture shields the lower troposphere from satellite view especially in the moisture channel wavelengths. Therefore, temperatures and dewpoint temperatures above 600 mb were kept constant at values consistent with the tropical eastern Pacific atmosphere in an attempt to stabilize RTM performance at upper levels.

3.2 Test soundings

Two real soundings, distinctly different from, but typical of the tropical eastern Pacific Ocean, were introduced to test the sounding identification and classification method. These soundings were not perturbed. They are shown in Fig. 3.

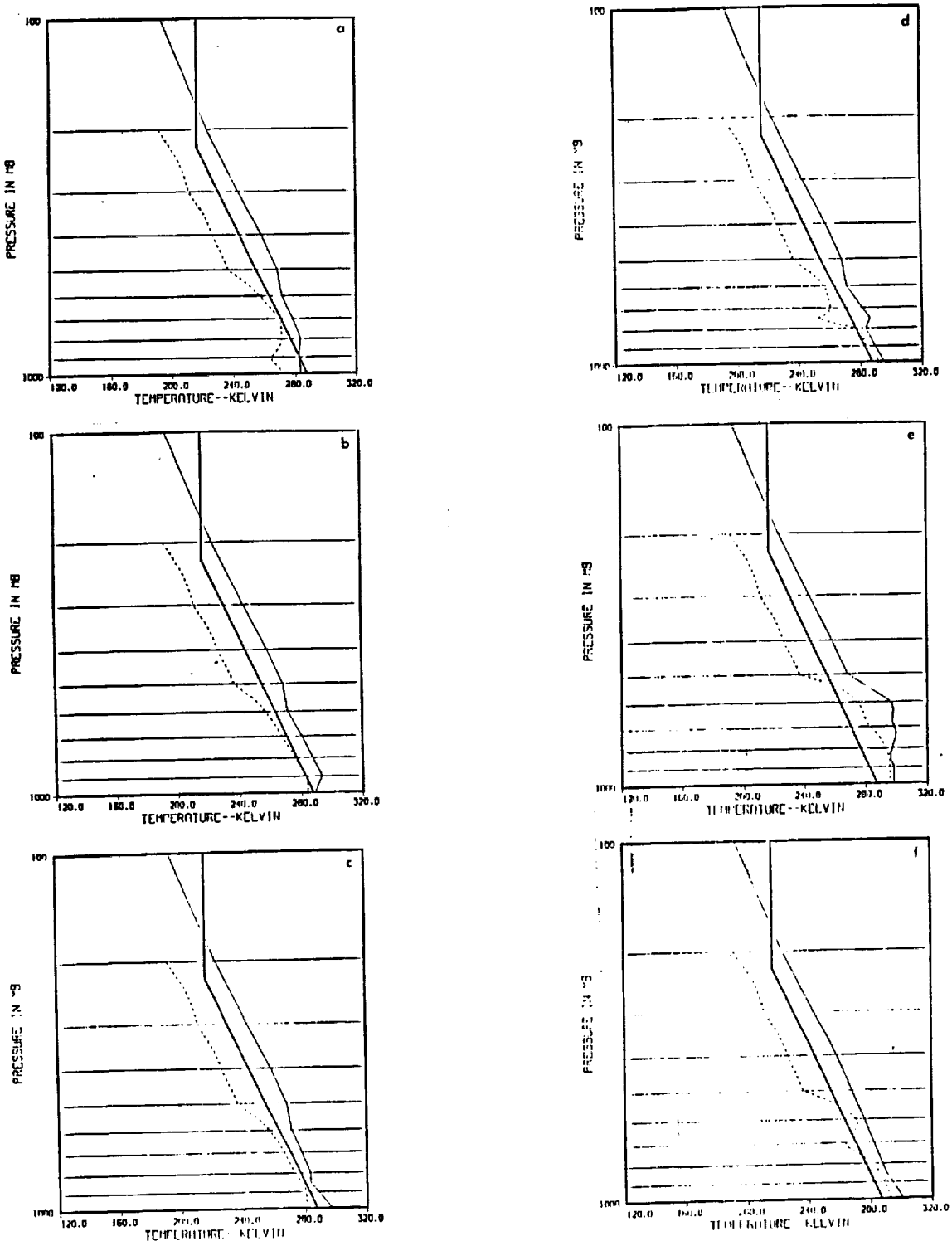

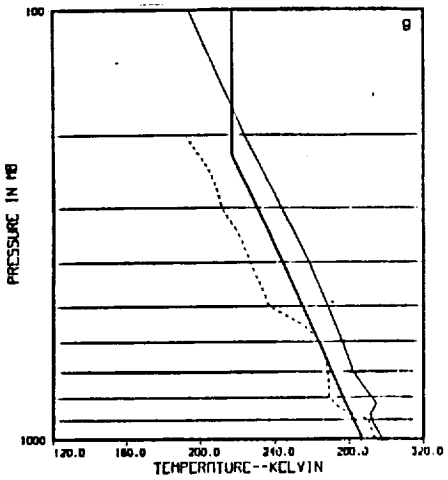

Fig. 1. Seed soundings for training data. Heavy line is tropical standard atmosphere, for reference. a) Sounding #1. Frontal inversion, surface to 850 mb. Cool surface temperature, dry throughout. b) Sounding #2. Radiation inversion, surface to 900 mb. Moist at surface, drying at inversion and remaining dry aloft. c) Sounding #3. Turbulence inversion resulting from well-mixed layer. Very dry at surface, turning moist at 850 mb. Inversion from 850 to 800 mb. Top of inversion starts dry layer to 600 mb. d) Sounding #4. Trade wind inversion, 800 to 750 mb. Moist surface layer, drying slightly at 900 mb, becoming moist again at 800 mb, then drying significantly at 750 mb. e) Sounding #5. Tropical cyclone. Warm and moist at surface, saturation at 850 mb, strong drying and significant warming aloft. Inversion, 850 to 650 mb. f) Sounding #6. Carrizal (9.5 °N, 67 °W). July. Warm surface, moist layer at 850 mb, with pronounced dryness at 700 mb, converging to moist layer at 600 mb. g) Sounding #7. Subsidence inversion in warm anticyclone. Warm and moist, surface to 850 mb. Inversion 850 to 800 mb with pronounced dry layer at 800 mb.

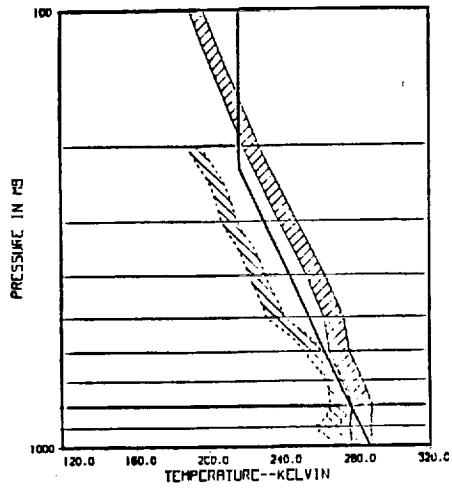

Fig. 2. As in Fig. 1a, with perturbation envelope shown. Random perturbation is ± 2%, distributed as white noise. Seed sounding makes vertical ascent through center of envelope.

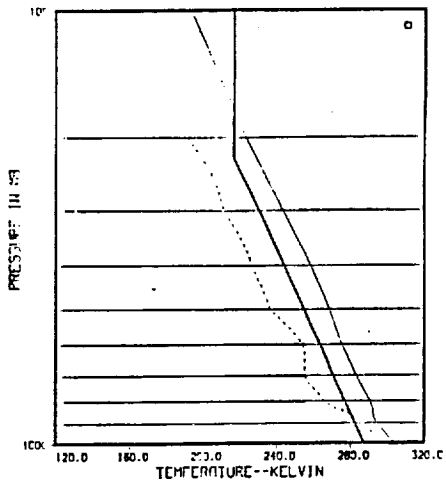

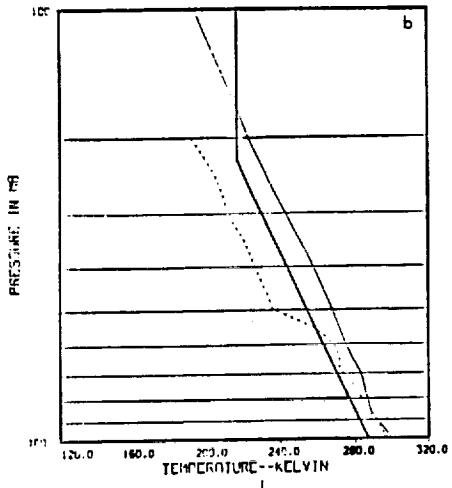

Fig. 3. Test soundings A and B, both 11 July 1957, 0000 UTC. a) Test sounding A. Kwajalein Island. b) Test sounding B. Majuro Island.

3.3 Brightness temperature vectors vs soundings

It should be remembered that the analysis procedure acts on brightness temperature vectors created for each sounding by the radiative transfer model. Conventional temperature and moisture sounding plots are shown for the seed and test soundings as a convenience in interpretation.

4. RESULTS

4.1 Cluster analysis

After evaluation by the RTM, the training data set brightness temperature vectors were classified and labeled according to their synoptic origins. The classifications were made two ways: (1) *a priori* through knowledge of the generating seed sounding, and (2) objectively through cluster analysis. In this study, both methods led essentially to the same results, i.e., cluster analysis reproduced almost the same sounding groupings as did the generating procedure.

4.2 Canonical discriminant analysis (CDA)

The linear combinations, or canonical variables of the channel brightness temperatures derived by CDA, explain between-sounding-class variance. The first canonical variable, CAN 1, carries nearly 90 percent of the variance. The second canonical variable, CAN 2, accounts for nearly 9 percent of the variance, and CAN 3 reveals slightly less than 1 percent. Cumulatively, the first three canonical variables account for nearly 99 percent of the between sounding class variance. These canonical variables may be accepted with confidence according to the results of Wilks' Lambda and associated T^2 tests.

4.3 Physical interpretation of CDA

Table 1 summarizes the interpretation of individual satellite channel membership in the first three canonical variables. CAN 1 is comprised of surface window and channels sensitive to lower-tropospheric temperature variations. The near surface water vapor channel, channel 10, is included in CAN 1.

CAN 2 is dominated by the mid-tropospheric moisture channels, 11 and 12, and most tropospheric temperature channels. One stratospheric channel makes a minor contribution.

Table 1. Satellite channel assignment to canonical variables.

CAN 1		
HIRS/MSU Channel	Level of peak Energy (mb)	Purpose of the radiance observation
7	900	Temperature sounding
8	Surface	Window
10	900	Water vapor sounding
13	1000	Temperature sounding
14	950	Temperature sounding
18	Surface	Window
19	Surface	Window
MSU 1	Surface	Surface emissivity
CAN 2		
HIRS/MSU Channel	Level of peak Energy (mb)	Purpose of the radiance observation
1	30	Temperature sounding
4	400	Temperature sounding
5	600	Temperature sounding
6	800	Temperature sounding
11	700	Water vapor sounding
12	500	Water vapor sounding
15	700	Temperature sounding
16	400	Temperature sounding
MSU 2	700	Temperature sounding
MSU 3	300	Temperature sounding
CAN 3		
HIRS/MSU Channel	Level of peak Energy (mb)	Purpose of the radiance observation
2	60	Temperature sounding
3	100	Temperature sounding
MSU 4	90	Temperature sounding

CAN 3 represents only about 1 percent of the between sounding group variance and is derived exclusively from stratospheric channels at or above 100 mb. No variation in channels sensitive to upper level radiation was expected, because temperature and dewpoint temperature in the original seed and test soundings were kept constant above 600 mb. A possible explanation of the variation is absorption from below and re-radiation at higher levels within the RTM.

4.4 Canonical variable plots

The canonical variables define sounding group separation as shown in Fig. 4. Plots of CAN 2 vs CAN 1 and CAN 3 vs CAN 1 depict sounding clusters and illustrate the between-group variance exhibited by the three canonical variables.

When plotted, the three canonical variables may be thought of as a three-dimensional representation of the variance of the sounding groups. Based on the physical interpretation of the canonical variables, the CAN 1 axis represents sounding group separation due to surface and near-surface temperature and moisture variability. The CAN 2 axis displays tropospheric temperature and moisture variability, and the CAN 3 axis describes minor variations of stratospheric temperature.

It is significant to note that the physical interpretation of variance groups revealed by this study is unique to this sounding climatology. Indeed, close examination of the seed soundings in Fig. 1 confirms that the greatest difference occurs in surface and near surface temperature in accordance with CDA results. Successive and thus lesser sounding differences are beyond the resolution of the seed sounding plots.

4.5 Identification of test brightness temperature vectors

The two test soundings introduced into the training data set and evaluated by the RTM appear as points A and B in Fig. 4. The points seem closest to seed sounding 6. The assignment is confirmed by the Mahalanobis distance calculations (a measure of cluster spacing) in Table 2.

Table 2. Mahalanobis distances between sounding classes.

Sound	A	B	1	2	3	4	5	6	7
A	.	25.91	88.06	67.30	29.44	36.27	35.01	19.19	26.26
B	25.91	.	70.19	49.89	18.60	22.13	20.90	8.98	12.25
1	88.00	70.19	.	21.76	59.73	52.13	68.46	75.12	63.71
2	67.30	49.89	21.76	.	39.51	31.43	48.16	54.52	42.70
3	29.44	18.60	59.73	39.51	.	9.18	28.21	18.70	9.62
4	36.27	22.13	52.13	31.43	9.18	.	27.22	24.83	13.14
5	35.01	20.90	68.46	48.16	28.21	27.22	.	23.52	20.01
6	19.19	8.93	75.12	54.52	18.70	24.83	23.52	.	12.74
7	26.26	12.25	63.71	42.70	9.62	13.14	20.01	12.74	.

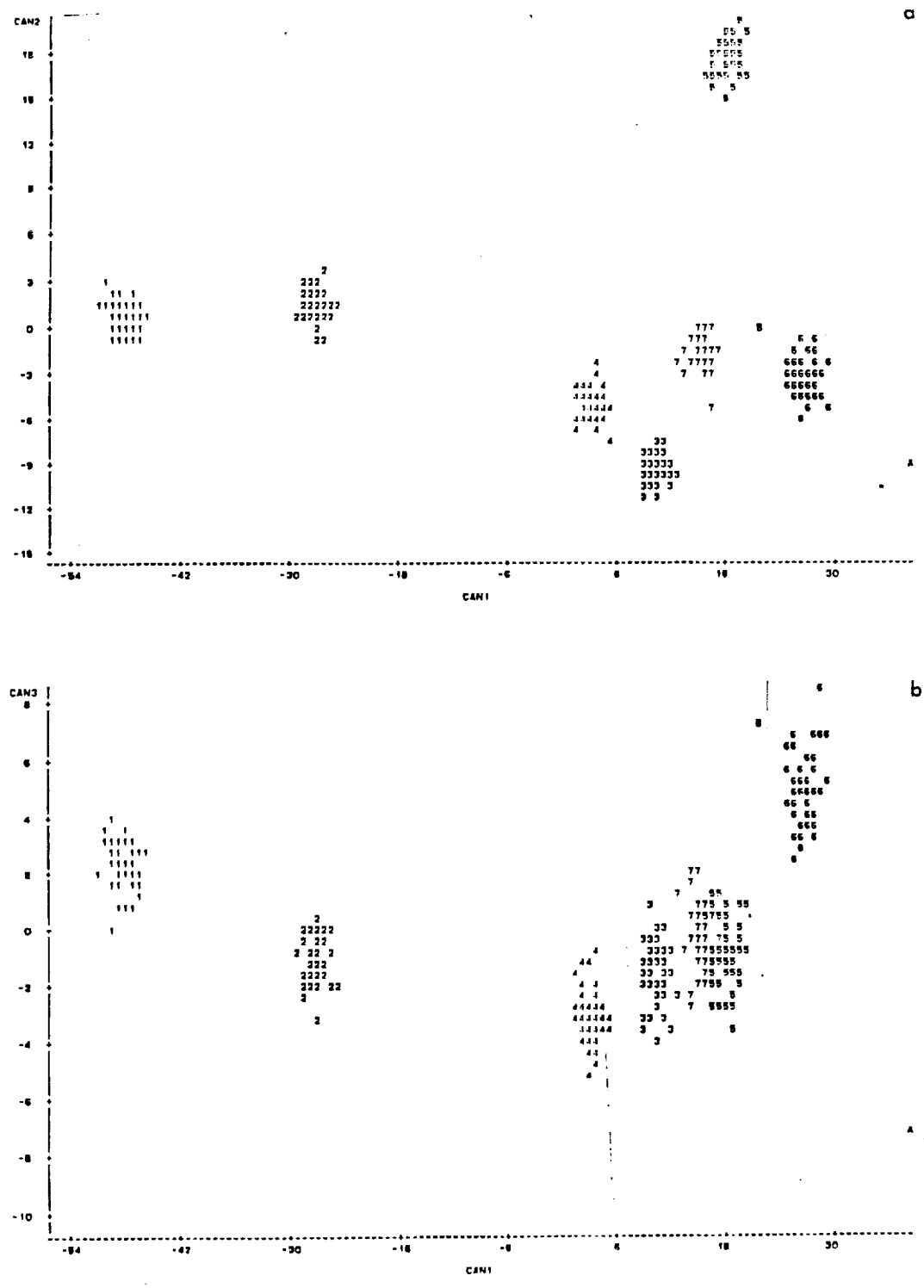

Fig. 4. Canonical discriminant analysis plots. Distribution of all synthetic soundings (1-7) and real soundings (A and B). For amplitudes of a) CAN 2 vs CAN 1, and b) CAN 3 vs CAN 1. Canonical variables are described in the text and in Table 1.

The physical characteristics of the two test soundings indeed are similar to seed sounding 6 (Fig. 1 f). Test sounding A is taken from Kwajalein (July) and test sounding B is taken from Majuro (July). Seed sounding 6 is based on Carrizal (July). All are warm at the surface. Carrizal and Majuro show increasing saturation from the surface to about 850 mb while a constant dewpoint depression is maintained from the surface to 850 mb at Kwajalein. From 850 mb to 700 mb, all three soundings present a layer of pronounced dryness which lapses into another moist layer at approximately 600 mb.

The Mahalanobis distance table confirms the next seed sounding with similar characteristics is 7 (Fig. 1 g). It is a composite sounding created to represent a warm anticyclone subsidence inversion. While not as warm at the surface, there is increasing moisture to about 850 mb, a layer of pronounced dryness at 800 mb (vice 700 mb), and a gradual increase in moisture from 800 mb to 600 mb. In general, the conditions are similar to seed sounding 6.

5. CONCLUSIONS

It has been shown that is it is possible to associate TIROS N channel brightness temperature vectors with synoptic features. The success of this approach is dependent entirely on the judicious choice of seed soundings, the allowable spread of soundings about the seed, and the quality of the radiative transfer model which produces the brightness temperatures from atmospheric variables.

The method is not without difficulties. Most of the variance is carried in the first canonical variable. Unfortunately, in this study, the channels appearing in CAN 1 are sensitive primarily to surface or near surface conditions. The atmospheric conditions of greatest interest—mid- to lower tropospheric temperature and moisture variations—appear in the second canonical variable, CAN 2, which carries a smaller percentage of the variance. The third canonical variable carries variance of little use in sounding identification.

One is reminded that canonical discriminant analysis focuses on the between-class variance. Within-class variances are an important, but often overlooked, byproduct of CDA. Evaluated properly, within-class variances may reveal how soundings within a given cluster differ and may lead to quantification of synoptic signatures directly from satellite channel brightness temperatures.

6. ACKNOWLEDGEMENTS

The research reported here is supported by NASA's George C. Marshall Space Flight Center, under Contract No. NAS8-37284. The radiative transfer model was provided by J. Susskind and D. Reuter of the NASA Goddard Laboratory for Atmospheres. R. Liles provided computational support. N. Streetman prepared figures and assembled the manuscript.

7. REFERENCES

Chahine, M. T., 1970: Inverse problems in radiative transfer: Determination of atmospheric parameters. *J. Atmos. Sci.*, 27, 960-967.

Johnson, R. A. and D. W. Wichern, 1982: *Applied Multivariate Statistical Analysis.* Prentice Hall, 594 pp.

McGuirk, J. P., L. L. Anderson and A. H. Thompson, 1985: Satellite-derived synoptic climatology in data-sparse regions. *Adv. Space Res.*, 5(6), 45-48.

———, A. H. Thompson and L. L. Anderson, 1986: Wintertime disturbances in the tropical Pacific: FGGE IIIb and satellite comparisons. Preprint from National Conference on Scientific Results of the First GARP Global Experiment, Miami, Jan. 1986, 4 pp.

Smith, W. L. and H. M. Woolf, 1976: The use of eigenvectors of statistical covariance matrices for interpreting satellite sounding radiometer observations. *J. Atmos. Sci.*, 66, 1127-1150.

———, H. M. Woolf, C. M. Hayden, D. Q. Wark and L. M. McMillin, 1979: The TIROS-N operational vertical sounder. *Bull. Am. Meteor. Soc.*, 58, 1177-1187.

Susskind, J., J. Rosenfield, D. Reuter and M. T. Chahine, 1982: The GLAS physical inversion method for analysis of HIRS2/MSU sounding data. NASA Tech. Memo. 84936, Goddard Space Flight Center, Greenbelt, MD, 101 pp.

Paper presented at: Tenth Conference on Probability and Statistics in the Atmospheric Sciences, American Meteorological Society, Edmonton, Canada, October 1987.

CANONICAL DISCRIMINANT ANALYSIS OF SYNOPTIC SIGNATURES IN SATELLITE BRIGHTNESS TEMPERATURES

G. A. White, III and J. P. McGuirk

Department of Meteorology
Texas A&M University
College Station TX 77843-3146

1. INTRODUCTION

Meteorological analysis over critically data-sparse areas, such as tropical oceans, must be accomplished, in part, with remotely sensed data from satellites. A portion of these data are employed as input to models which yield vertical profiles of the atmosphere. Additional synoptic information in the satellite channel brightness temperature data is needed and may be present, but appears to remain unused. In a study of synoptic variability of satellite data, McGuirk *et al.* (1986) found that individual channel brightness temperatures may be preferable to reconstructed temperature and moisture profiles because the reconstructions are smoothed both horizontally and vertically.

The objective of this study is to identify and recover the signatures of synoptic features directly from individual satellite channel brightness temperatures. Of special interest are the meteorologically important elements of an atmospheric sounding; namely, the near discontinuities in temperature and moisture found typically in fronts and inversions. Conventional reconstructed temperature and moisture profiles from satellite-borne radiometer data unavoidably smear these discontinuities and contaminate their signatures. In pursuit of the objective, this study poses two main questions: can atmospheric soundings as viewed by satellite, be sorted by synoptic signature, and can the signatures be quantified?

To test this possibility, a set of fictitious atmospheric temperature and moisture soundings was created, each of which represented a specific synoptic feature. The temperature and water vapor variables for each of these "seed soundings" were perturbed randomly, within limits, to create a group of 60 soundings. Each sounding was transformed by a radiative transfer model (RTM) to a vector of individual satellite channel brightness temperatures which would have been observed by radiometers aboard the TIROS-N satellite had they viewed that vertical section of the atmosphere.

The brightness temperature vectors arising from the sounding groups were classified and labeled as to their known synoptic origins as they were created by the RTM. The classifications could have been made *a priori* through knowledge of the generating seed sounding or objectively through cluster analysis (Johnson and Wichern, 1982). If the goal is to identify synoptic features from satellite-derived data, cluster analysis is appropriate; if diagnosis of a specific feature is intended, physical assignment is appropriate. In this study, both methods led to identical results, i.e., cluster analysis reproduced the same sounding groupings as did the generating procedure.

Finally, the brightness temperature vectors arising from the sounding groups were subjected to canonical discriminant analysis (CDA), which serves two purposes: first, it confirms (or denies) the initial classifications of the sounding groups based on their statistical properties; and second, it quantifies the basis for synoptic classification (Johnson and Wichern, 1982). Each satellite channel is sensitive to upwelling radiation within a specific wavelength band from certain atmospheric constituents (Smith and Woolf, 1979). By determining which channels and thus which atmospheric constituents contribute to the separation of sounding groups, physical significance may be assigned to the linear combinations of the individual satellite channel brightness temperatures which appear as canonical variables in CDA.

2. RADIATIVE TRANSFER MODEL

Since the objective of this study is to recover synoptic information directly from satellite channel brightness temperatures, a source for the satellite data was required. There were two options: (1) collocated satellite observations and upper air data; or, (2) a radiative transfer model (RTM) capable of simulating a vector of individual satellite channel brightness temperatures for specified soundings. The RTM was chosen because it gave better control for technique development; it allowed the flexibility to study any synoptic feature for which atmospheric vertical profiles could be drawn; and, it removed the spurious signals found in real soundings.

The RTM was developed at NASA Goddard Space Flight Center's Laboratory for Atmospheres and documented by Susskind *et al.* (1982). It is a non-linear 66-layer (surface to 1 mb) rapid transmission algorithm which directly calculates brightness temperatures for 22 of the 24 HIRS2 and MSU channels on board TIROS-N. Because of its non-linearity, the model increases the variability of the atmospheric temperature and dewpoint information. The model simulates the vertical-integrating property of radiative transfer and thus smears the signal from detailed atmospheric features.

3. DATA DESCRIPTION

Four fictitious seed soundings were used in this study. The soundings are distinct and representative of conditions over the tropical eastern Pacific Ocean. They were chosen to contain considerable overlap of temperature and dewpoint throughout the troposphere. The soundings are nearly identical above 600 mb and contain varying features between the surface and 700 mb.

The first sounding (Fig. 1a) depicts a shallow trade wind inversion between 900 and 850 mb. The second sounding (Fig. 1b) shows a frontal inversion. The third sounding (Fig. 1c) illustrates a subsidence inversion, or a higher trade wind inversion. The fourth sounding (Fig. 1d) is a smooth profile containing no discontinuities in temperature or moisture.

Each seed sounding was perturbed randomly to create groups of soundings which illustrate synoptic features and their natural variability. The perturbation was accomplished by varying randomly the seed sounding temperature and mixing ratio by as much as plus or minus 2 percent in each of the 66 layers of the RTM; the variability was distributed as white noise. Fifty perturbation iterations were made from each of the four seed soundings.

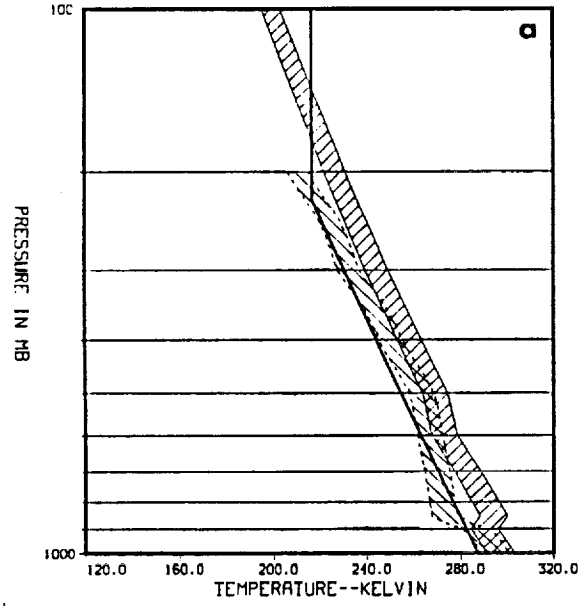

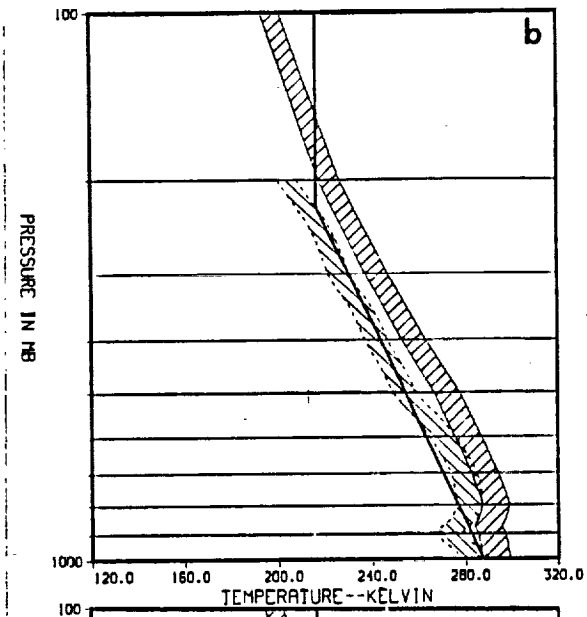

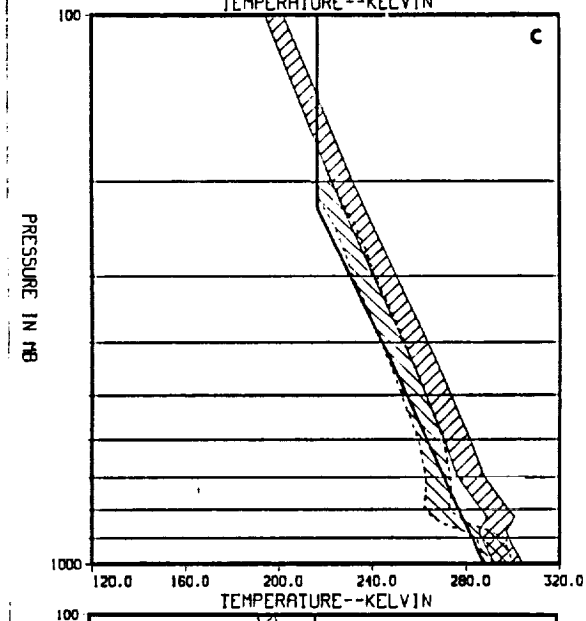

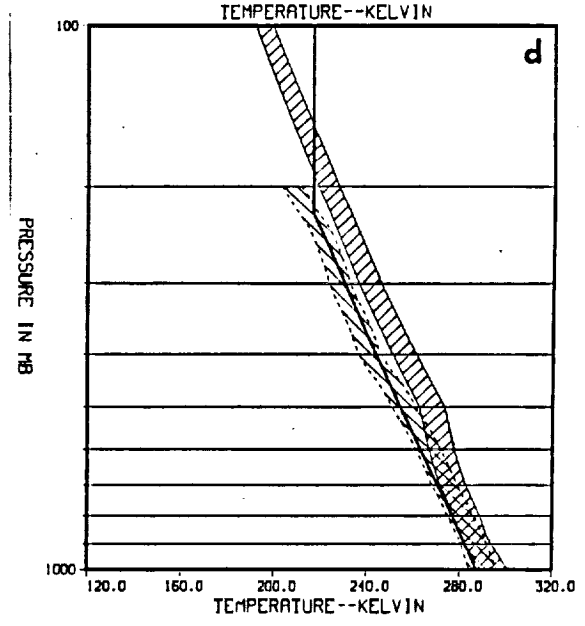

Fig. 1. Fictitious soundings used in this study. The envelopes depict variability of temperature and dewpoint. Moisture values above 200 mb are fixed. The heavy line is the ICAO standard atmosphere and is included for reference. a) Shallow trade wind inversion. b) Frontal inversion. c) Subsidence or higher trade wind inversion. d) Smooth profile containing no temperature or moisture discontinuities.

4. SOUNDING CLASSIFICATION

All members of each 50-sounding group was coded according to the parent seed sounding. The synoptic classification assignments also could have been made objectively using cluster analysis. - Membership in a cluster is determined by an individual sounding's minimum squared distance to the nearest cluster mid-point. Clusters are defined by minimizing the sum of squares of the distance of all soundings to their respective group means.

Cluster analysis works best when data distribution is grouped around central means with small variances as shown in Fig. 2. With short data distribution tails, there is small overlap between groups, and assignment of individual points to a group is unambiguous. For large variability, cluster algorithms have two main problems. First, the number of clusters may be unclear, and the process may need to be forced to select the optimum number of groups. Second, after the clusters are chosen, it may be difficult to assign points lying within two data distribution tails to the correct group. The 200 soundings used in this study were clustered after their synoptic classifications were assigned by the creation algorithm; cluster analysis found four groups and assigned each sounding correctly.

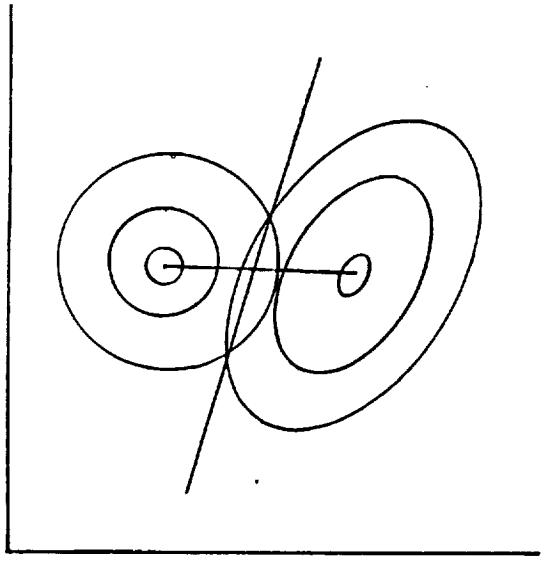

Fig. 2. Data distribution in two dimensions. Contours are isopleths of standard deviation. Variance in data is shown by relative size of ellipse and spacing of contours. When overlap occurs among ellipses from more than one data group, assignment of individual points to proper groups becomes ambiguous.

5. CANONICAL DISCRIMINANT ANALYSIS

Canonical correlation analysis is a generalization of regressing one variable on another; i.e., regressing one vector on another vector. Canonical discriminant analysis (CDA) extends this concept by regressing the random variables of satellite channel brightness temperatures on dummy variables (class of atmospheric sounding, in this case). CDA is related to empirical orthogonal function (EOF) analysis; the main difference is that EOF analysis seeks to interpret total variance while CDA attempts to explain between-class variance. Thus CDA minimizes within class means and serves to discriminate among groups by responding to between-class variance.

Analyzing the satellite channel brightness temperature data with canonical discriminant analysis has two purposes. The first is to confirm the classification of individual soundings. The second is to find sets of linear combinations of variables that best describe the physical differences of the of the four sounding groups (in this example).

5.1 Training data set

The 200 brightness temperature vectors with their initial classifications form a training data set. While CDA is incapable of making initial classification assignments for the entire data set, if additional vectors are introduced without classification information, CDA places each new vector with the group having similar variance characteristics. In this fashion, CDA serves to confirm the initial classification assignments and may classify new vectors introduced into the data base.

5.2 Linear combinations

CDA derives several linear combinations, or canonical variables, of the channel brightness temperature variables that explain between sounding class variance. The greatest variance is explained by the first canonical correlation, and successively smaller amounts of variance are explained by additional canonical correlations.

5.3 Physical interpretation of CDA

Within each canonical variable, a correlation coefficient was calculated for each satellite channel brightness temperature. A large coefficient (absolute value) indicates that a channel was a significant contributor to the variance for a given canonical variable. With a knowledge of channel sensitivities and a summary of between-class canonical correlation coefficients, each brightness temperature channel was assigned membership in canonical variable 1 (CAN 1), canonical variable 2 (CAN 2) or canonical variable 3 (CAN 3). In this manner a physical pattern emerged which explained the source of the variance of the channel brightness temperature vectors which defined the four sounding groups.

Since most of the between-class variance (nearly 87 percent) is associated with CAN 1, the greatest separation of sounding groups is revealed by this canonical variable. Lesser separation (11 percent) is shown by CAN 2 and very little (2 percent) is carried by CAN 3. The first canonical variable results from contributions of surface

temperature and mid- to lower tropospheric water vapor content. Fig. 1 a-d reveal subtle yet distinct differences in surface temperature and dewpoint profiles below 600 mb. The second canonical variable arises from contributions by mid-tropospheric temperature variability and near surface water vapor content. Slight stratospheric temperature variability appears in the third canonical variable. The separation of the brightness temperature vectors according to the amplitudes of the three canonical variables is shown in Fig. 3.

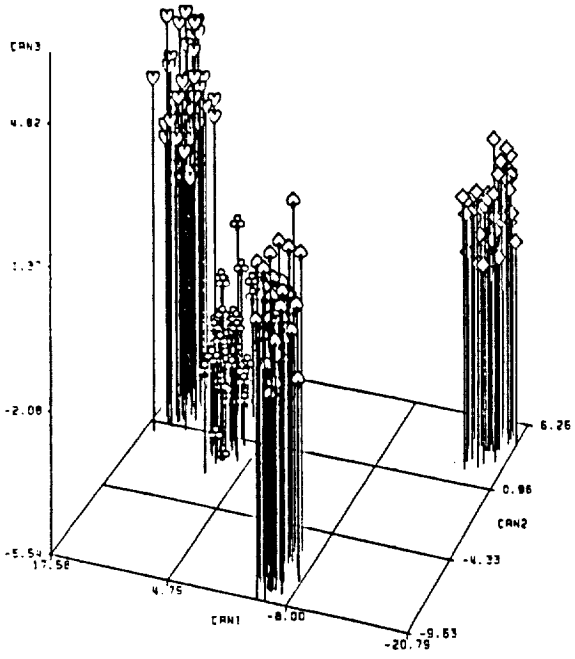

Fig. 3. Canonical discriminant analysis of four sounding groups. Maximum separation occurs in the first canonical variable which results from contributions of surface temperature and mid- to lower tropospheric water vapor content. The second canonical variable arises from contributions by mid-tropospheric temperature variability and near surface water vapor content. Slight stratospheric temperature variability appears in the third canonical variable. The symbols clubs, diamonds, hearts, and spades represent the soundings in Fig. 1 a-d, respectively.

6. CONCLUSIONS

The major achievement of this study is the recovery of the synoptic variability of temperature and dewpoint differences as detected in individual satellite channel brightness temperatures. The techniques employed in this study revealed the physical source of the brightness temperature variance and confirmed that the physical differences of the sounding groups had the same origins as in the original seed soundings.

EOF analysis and CDA do not reveal the same information. In their analysis of satellite channel data, McGuirk *et al.* (1986) found that the typical first principal component represents tropospheric mean temperature and carries about 60 percent of the variance. The second principal component represents mean tropospheric moisture and carries 15 to 20 percent of the variance. In contrast, the first canonical variable separated the four sounding groups by differences in surface temperature and mid- to lower tropospheric water vapor content. The second canonical variable separated the groups by differences in tropospheric temperature and near surface water vapor.

Although not an major part of this study, cluster analysis was shown to be able to classify satellite channel brightness temperature vectors into groups based on the physical characteristics of the atmospheric soundings from which the satellite information was taken. Cluster analysis, coupled with canonical discriminant analysis, suggests that satellite channel data may contribute more directly to meteorological analysis over otherwise data-sparse areas.

7. ACKNOWLEDGEMENTS

The research reported here is supported by NASA's George C. Marshall Space Flight Center, under Contract No. NAS8-37284. The radiative transfer model was provided by J. Susskind and D. Reuter of the NASA Goddard Laboratory for Atmospheres. E. Rieger and B. Batson provided computational support.

8. REFERENCES

Johnson, R. A. and D. W. Wichern, 1982: *Applied Multivariate Statistical Analysis.* Prentice Hall, 594 pp.

McGuirk, J. P., L. L. Anderson and A. H. Thompson, 1986: Tropical synoptic interpretation of inter-channel correlations from TIROS N. Preprint from Second Conference on Satellite Meteorology/Remote Sensing and Applications, Williamsburg, VA, Amer. Meteor. Soc., 5 pp.

Smith, W. L. and H. M. Woolf, 1976: The use of eigenvectors of statistical covariance matrices for interpreting satellite sounding radiometer observations. *J. Atmos. Sci.*, 66, 1127-1150.

Susskind, J., J. Rosenfield, D. Reuter and M. T. Chahine, 1982: The GLAS physical inversion method for analysis of HIRS2/MSU sounding data. NASA Tech. Memo. 84936, Goddard Space Flight Center, Greenbelt, MD, 101 pp.

Paper presented at: Twelfth
Climate Diagnostics Workshop,
NOAA, Salt Lake City UT,
October 1987.

Climatology of Various Synoptic Systems over the Tropical North Pacific

James P. McGuirk
Department of Meteorology, Texas A&M University
College Station, TX 77843

Studies of low frequency variability in the tropics show systematic differences in behavior as a function of longitude. The atmospheric manifestations of most ENSO events do not seem to propagate beyond the dateline; their east Pacific behavior often does not change until the SST anomalies appear off the coast of South America and spread to the west-- certainly, 1982-83 is an exception to this behavior. The SPCZ seldom extends significantly eastward of the dateline. Certain aspects of the 30-60 d wave are restricted to east Asia and the western Pacific. It has been suggested that this wave may act as a propagating wave between the east coast of Africa and the dateline, and as a standing wave across the east Pacific and the Atlantic. The first part of this summary describes interaction of synoptic scale systems with tropical low frequency behavior for several different longitude bands.

1) Western Pacific. Madden and Julian's original work on the 30-60 d wave reveal a sea level pressure oscillation with about 2 mb amplitude (peak-to-peak) at Canton Island, just to the east of the area of preferred typhoon origin. Eighty-one typhoons, occurring between 1960-64, were composited and stratified as a function of the pressure wave at Canton. The results are summarized in the histograms of Fig. 1. The top panel shows that more typhoons occur when the pressure at Canton is at a minimum or is rising (47 vs. 34). If the pressure data are backshifted two days, to center the pressure extrema over the typhoon origin region west of Canton, the frequency variation sharpens considerably About twice as many typhoons initiate at pressure minima or during the subsequent rise. When stratified by quarters, the signal strengthens even more. Only 8 typhoons developed after a pressure peak, whereas 34 initiated after pressure minima. The backshifted results are significant with a confidence exceeding 99%. The five typhoon seasons are summarized, showing the interannual variability; the dependence on the 30-60 d wave appears in every year examined.

2) Eastern Pacific. A climatology of a type of tropical/subtropical system manifested by a SW-NE line of cirrus and convective cloud is shown in Fig. 2. The dark bars indicate individual systems. The period is the 1981-82 cool season. The shading designates the 200 mb divergence pattern (from Knudson and Weickmann) associated with the 30-60 d wave. The link between the synoptic events and the 30-60 d wave is suggestive, but not compelling. Association between the December and March cycles is strong, but non-existent for the December/January wave. Synoptic evolution is common during the upper level convergent phases as well. If a relation exists, it is weak. The western Pacific was not examined for these synoptic disturbances because they do not occur so commonly there.

3) Gulf of Mexico. Indications of the 30-60 d wave are not strong in this region. A number of parameters were examined, but results are inconclusive. The strongest coupling was found in percentage cloud cover of a rectangular area over the Gulf (bounded by 10 and 20º N latitude and 85 and 100º W longitude. The cloud cover was inferred from GOES E infrared imagery during the spring and summer of 1979. Figure 3 displays the smoothed traces of percentage cloud cover at 00 and 12 UTC. The bars at the bottom indicate maxima of Selkirk's EOF pattern 2 of upper level divergence. This pattern, with EOF 3, represents the travelling component of the 30-60 d wave. Correspondence is good, except in March. At this cycle a major change in the behavior of the time series of EOF 3 was observed. With four of the cycles, cloud cover fluctuations of 10-20% were detected at both 00 and 12 UTC.

The second part of this summary examines systems as they cross the Pacific and how they interact with the zonally symmetric Hadley cell (at least over the Pacific). Figure 4 displays an introductory analysis of the OLR signatures of synoptic disturbances crossing the Pacific, over a seven day period. The heavy line tracks a cyclone triggered by an east Asian cold surge; the light line to the west is the cold surge itself. The light line to the east is the remnant of another cyclone. The cloud bands with arrows, over the eastern Pacific, represent the synoptic systems discussed in (2) above. A number of authors have suggested that these cloud bands are triggered by midlatitude troughs, as indicated by the propagation lines. Three points are relevant in this figure:

i) Why did these propagating troughs not initiate any of these synoptic disturbances in the west Pacific?

ii) Why is there not a clearer relationship between the "initiating" midlatitude disturbances and the "resulting" tropical system, either in terms of cloud connection or proximity of initiation and result?

iii) Is the tropical convection, apparent in the lower right hand corner from the 22nd onward (but not continuous in time), relevant?

Finally, the behavior of the ITCZ is contrasted between periods of zonally symmetric behavior, and periods dominated by a tropical synoptic scale wave regime. McGuirk has already presented data supporting the hypothesis that the east Pacific Hadley cell operates in two different modes (a zonally symmetric mode-- during summer and ENSO events, and an intense eddy mode--during wintertime synoptic events). Figure 5 displays composites of 35 synoptic events, aligned at their ITCZ origin points, in both latitude and longitude. Thus, the 0º latitude line is approximately at 7º N. The data for the composites come from the 6.7 μm water vapor channel on VAS. This channel is sensitive to the temperature of the first layer of atmospheric moisture it sees, looking downward. The 16-level false coloring on images was reduced to 4, with 1 being wettest, and 4 driest. For numbers larger than about 2.6, clouds will not be present.

The lower left panel is a composite of the systems at their maturity. The panel to the right represents conditions when no synoptic activity is present. The differing appearances are obvious. The synoptic system is clearly tropical, centered on about 12º N; the wavelength is approximately 4000 km, and the ITCZ wave is obvious. The ITCZ in the right panel is much better defined in water vapor imagery than in OLR climatologies, even when there is no strong synoptic scale convective signature.

The two upper panels represent composites 48 and 24 h before system maturity. The shaded (wet) and hatched (dry) regions are distinguishing features of the precursor atmosphere to synoptic development. Cloud development with the system typically does not occur until about 36 h after the upper left panel. Using this panel as a template for future synoptic development captured 60% of the developing systems, both in time and in location at least 24 h in advance on an independent data set. The main reason for misforecasting was the existence of multiple systems in the Pacific and their interaction. A comparison of composited water vapor imagery with a similar composite prepared by Mock and Lin from OLR data revealed two important biases: The OLR data center the systems nearly 10º north of the water vapor composite, suggesting a midlatitude system; the strength of the ITCZ wave is underestimated by the OLR composite.

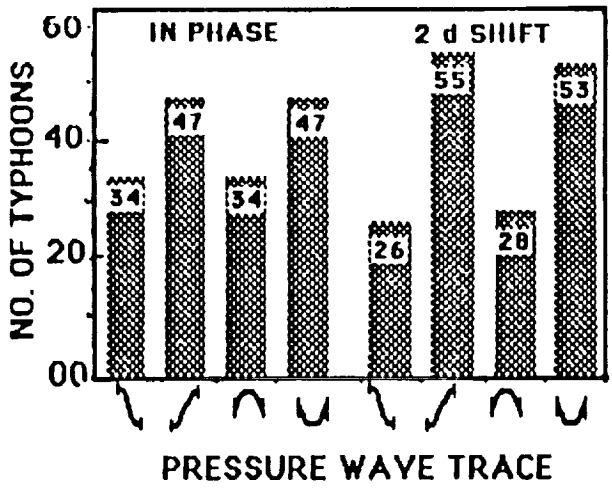

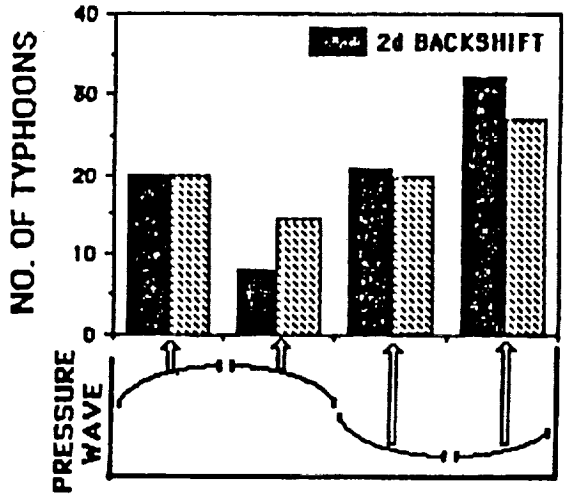

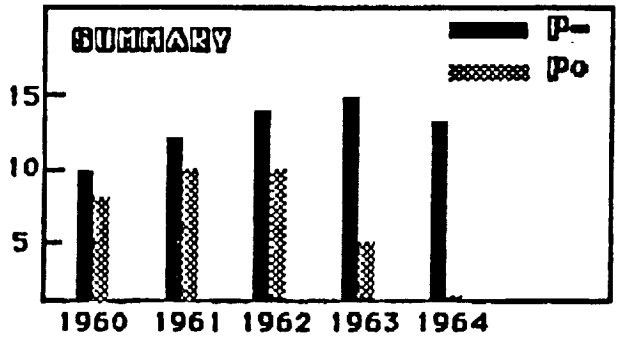

Fig. 1. Histograms of typhoon frequency as a function of 30-60 d wave phase of sea level pressure at Canton Island from 1960-1964. In top two panels the wave phase is shown schematically below the histograms. The "backshifted" pressure data move the extrema westward to the region of typhoon genesis. The bottom panel summarizes the interannual variations for pressure extrema.

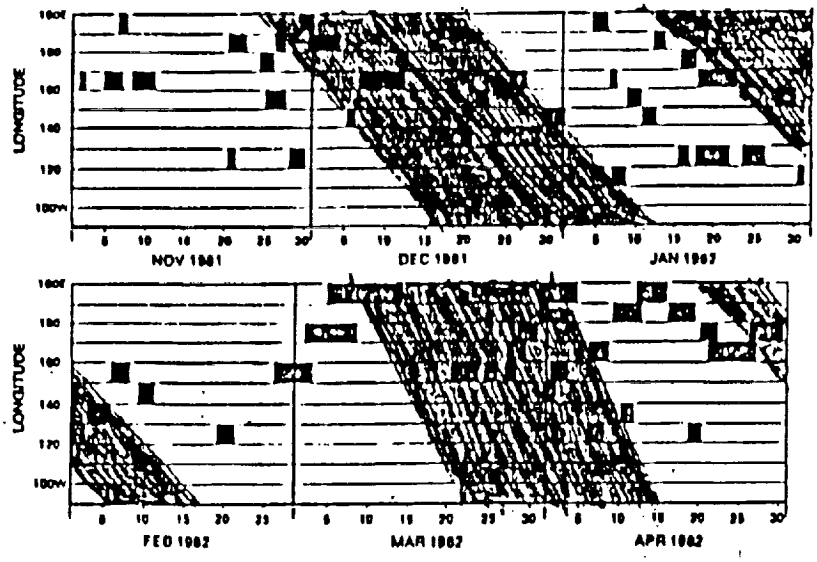

Fig. 2. Occurrence of tropical/subtropical synoptic systems (black bars) as a function of time and longitude of initiation. Shaded regions represent the propagation of 200 mb divergence associated with the 30-60 d wave (from Knudson and Weickmann).

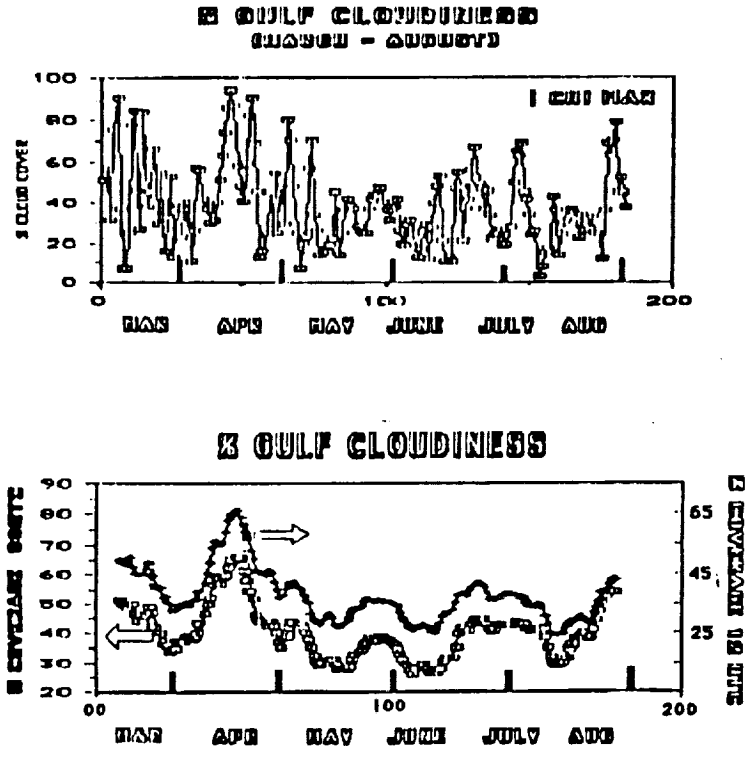

Fig. 3. Smoothed percent coverage of IR detected cloudiness over the Gulf of Mexico between 85 and 100°W, and 10 and 20°N during 1979. Bars along bottom represent maxima from Selkirk's 200 mb divergence EOF.

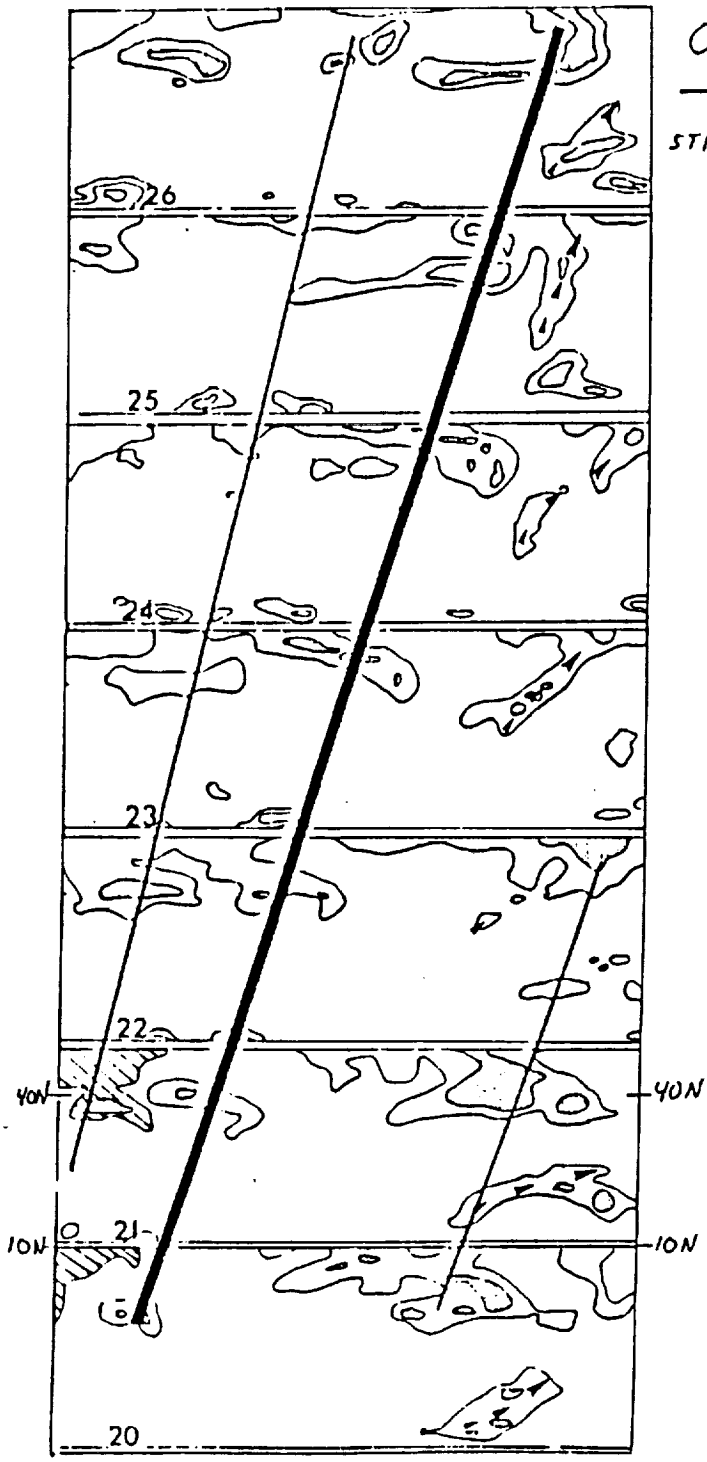

Fig. 4. Seven day sequence of OLR data between 120°W and 120°E, and 10°N and 50°N. Slanted lines follow propagating synoptic cloud mass; hatching denotes east Asian cold surge. Arrows denote tropical/subtropical systems.

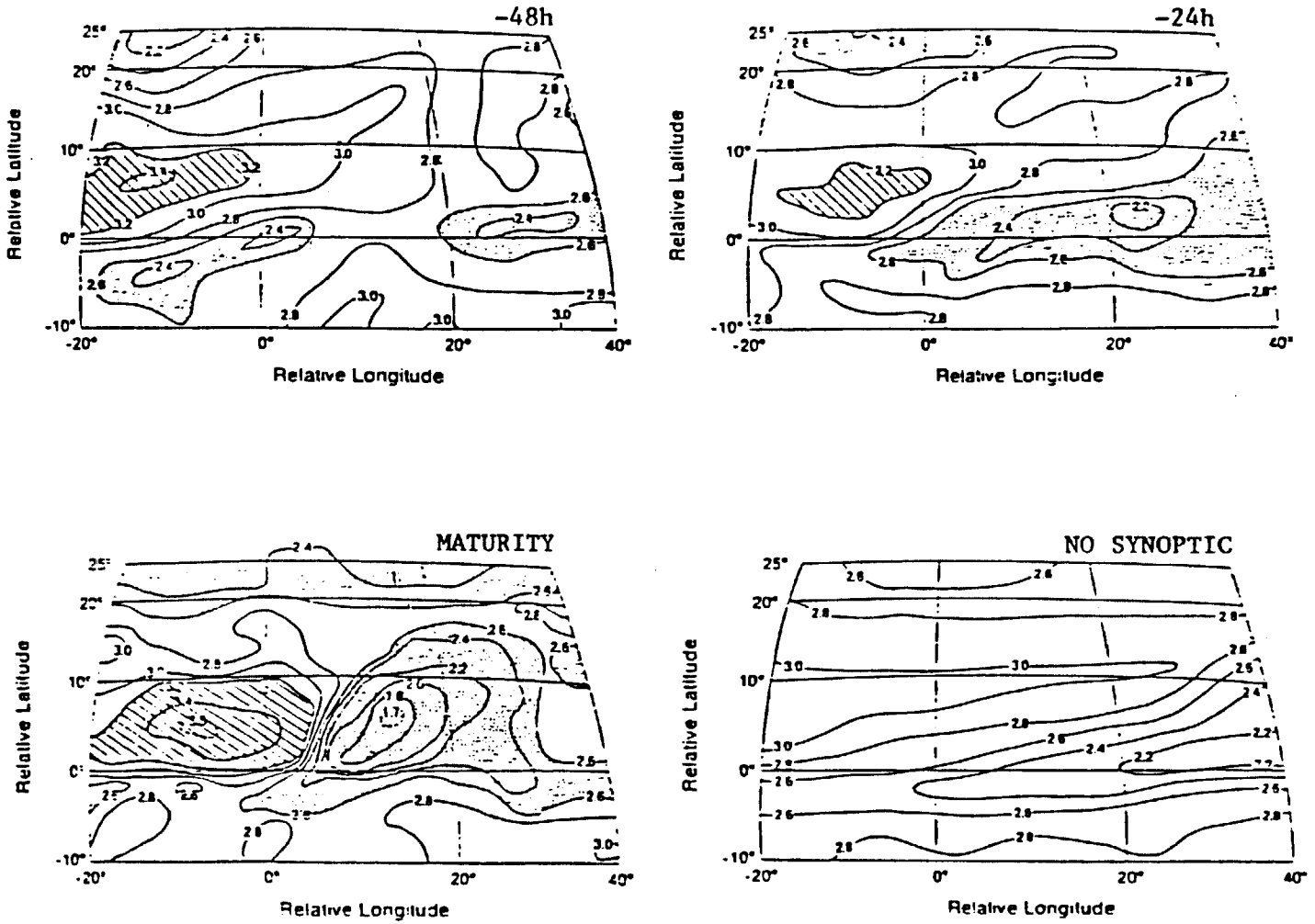

Fig. 5. Thirty-five event composites of evolution of tropical/subtropical system for 48h and 24h before maturity, for maturity and for no synoptic signal. The data are 6.7 μm water vapor imagery indexed to four integers, with 1 being wettest and 4 driest. Synoptic composites are adjusted in space with their ITCZ origin located at 0°,0° lat/long.

NASA
National Aeronautics and Space Administration

Report Documentation Page

1. Report No.	2. Government Accession No.	3. Recipient's Catalog No.
N/A		

4. Title and Subtitle
Tropical Pacific Moisture Variability: Its Detection, Synoptic Structure and Consequences in the General Circulation

5. Report Date
September 1990

6. Performing Organization Code

7. Author(s)
James P. McGuirk

8. Performing Organization Report No.

10. Work Unit No.
146-73-07-91

9. Performing Organization Name and Address
Department of Meteorology
Texas A&M Unuveristy
College Station, TX 77843-3146

11. Contract or Grant No.
NAS8-37284

13. Type of Report and Period Covered
Final
December 6,1986-August31,1990

12. Sponsoring Agency Name and Address
National Aeronautics and Space Administration
Washington D.C. 20546-0001
George C. Marshall Space Flight Center

14. Sponsoring Agency Code

15. Supplementary Notes

16. Abstract This study develops satellite data analysis tools and implements them for the diagnosis of atmospheric circulation systems over the tropical Pacific Ocean. The tools include statistical multi-variate procedures, a multi-spectral radiative transfer model, and the global spectral forecast model at NMC. Data include *in situ* observations; satellite observations from VAS (moisture, infrared and visible), NOAA polar orbiters (including TOVS multi-channel sounding data and OLR grids) and SMMR; and ECMWF analyses.

A primary goal is a better understanding of the relation between synoptic structures of the area, particularly tropical plumes, and the general circulation, especially the Hadley circulation. A second goal is the definition of the quantitative structure and behavior of all Pacific tropical synoptic systems.

Finally, this study examines strategies for extracting new and additional information from existing satellite observations. Although moisture structure is emphasized, thermal patterns are also analyzed. Both horizontal and vertical structures are studied and objective quantitative results are emphasized.

17. Key Words (Suggested by Author(s))	18. Distribution Statement
Tropical, Plumes, Moisture, Satellite, Radiative transfer	Unclassified/Unlimited

19. Security Classif. (of this report)	20. Security Classif. (of this page)	21. No. of pages	22. Price
Unclassified	Unclassified	124	